POLITECNICO
MILANO 1863

SCUOLA DI INGEGNERIA INDUSTRIALE
E DELL'INFORMAZIONE

Executive Summary of the Thesis

Model identification and statistical analysis in visual odometry on an UAV

Master of Science in Aeronautical Engineering

Author: Pietro Giannagostino

Advisor: Prof. Marco Lovera

Co-advisor: Gabriele Roggi

Academic year: 2021-2022

My thesis is mainly about Visual Odometry, that is the process of estimation of the position and/or the motion of a body through comparisons in images taken by a camera mounted on it.
Visual Odometry, from now on VO, has been improved a lot and has found an increasing number of application across the last years, but few attempts have been done to characterize the dynamic of errors in VO systems and to find out how it depends on environmental conditions.

1. Experimental setup

Visual Odometry can use Feature Based methods, that track only some features of the pictures, and Direct Methods, that track all pixels.
It has been chosen to do a *factorial design of experiments*, based on the $factors$, the variables that can influence the experimental outcomes, and on their *levels*. The effect of a change in the level of a single factor is called $maineffect$; if the effect of a factor varies in relationship with the level of another factor, the two factors are said to have an *interaction*.
For the purpose of this thesis, it has been used a quadrotor UAV called ROG-1, built by students and research fellows of Politecnico di Milano, that has been operated inside an indoor arena with a Motion Capture system, in order to have a sort of "ground truth" in the estimation of the position. The reference frame is centered in the point of coordinates (0,0,0) and has the x, y ans z axes pointing, respectively, East, North and upward.
The VO system was a Stereolabs ZED stereoscopic camera with an embedded algorithm.
The flight trajectory contained vertical, horizontal and circular parts.
Four factors, each with two levels, have been considered (2^k design, with $k = 4$): the height, the angular velocity of the circular part of the flight (from now on TAV), the state of the Yaw Following (from now on YF) and the light in the arena. Sixteen experimental runs have been performed.

2. Statistical analysis

To build a dynamic model for the noise, the *Allan Variance* (AVAR) technique has been used [1].
It is based on splitting a dataset into clusters and computing the variance of the difference of mean values of adiacent clusters.
The AVAR and its square root, the Allan Devi-

ation (ADEV), are connected by the so-called *integral transformation* to the Power Spectral Density (PSD).
The considered noise dynamics has as input a white driving noise, as output the total noise and, as states, some *fundamental noises*:

- Angular Random Walk (ARW)
- Rate Random Walk (RRW)
- Bias instability
- Gauss-Markov noise
- Drift Rate Ramp noise

These noises provide a total PSD of the noise with five coefficients: N, K, T_B, Q_B and R.
A study on how the first four coefficients depend on the four factors has been done using a method from inference statistics, the Analysis of Variance (ANOVA) [3].
It is a method that inspects the variability *between* groups of data and the variability *within* each group; based on the so-called *null hypotheses*, it is the procedure to test them. If the mean squared errors between and within experimental treatments are good estimators of the variance of the stochastic error that is intrinsic in the data, called σ^2, the dependence of the studied quantity on the considered factor or interaction is not relevant.
ANOVA requires that the data follow a specific data model and that the stochastic errors in the data are normally distributed with null mean and variance σ^2; these assumption can be checked through the Normal Probability Plots of the residuals.
ANOVAs on AVAR coefficients put in evidence that:

- K mainly depends on the TAV, on the height and on their interaction;
- N is mainly influenced by the height, by the interaction between the YF and the light and by the interaction between the height and the TAV;
- T_B is not affected in a recurrent way by the factors;
- Q_B mainly depends on the height, on the TAV and on two interactions involving the light.

3. Model identification and Kalman prediction

Using as input the position estimates and as output the position errors, a *black-box model identification* process of the discrete-time error dynamics has been performed, using an algorithm called *MOESP-PO*, that is a *subspace* algorithm [2]. It starts, basically, from the *MOESP algorithm*, suitable in deterministic cases, that elaborates a projection of a data equation that contains Hankel matrices, uses this projection to recover a column space, constructs a basis for this column space and, in the end, estimates the matrices of the state-space representation through shift invariance and through the least-squares method.
The MOESP-PO algorithm is a generalization of the MOESP algorithm for stochastic cases, with process and measurement noise; in such case the projection procedure does not lead to an unbiased estimation. This problem is solved through the use of the so-called *Instrumental Variables* (IVs), splitting the dataset into two groups, one shifted ahead in time, and using the previous data as IVs for the subsequent data.
Sixteen models have been identified, all having A matrices similar to identity matrices and B and C matrices without specific trends.
In order to evaluate the performance of the models, two sets of one-step ahead *Kalman predictors* have been built, one using the complete position estimates and the other using only the vertical components. They have been evaluated through the inspection of mean values and standard deviations of prediction errors; the prediction errors have tended to be bigger with the height and TAV at higher level.
In the end, the study of the influence of the factors through the ANOVA has been done also on three characteristics of the models, analyzing also the mean variation of them when the factors change level:

- $\Delta\sigma_B^{max}$, the maximum excursion of the singular values of the matrices B, that mostly depends on the height (that makes it increase a lot), the TAV and the interaction between the TAV and the YF;
- σ_{G1}^{max}, σ_{G2}^{max}, σ_{G3}^{max}, the maximum values of the singular values of the frequency response matrices $G(j\omega)$, that are mainly influenced by the TAV and by the YF (that, when activated, makes σ_{G2}^{max}, σ_{G3}^{max} much smaller);
- The error in the position estimation in absolute value $e = \sqrt{y_x^2 + y_y^2 + y_z^2}$, that mainly

depends on the height, on the TAV and on the interaction between height and YF.

All these characteristics, in the end, have big increases when the TAV is raised to 0.6 rad/s.

4. Parametric modeling

The following, important part of the work has been the construction of parametric linear models for the coefficients K, N, T_B and Q_B on the Cartesian axes from the AVAR analysis, using the factors as independent variables and using the least-squares interpolation method.

In this case, in order to not neglect the influence of the YF, the only factor with qualitative levels, two separate procedures have been carried out, one with the data with the YF and another without it, bringing to a total of 24 models.

The used models have one, two or three independent variables, that have been chosen starting from the dependences put in evidence by the ANOVAs.

In the case without the YF all the variables have been used in an almost equal manner; in the case with the YF the light has come into play much less times and the coefficients T_B and Q_B have required less variables to be modeled than in the other case. In both cases, T_B and Q_B have more complex models than K and N.

In the end, the process of linear interpolation has been done also on the matrices A, B, C and K from the model identification process [4]. The choice of what terms to interpolate (the other terms have been considered as constant and equal to their mean value) has been done looking mainly to the difference of their mean values between the two TAV levels. It resulted that the C and K matrices were more influenced than the A and B matrices by the variation of the TAV.

5. Equations, Figures and Tables

5.1. Equations

Here there are some important equations and formulas used in the thesis.

Visual Odometry transformation

$$C_{t_i} = C_{t_{i-1}} T_i \begin{bmatrix} R_{i,i-1} & t_{i,i-1} \\ 0 & 1 \end{bmatrix} \tag{1}$$

Allan variance, with M clusters of data, each with mean value $\bar{y}_i$

$$\sigma^2(\tau) = \frac{1}{2(M-1)} \sum_{i=1}^{M-1} (\bar{y}_{i+1} - \bar{y}_i)^2 \tag{2}$$

Integral transformation, linking AVARs and PSDs, with $f = \frac{\omega}{2\pi}$

$$\sigma^2(\tau) = 4 \int_0^\infty S(f) \frac{\sin^4(\pi f \tau)}{(\pi f \tau)^2} df \tag{3}$$

Total noise PSD

$$S_{tot}(f) = N^2 + \left(\frac{K}{2\pi f}\right)^2 + \frac{Q_B}{\left(\frac{1}{T_B}\right)^2 + (2\pi f)^2} + \frac{R^2}{(2\pi f)^3} \tag{4}$$

ANOVA quantities

$$\bar{y}_i = \frac{\sum_{j=1}^{n} y_{ij}}{n} = \frac{y_i}{n} \tag{5}$$

$$\bar{y} = \frac{\sum_{i=1}^{a} \sum_{j=1}^{n} y_{ij}}{an} \tag{6}$$

ANOVA identity

$$\sum_{i=1}^{a} \sum_{j=1}^{n} (y_{ij} - \bar{y})^2 = n \sum_{i=1}^{a} (\bar{y}_i - \bar{y})^2 + \sum_{i=1}^{a} \sum_{j=1}^{n} (y_{ij} - \bar{y}_i)^2 \tag{7}$$

$$SS_T = SS_{Tr} + SS_E \tag{8}$$

ANOVA: data model in the single factor case, with μ overall mean effect, τ_i main effect of the i-th level of the factor and ϵ_{ij} random error component

$$y_{ij} = \mu + \tau_i + \epsilon_{ij} \begin{cases} i = 1, 2...a \\ j = 1, 2...n \end{cases} . \tag{9}$$

ANOVA: data model in the two factors case, with μ overall mean effect, τ_i effect of the i-th level of the first factor, β_j effect of the j-th level of the second factor, $(\tau\beta)_{ij}$ interaction of the two factors and ϵ_{ij} random error component

$$y_{ij} = \mu + \tau_i + \beta_j + (\tau\beta)_{ij} + \epsilon_{ij}, \tag{10}$$

ANOVA: bigger values of F mean a not negligible dependence

$$F = \frac{MS_{Tr}}{MS_E} = \frac{SS_{Tr}}{a-1}\frac{N-a}{SS_E} \tag{11}$$

ANOVA: null hypotheses in the single factor case

H_0: $\tau_1 = \tau_2 = ... = \tau_a = 0$
H_1: there is at least one $\tau_i \neq 0$

ANOVA: null hypotheses in the two factors case

H_0: $\tau_1 = \tau_2 = ... = \tau_a = 0$
H_1: there is at least one $\tau_i \neq 0$
H_0: $\beta_1 = \beta_2 = ... = \beta_b = 0$
H_1: there is at least one $\beta_i \neq 0$
H_0: $(\tau\beta)_{ij} = 0$ for all i, j
H_1: there is at least one $(\tau\beta)_{ij} \neq 0$

Structure of the identified discrete-time models, deterministic case

$$\begin{cases} x(t+1) = Ax(t) + Bu(t) \\ y(t) = Cx(t) \end{cases} \tag{12}$$

Structure of the identified discrete-time models, stochastic case

$$\begin{cases} x(t+1) = Ax(t) + Bu(t) + w(t) \\ y(t) = Cx(t) + v(t) \end{cases} \tag{13}$$

MOESP algorithm: data equation

$$Y_{tij} = \Gamma_i X_{t,j} + H_i U_{t,i,j}. \tag{14}$$

MOESP algorithm: orthogonal projection

$$U_{t,i,j}\Pi = 0 \tag{15}$$

$$\Pi = I - U_{t,i,j}^T (U_{t,i,j} U_{t,i,j}^T)^{-1} U_{t,i,j} \tag{16}$$

MOESP algorithm: A and C estimated through shift invariance

$$\Gamma_\uparrow A = \begin{bmatrix} C \\ CA \\ CA^2 \\ \vdots \\ CA^{i-2} \end{bmatrix} A = \begin{bmatrix} CA \\ CA^2 \\ CA^3 \\ \vdots \\ CA^{i-1} \end{bmatrix} = \Gamma_\downarrow. \tag{17}$$

MOESP algorithm: B and D estimated through LS method

$$B, D = \arg\min_{B,D} \sum_{k=0}^{s} [y(t) - \hat{y}(t)]^2 \tag{18}$$

$$\hat{y}(t) = Du(t) + \sum_{r=0}^{t-1} CA^{t-r-1} Bu(r) \tag{19}$$

MOESP-PO algorithm: Instrumental Variables (matrix Z)

$$rank(\lim_{N\to\infty} \frac{1}{N}(X_{t,j}\Pi)Z^T) = n \tag{20}$$

$$\lim_{N\to\infty} \frac{1}{N}(E_i W_{t,i,j} + V_{t,i,j})Z^T = 0 \tag{21}$$

MOESP-PO algorithm: modified data equation

$$Y_{t,i,j}\Pi Z^T = \Gamma X_{t,j}\Pi Z^T + (E_i W_{t,i,j} + V_{t,i,j})\Pi Z^T \tag{22}$$

Kalman predictor: general structure

$$\begin{cases} x_p(t+1) = A_p(t)x_p(t) + B_p(t)u_p(t) \\ y_p(t) = C_p(t)x_p(t), \end{cases} \tag{23}$$

Matrices of the complete Kalman predictor, built from 12, being K the gain matrix

$$A_p = A - KC \tag{24}$$

$$B_p = \begin{bmatrix} B & K \end{bmatrix} \tag{25}$$

$$C_{p1} = C \tag{26}$$

$$u_p = \begin{bmatrix} u & y, \end{bmatrix} \tag{27}$$

Matrices of the partial Kalman predictor, built from 12, being K the gain matrix

$$A_p = A_- \begin{bmatrix} K(1,3) \\ K(2,3) \\ K(3,3) \end{bmatrix} \begin{bmatrix} C(1,3) \\ C(2,3) \\ C(3,3) \end{bmatrix} \tag{28}$$

$$B_p = \begin{bmatrix} B & \begin{bmatrix} K(1,3) \\ K(2,3) \\ K(3,3) \end{bmatrix} \end{bmatrix} \tag{29}$$

$$C_p = C \tag{30}$$

$$u_p = \begin{bmatrix} u & \begin{bmatrix} y(1,3) \\ y(2,3) \\ y(3,3) \end{bmatrix} \end{bmatrix} \tag{31}$$

5.2. Figures

Here there are some figures, for illustrative purpose only; all the figures and plots that illustrate the results are retrievable in the main thesis document.

Analysis of Variance

Source	Sum Sq.	d.f.	Mean Sq.	F	Prob>F
Height	0.01572	1	0.01572	2.81	0.1547
TAV	0.02541	1	0.02541	4.54	0.0864
YF	0.00285	1	0.00285	0.51	0.5079
Light	0.00003	1	0.00003	0.01	0.9461
Height*TAV	0.00359	1	0.00359	0.64	0.4595
Height*YF	0.01632	1	0.01632	2.91	0.1486
Height*Light	0.00051	1	0.00051	0.09	0.774
TAV*YF	0.00493	1	0.00493	0.88	0.3911
TAV*Light	0.00046	1	0.00046	0.08	0.7857
YF*Light	0	1	0	0	0.9943
Error	0.02801	5	0.0056		
Total	0.09785	15			

Constrained (Type III) sums of squares.

Figure 1: A 2-ways ANOVA table (the one of the estimation error e)

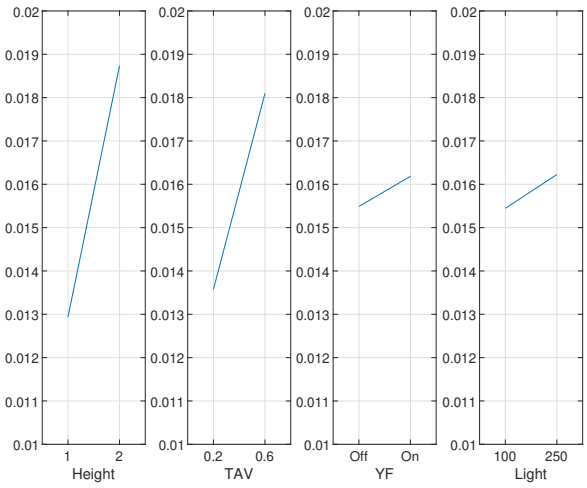

Figure 2: A plot of the main effects of the factors (on $\Delta\sigma_B^{max}$)

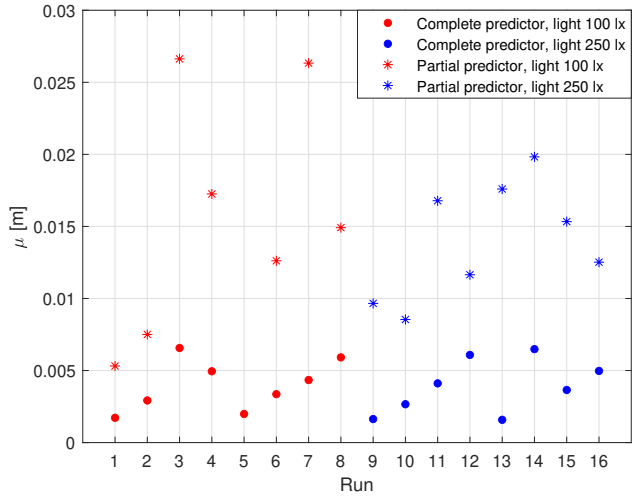

Figure 3: A comparison of the mean values of the prediction errors (with respect to the light)

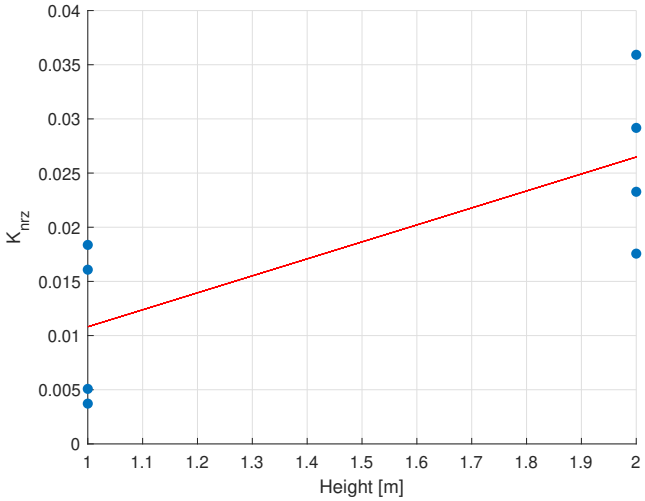

Figure 4: The plot of a parametric model with 1 variable (the one of K on z axis without YF

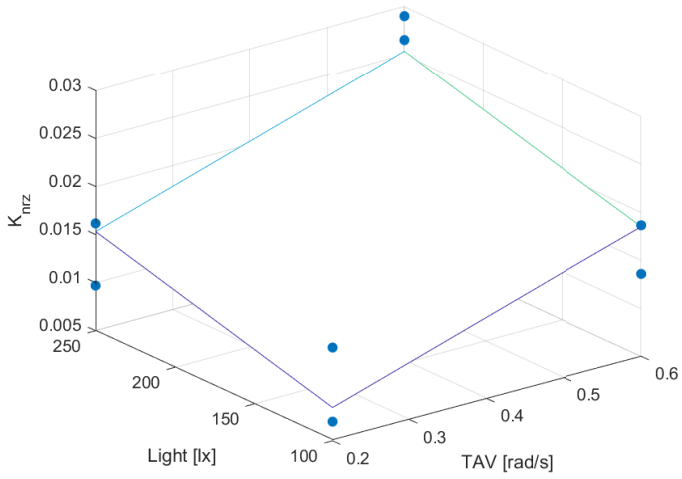

Figure 5: The plot of a parametric model with 2 variables (the one of K on z axis with YF

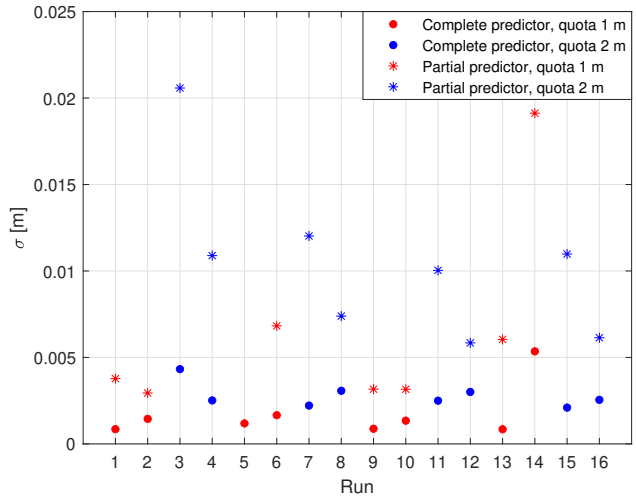

Figure 6: A comparison of the standard deviations of the prediction errors (with respect to the TAV)

5.3. Tables

Run number	Height	TAV	YF	Light
1	1 m	0.2 rad/s	No	100 lx
2	2 m	0.2 rad/s	No	100 lx
3	1 m	0.6 rad/s	No	100 lx
4	2 m	0.6 rad/s	No	100 lx
5	1 m	0.2 rad/s	Yes	100 lx
6	2 m	0.2 rad/s	Yes	100 lx
7	1 m	0.6 rad/s	Yes	100 lx
8	2 m	0.6 rad/s	Yes	100 lx
9	1 m	0.2 rad/s	No	250 lx
10	2 m	0.2 rad/s	No	250 lx
11	1 m	0.6 rad/s	No	250 lx
12	2 m	0.6 rad/s	No	250 lx
13	1 m	0.2 rad/s	Yes	250 lx
14	2 m	0.2 rad/s	Yes	250 lx
15	1 m	0.6 rad/s	Yes	250 lx
16	2 m	0.6 rad/s	Yes	250 lx

Table 1: List of the 16 experimental runs with their conditions

Number of factors	Equation
1	$y = a + bx$
2	$y = a + bx_1 + cx_2$
3	$y = a + bx_1 + cx_2 + dx_3$

Table 2: General forms of the parametric models for the AVAR coefficients

Coefficient	Axis	Height	TAV	Light
K	x		✓	
K	y		✓	✓
K	z		✓	✓
N	x	✓		✓
N	y	✓		✓
N	z			✓
T_B	x	✓	✓	✓
T_B	y	✓	✓	
T_B	z	✓	✓	✓
Q_B	x	✓	✓	
Q_B	y	✓	✓	✓
Q_B	z	✓	✓	✓

Table 3: Summary of the used independent variables for the AVAR coefficients without the YF

Coefficient	Axis	Height	TAV	Light
K	x	✓	✓	
K	y	✓	✓	
K	z	✓		
N	x	✓		
N	y	✓		
N	z		✓	✓
T_B	x		✓	✓
T_B	y	✓	✓	✓
T_B	z	✓		✓
Q_B	x		✓	
Q_B	y		✓	
Q_B	z	✓	✓	

Table 4: Summary of the used independent variables for the AVAR coefficients with the YF

6. Conclusions

In the end, the factors that appeared to be more important in affecting the studied characteristics of the VO dynamics were the height, the TAV and their interaction.
The light, instead, has not appeared to be very relevant
An important step of the process would have been a *validation* of the identification and modeling processes, with other data or with the cross-validation technique, not done only due to logistical issues.
In general, a better analysis can be carried out through a more complex experimental campaign and/or through the collection of a bigger amount of data.

7. Acknowledgements

My work is dedicated to everbody who has been near me in last years; as an Italian famous man that passed away some months ago said, *"Nessuno è al sicuro, da solo"*, that means "Nobody is safe when alone".

References

[1] F. Chiarlo. A statistical analysis of position estimation error in visual odometry. *School of Industrial and Information Engineering, Politecnico di Milano*, 2021.

[2] M. Lovera. Identification of MIMO linear models: introduction to subspace methods. *Dipartimento di Scienze e Tecnologie Aerospaziali, Politecnico di Milano*, 2021.

[3] D.C. Montgomery. *Design and Analysis of Experiments, Ninth Edition*. Wiley, 2017.

[4] Hecker S. and Pfifer H. Generation of optimal linear parametric models for lft-based robust stability analysis and control design. *IEEE Transactions on Control System Technology*, 2011.

Politecnico di Milano
School of Industrial and Information Engineering
Master of Science in Aeronautical Engineering

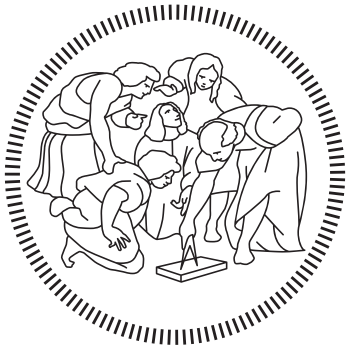

Model identification and statistical analysis in visual odometry on an UAV

Advisor: Prof. Marco LOVERA
Co-Advisor: Eng. Gabriele ROGGI

Thesis by:
Pietro GIANNAGOSTINO Matr. 952859

Academic Year 2021–2022

To everbody who spent even only one positive thought about me.

Acknowledgments

I started this amazing study path six years ago, knowing that it would have been very difficult but very challenging at the same time, and now I can say that I was right.

The fact that now all this is coming to an end is very difficult to believe but, at the same time, brings a lot of happiness and hope for the future.

I have obviously done my part, but goals are never achieved alone and there are a lot of people that have been important in these years; I will try to be general and, at the same time, to not leave anyone apart.

I want to thank my supervisors Professor Lovera and Engineer Roggi for the support, the availability, the patience and the courtesy shown towards me; they have made me interested in these topics and nothing in this work would have been possible without them.

This work and this fundamental milestone that I am reaching in my life are dedicated to my supervisors, to my family, to my parents, to all the colleagues I met in my study years, to my older and newer friends, to all people who believed in me, helped me and/or simply have been kind with me, even if they are no longer here; there are no words to say how grateful I am to who has been present for me.

I want to say to these people that, during the last years, some moments have been filled with happiness, jubilation and satisfaction, whereas in other moments there have been sadness, anxiety and bad thoughts: we shared all these moments and these emotions, all them would have not been the same without you and I hope that in our lives we will continue to be next to each other.

There is a thing I want to say some particular people, that I met in the classrooms of Politecnico di Milano and in the other places were I applied to my studies, and who has to understand will understand: the "construction sites" of our lives have allowed us to met, but I chose you as friends every day only because of the people we are.

I want to close and summarize my acknowledgments with a quote from an Italian pressman and politician who has prematurely passed away in January 2022, that I think to be extremely right:

"*Nessuno è al sicuro, da solo*", that in Italian means "*Nobody is safe when alone*".

Abstract

During the last years, the process of Visual Odometry (VO) has acquired a relevant importance in unmanned machines, such as robots and both ground and aerial vehicles, thanks mainly to the constant cost decrease and performance improvement in technologies.

VO can be used in sinergy with other tools in order to acquire a greater precision and has the advantage to be totally independent from external infrastructures and radio signals.

Few attempts, however, have been done to study the effects of environmental conditions on behavior and time accumulation of errors in VO systems.

The purpose of this thesis is to model the errors in the estimation of position in a VO system on a drone and to identify dependences on environmental conditions in the odometry process.

A campaign of experimental flights has been designed and carried out; the dynamics of the errors in the resulting data has been studied using both the Allan Variance (AVAR) technique and a model identification algorithm; Kalman predictors have been built in order to compare errors from the identified models with real errors.

The effects on experimental conditions on some relevant quantities have been studied using the Analysis of Variance (ANOVA) and some involved quantities have been parametrically modeled.

Sommario

Negli ultimi anni, il processo di odometria visuale ha acquisito una certa importanza nei macchinari, come robot e veicoli aerei e terrestri, principalmente grazie al costante abbassamento dei costi ed al costante miglioramento tecnologico.

L'odometria visuale può essere impiegata unitamente ad altri sistemi allo scopo di ottenere una precisione migliore ed ha il vantaggio di essere totalmente indipendente da infrastrutture e segnali in radiofrequenza esterni.

Pochi sono stati, tuttavia, i tentativi di studiare come le condizioni ambientali influiscano sul comportamento e sulla modalità di accumulazione nel tempo degli errori nei sistemi di odometria visuale.

Questa tesi è finalizzata a presentare un processo di modellazione degli errori di stima della posizione nel sistema di odometria visuale di un drone ed a individuare dipendenze dalle condizioni ambientali all'interno del processo di odometria.

È stata progettata e messa in opera una campagna di voli sperimentali del drone; la dinamica degli errori è stata analizzata a partire dai dati raccolti impiegando la tecnica delle Varianze di Allan ed un algoritmo per l'identificazione di modelli; sono stati costruiti dei predittori di Kalman per comparare gli errori calcolati con i modelli identificati e gli errori reali.

L'influenza delle condizioni sperimentali su alcune quantità di interesse è stata studiata mediante Analisi della Varianza; di alcune quantità coinvolte sono stati realizzati modelli parametrici.

Contents

Acknowledgments I

Abstract III

Sommario V

List of figures IX

List of tables XIII

Introduction 1

1 Visual odometry and experimental setup 3
- 1.1 What is Visual Odometry (VO) . . . 3
- 1.2 Design of experiments . . . 4
- 1.3 Experimental setup . . . 5
  - 1.3.1 UAV . . . 5
  - 1.3.2 Flying arena . . . 6
  - 1.3.3 VO system . . . 6
  - 1.3.4 Motion capture system . . . 6
  - 1.3.5 Reference frame . . . 7
  - 1.3.6 Trajectory . . . 7

2 Statistical analysis 9
- 2.1 Allan Variance . . . 9
  - 2.1.1 Definition . . . 9
  - 2.1.2 Fundamental noises . . . 10
- 2.2 Analysis of Variance (ANOVA) . . . 13
- 2.3 ANOVA on AVAR coefficients . . . 16
  - 2.3.1 Overview of the results . . . 29

3 Model identification and Kalman prediction 31
- 3.1 MOESP-PO black-box model identification . . . 31
- 3.2 Kalman predictors . . . 36

3.2.1 Definition 36
3.2.2 Application 39
3.3 ANOVA on model characteristics 50
3.3.1 Overview of the results 62

4 Parametric modeling **63**
4.1 Linear regression 63
4.2 Interpolations on AVAR coefficients 64
4.2.1 Data without yaw following 64
4.2.2 Data with yaw following 76
4.2.3 Overview of the results 89
4.3 Interpolations on matrices 90

Conclusions **93**

List of Figures

2.1 Table of the 1-way ANOVA of K along x axis 17
2.2 Table of the 2-ways ANOVA of K along x axis 17
2.3 Table of the 1-way ANOVA of K along x axis 18
2.4 Table of the 2-ways ANOVA of K along x axis 18
2.5 Table of the 1-way ANOVA of K along z axis 19
2.6 Table of the 2-ways ANOVA of K along z axis 19
2.7 Table of the 1-way ANOVA of N along x axis 20
2.8 Table of the 2-ways ANOVA of N along x axis 20
2.9 Table of the 1-way ANOVA of N along y axis 21
2.10 Table of the 2-ways ANOVA of N along y axis 21
2.11 Table of the 1-way ANOVA of N along z axis 22
2.12 Table of the 2-ways ANOVA of N along z axis 22
2.13 Table of the 1-way ANOVA of T_B along x axis 23
2.14 Table of the 2-ways ANOVA of T_B along x axis 23
2.15 Table of the 1-way ANOVA of T_B along y axis 24
2.16 Table of the 2-ways ANOVA of T_B along y axis 24
2.17 Table of the 1-way ANOVA of T_B along z axis 25
2.18 Table of the 2-ways ANOVA of T_B along z axis 25
2.19 Table of the 1-way ANOVA of Q_B along x axis 26
2.20 Table of the 2-ways ANOVA of Q_B along x axis 26
2.21 Table of the 1-way ANOVA of Q_B along y axis 27
2.22 Table of the 2-ways ANOVA of Q_B along y axis 27
2.23 Table of the 1-way ANOVA of Q_B along z axis 28
2.24 Table of the 2-ways ANOVA of Q_B along z axis 28

3.1 Mean values of the prediction error at the two different levels of the height 42
3.2 Standard deviations of the prediction error at the two different levels of the height 43
3.3 Mean values of the prediction error at the two different levels of the TAV 44
3.4 Standard deviations of the prediction error at the two different levels of the TAV 45

3.5 Mean values of the prediction error at the two different levels of the YF . . . 46
3.6 Standard deviations of the prediction error at the two different levels of the YF . . . 47
3.7 Mean values of the prediction error at the two different levels of the light . . . 48
3.8 Standard deviations of the prediction error at the two different levels of the light . . . 49
3.9 Normal Probability Plot of the residuals of the 2-ways ANOVA of $\Delta\sigma_B^{max}$ . . . 51
3.10 Table of the 2-ways ANOVA of $\Delta\sigma_B^{max}$ . . . 51
3.11 Mean variations of $\Delta\sigma_B^{max}$ between the levels of the factors . . . 52
3.12 Normal Probability of the residuals of the 1-way ANOVA of σ_{G1}^{max} 53
3.13 Normal Probability Plot of the residuals of the 2-ways ANOVA of σ_{G1}^{max} . . . 53
3.14 Table of the 1-way ANOVA of σ_{G1}^{max} . . . 54
3.15 Mean variations of σ_{G1}^{max} between the levels of the factors . . . 54
3.16 Normal Probability Plot of the residuals of the 1-way ANOVA of σ_{G2}^{max} . . . 55
3.17 Normal Probability Plot of the residuals of the 2-ways ANOVA of σ_{G2}^{max} . . . 55
3.18 Table of the 1-way ANOVA of σ_{G2}^{max} . . . 56
3.19 Table of the 2-ways ANOVA of σ_{G2}^{max} . . . 56
3.20 Mean variations of σ_{G2}^{max} between the levels of the factors . . . 57
3.21 Normal Probability Plot of the residuals of the 2-ways ANOVA of σ_{G3}^{max} . . . 58
3.22 Table of the 2-ways ANOVA of σ_{G3}^{max} . . . 58
3.23 Mean variations of σ_{G3}^{max} between the levels of the factors . . . 59
3.24 Normal Probability Plot of the residuals of the 1-way ANOVA of e 60
3.25 Normal Probability Plot of the residuals of the 2-ways ANOVA of e 60
3.26 Table of the 1-way ANOVA of e . . . 61
3.27 Table of the 2-ways ANOVA of e . . . 61
3.28 Mean variations of e between the levels of the factors . . . 62

4.1 1-way ANOVA of K on x axis without YF . . . 65
4.2 Plot of the model for K on x axis without YF . . . 65
4.3 1-way ANOVA of K on y axis without YF . . . 66
4.4 Plot of the model for K on y axis without YF . . . 66
4.5 1-way ANOVA of K on z axis without YF . . . 67
4.6 Plot of the model for K on z axis without YF . . . 67
4.7 1-way ANOVA of N on x axis without YF . . . 68
4.8 Plot of the model for N on x axis without YF . . . 68
4.9 1-way ANOVA of N on y axis without YF . . . 69

4.10 Plot of the model for N on y axis without YF 69
4.11 1-way ANOVA of N on z axis without YF 70
4.12 Plot of the model for N on z axis without YF 70
4.13 1-way ANOVA of T_B on x axis without YF 71
4.14 1-way ANOVA of T_B on y axis without YF 72
4.15 Plot of the model for T_B on y axis without YF 72
4.16 1-way ANOVA of T_B on z axis without YF 73
4.17 1-way ANOVA of Q_B on x axis without YF 74
4.18 Plot of the model for Q_B on x axis without YF 74
4.19 1-way ANOVA of Q_B on y axis without YF 75
4.20 1-way ANOVA of Q_B on z axis without YF 76
4.21 1-way ANOVA of K on x axis with YF 77
4.22 Plot of the model for K on x axis with YF 77
4.23 1-way ANOVA of K on y axis with YF 78
4.24 Plot of the model for K on y axis with YF 78
4.25 1-way ANOVA of K on z axis with YF 79
4.26 Plot of the model for K on z axis with YF 79
4.27 1-way ANOVA of N on x axis with YF 80
4.28 Plot of the model for N on x axis with YF 80
4.29 1-way ANOVA of N on y axis with YF 81
4.30 Plot of the model for N on y axis with YF 81
4.31 1-way ANOVA of N on z axis with YF 82
4.32 Plot of the model for N on z axis with YF 82
4.33 1-way ANOVA of T_B on x axis with YF 83
4.34 Plot of the model for T_B on x axis with YF 83
4.35 1-way ANOVA of T_B on y axis with YF 84
4.36 1-way ANOVA of T_B on z axis with YF 85
4.37 Plot of the model for T_B on z axis with YF 85
4.38 1-way ANOVA of Q_B on x axis with YF 86
4.39 Plot of the model for Q_B on x axis with YF 86
4.40 1-way ANOVA of Q_B on y axis with YF 87
4.41 Plot of the model for Q_B on y axis with YF 87
4.42 1-way ANOVA of Q_B on z axis with YF 88
4.43 Plot of the model for Q_B on z axis with YF 88

List of Tables

1.1 Runs and experimental conditions 5

4.1 General form of regression models 63
4.2 Summary of the used independent variables for AVAR coefficients without YF 89
4.3 Summary of the used independent variables for AVAR coefficients with YF 90

Introduction

This thesis is about Visual Odometry (VO), that is term used to identify all the procedures that allow to localize an object and/or to estimate its motion through the progressive comparison of images taken by one or more cameras placed on the object itself.

Used since 1980s, Visual Odometry has been extensively studied and has found an increasing number of application across years, both in the Aerospace field and in other areas of industrial engineering and both on Unmanned Ground Vehicles (UGVs) and on Unmanned Aerial Vehicles (UAVs), the latter commonly known as *drones*. It has been used both alone and in sinergy with other localization systems, such as satellite-based systems (for example the GPS) or Inertial Navigation Systems (INS), in order to improve the overall performance of the motion estimation. This has been possible because of the constant decrease in cost of electronic equipments.

Visual Odometry systems have been improved a lot in terms of speed and precision, but few attempts have been done to characterize the noise affecting their dynamics, to give state-space representation of such dynamics and to find out how the odometry process is affected by environmental conditions.

This thesis had as objective to do such a process. Using the factor-based design of experiments, an experimental campaign made of sixteen experiments with a flying drone, each one with a different setting of four experimental variables (factors), has been designed and carried out. The collected data have been about the position of the drone and the difference between the position detected by the Visual Odometry system, equipped with a Stereolabs ZED camera, and the position measurements coming from a Motion Capture (MOCAP) system.

From these data, an attempt to model and characterize the dynamics of the Visual Odometry system has been done using the statistical technique of the Allan variance (AVAR), that allows to build a state-space model of the dynamics of the noise based on some fundamental noises with some coefficients, and the MOESP-PO black-box model identification algorithm, that allows to go directly from the Visual Odometry position estimates to the estimation errors. In order to evaluate the ability of models to capture the evolution of the errors, two types of one-step ahead Kalman predictors have been built and a simple analysis, based on mean values and standard deviations, has been done on the prediction results.

The coefficients from the AVAR and some characteristics of the identified models have been treated with another statistical technique, the Analysis of Variance, known as the ANOVA, that basically determines if and how much a quantity is affected by a change in other quantities through the analysis of the variability between and within groups of data.

The last part of the work has been the creation of parametric models having as independent variables the factors and as dependent values the AVAR coefficients and the terms of the matrices in the state-space representations of the models and the predictors, using the least-squares regression method.

The thesis is organized in four Chapters:

- Chapter 1 starts with an overview on Visual Odometry, then the experimental setup (the drone, its Visual Odometry system and the flying environment) is introduced, the technique used to design the experimental campaign is presented and the sixteen experiments with different environmental conditions that have been performed are explained.

- Chapter 2 is mainly dedicated to the statistical analysis tools that have been used, the Allan variance and the Analysis of Variance (ANOVA). As regards the AVAR, some fundamental noises are described in terms of their Power Spectral Densities (PSDs) and of the AVAR-based approach. The results the ANOVA provided on the data from the AVAR-based analysis are also listed and commented.

- Chapter 3 contains the explanation of the MOESP-PO identification algorithm. Kalman predictors are then introduced, with a general overview, the procedure used to construct them in this work and a brief analysis of the prediction results. The last part contains, again, a statistical analysis with the ANOVA, done on some characteristics of the models.

- Chapter 4 is about the least-squares (LS) interpolation processes that have been carried out in order to parametrically model the AVAR coefficients and the state-space matrices, as functions of one or more factors.

Chapter 1

Visual odometry and experimental setup

This chapter presents a brief overview on Visual Odometry and introduces the experimental processes at the basis of this work.

1.1 What is Visual Odometry (VO)

The term *Visual Odometry* (acronym VO) has been introduced in 1996 and indicates the process of estimating the position of a body through the examination of the changes due to motion of pictures taken by cameras mounted on the body itself. It is called Monocular VO if the camera is one and Stereo VO if there is a stereoscopic camera [1] [2].

VO can be used as a complement or a substitute to other tools, such as wheel odometry (that is less accurate), inertial navigation systems (INU) and satellite positioning systems, such as GPS (that can be not always available). The first time VO has been used out of Earth has been in 2004 on Spirit and Opportunity Mars rovers.

VO computes the followed path incrementally. Let's consider two subsequent time instants, called t_{i-1} and t_i, and the camera poses $C_{t_{i-1}}$ and C_{t_i}; what here is called "pose" is, actually, the rigid transformation matrix from the fixed ground reference frame to the camera reference frame. Visual Odometry consists in finding, for each instant time, the transformation matrix T_i for which

$$C_{t_i} = C_{t_{i-1}} T_i \tag{1.1}$$

holds.

The structure of T_i is:

$$T_i = \begin{bmatrix} R_{i,i-1} & t_{i,i-1} \\ 0 & 1 \end{bmatrix} \tag{1.2}$$

There are many methods to estimate transformation matrices, mainly divided in Feature Based methods, that track how only some particular features of the images evolve in time, and Direct Methods, tracking the time evolution of all pixels.

1.2 Design of experiments

Design of experiments is the problem of defining appropriate input sequencies and experimental conditions for MIMO model identification [3], that is explained in Section 3.1.

The dynamic system needs to be excited in such a way that collected data contain sufficient information and, at the same time, respects operational constraints, imposed by safety and/or by system performance limits.

The data have also to be structured in a way so that they can be easily analyzed with statistical instruments. It is necessary to select some experimental conditions that are supposed to have an influence on the results; these variables are called *factors* and, usually, can assume a finite number of values, that are called *levels*. The variation in the response of the under-test system when the level of a factor is changed is called the *effect* of the factor.

Having identified the factors, it is necessary to decide which of them can be controlled during experimentation and have an effect being of interest for the purpose of the experiment; there can be the so-called *held-constant* factors, the ones whose effects are not of interest, and the so-called *allowed-to-vary* factors, that cannot be controlled by the experimenter.

To design the testing procedure in this case, the so-called *factorial design* has been used, in which all the possible levels of all the factors are taken into account.

When a single factor is modified, the consequence is called *main effect*. When the difference in response between two levels of a factor is not the same at all levels of the other factors, an *interaction* between factors is coming into play.

Factorial design of experiments has the advantages to avoid erroneous conclusions when interactions between factors are suspected to be present and to estimate the effect of each factor at several levels of the other factors, bringing results that can be applied to a wide range of experimental conditions.

In this case, the design has been done following a particular case of factorial design, the so-called 2^k design, that is used when the experiment has k factors, each one with two levels, that can be quantitative, such as two possible values of a physical quantity, or qualitative, for example an experimental feature that can be used or not. A complete execution of an experimental campaign designed in this way requires exactly 2^k experimental runs.

It has been decided to have $k = 4$ and to choose as relevant factors:

- *Height* [m]: two values of maximum height in the flight trajectory have been alternated during the runs;

- *Trajectory Angular Velocity (TAV)* [$\frac{rad}{s}$]: a part of the flight trajectory, following a circular path, has been covered with two different and alternated values of speed during the runs;
- *Yaw following* (YF): this is a logical variable, since the YF is a feature of the used drone that can be activated and de-activated. When the YF is activated, the attitude of the UAV is adjusted in order to have a defined body axis always parallel to the velocity vector;
- *Light* [lux]: the intensity of neon lamps in testing environment has been alternated between two values during the runs.

It is evident that height, TAV and light have quantitative levels, whereas YF has qualitative levels.

As described in detail in Table (1.1), sixteen experiments have been performed, each one characterized by different levels of these four factors.

Run number	Height	TAV	YF	Light
1	1 m	0.2 rad/s	No	100 lx
2	2 m	0.2 rad/s	No	100 lx
3	1 m	0.6 rad/s	No	100 lx
4	2 m	0.6 rad/s	No	100 lx
5	1 m	0.2 rad/s	Yes	100 lx
6	2 m	0.2 rad/s	Yes	100 lx
7	1 m	0.6 rad/s	Yes	100 lx
8	2 m	0.6 rad/s	Yes	100 lx
9	1 m	0.2 rad/s	No	250 lx
10	2 m	0.2 rad/s	No	250 lx
11	1 m	0.6 rad/s	No	250 lx
12	2 m	0.6 rad/s	No	250 lx
13	1 m	0.2 rad/s	Yes	250 lx
14	2 m	0.2 rad/s	Yes	250 lx
15	1 m	0.6 rad/s	Yes	250 lx
16	2 m	0.6 rad/s	Yes	250 lx

Table 1.1: Runs and experimental conditions

1.3 Experimental setup

1.3.1 UAV

The drone used to perform the experiments is called ROG-1 and has been designed by students and research fellows of Politecnico di Milano for the Leonardo Drone Contest, held in Turin, Italy. Its characteristics are [4] [5]:

- 4 rotors
- 8 plastic propellers
- 4 KDE2315XF-965 DC brushless motors
- Size: 50x50x35 cm
- Weight: 3.75 kg
- LiPo 16000 mAh rechargeable battery

1.3.2 Flying arena

All the experiments have been performed in the indoor flying arena of the ASCL (Aerospace System & Control Laboratory) of Politecnico di Milano. Its size is 12 x 6 x 4 m.

1.3.3 VO system

The images to perform the VO process have been taken by a Stereolabs ZED stereoscopic camera, that has been rigidly mounted on the UAV. It takes pictures and integrates the VO algorithm that processes the pictures and provides the data about the estimated position in Cartesian coordinates [4] [6].

The sampling frequencies of these data is around 15 Hz, that has been the value used for the computations related to the Allan variances (see Section 2.1), whereas when identifying models using the MOESP-PO algorithm (see Section 3.1), each experiment has been given a specific sampling frequency F_s, obtained in Equation (1.3):

$$F_s = \frac{n_s - 1}{T} \tag{1.3}$$

where T is the duration of the sampling period and n_s is the number of sampled data in the same period.

1.3.4 Motion capture system

In order to have a "ground truth" about the position of the drone to be compared with the results of the VO algorithm and to the identified models, the flying arena Motion Capture system, acronym MOCAP, has been used. The MOCAP consists of eight OptiTrack Prime 13 cameras, connected to a desktop computer equipped with the OptiTrack Motive Tracker software [4] [7].

1.3.5 Reference frame

Both the ZED odometer and the motion capture system use a reference frame centered in the point with coordinates (0,0,0) and with the x axis pointing East, the y axis pointing North and the z axis pointing upwards. The coordinates in these reference frame have the meter ([m]) as measurement unit.

1.3.6 Trajectory

The drone has been requested to follow this trajectory when flying:

- Take off from the reference frame origin
- Vertical climb to a fixed height z, reaching point (0,0,z)
- Movement on a straight line to point (0,1,z)
- Movement on a circular path centered in point (0,1,z), doing a precise number of circles at constant height, the last of which ending in point (0,1,z) again
- Movement on a straight line to point (0,0,z)
- Vertical descent and landing in point (0,0,0)

This is the setup used for all the previously mentioned sixteen experiment with four factors, each one with two levels.

Chapter 2

Statistical analysis

This chapter presents the most important statistical analysis tools used in this thesis, the Allan Variance and the Analysis of Variance, and an application of the second tool on the results from the first one.

2.1 Allan Variance

2.1.1 Definition

The Allan Variance (AVAR) is a mathematical tool first proposed by David Allan to study errors in atomic clocks; in this thesis it will be used in the time domain, as typically done when studying noises in rate gryos, despite its original use was in frequency domain [4] [8] .

Let's consider n values of the studied error y_i, with $i = 1, 2...n$, and split this vector into M clusters each containing τ values (with $\tau < \frac{n}{2}$), each with average value $\bar{y_i}$, with $i = 1...M$. The Allan variance is now defined as the variance of the random difference ξ between the averages of two adiacent clusters:

$$\xi_{i+1,i} = \bar{y}_{i+1} - \bar{y}_i. \tag{2.1}$$

Consequently, the AVAR expression turns out to be:

$$\sigma^2(\tau) = \frac{1}{2(M-1)} \sum_{i=1}^{M-1} (\xi_{i+1,i})^2. \tag{2.2}$$

Later on, the Allan Deviation (ADEV), defined as the square root of the AVAR, will be used.

Let's now define the Power Spectral Density (PSD) of a random process, that is a quantity representing the energy content of the process at various frequencies. The PSD $S_o(\omega)$ of a rational random process is the Fourier transform of its covariance. Being $H(j\omega)$ the frequency response of the transfer function of the

process $H(s)$ and $S_w(\omega)$ the PSD of a white noise, that is, by definition, constant, it holds that

$$S_o(\omega) = |H(j\omega)|^2 S_w(\omega). \tag{2.3}$$

The AVAR and the PSD of a process are linked by the integral transformation:

$$\sigma^2(\tau) = 4 \int_0^\infty S(f) \frac{\sin^4(\pi f \tau)}{(\pi f \tau)^2} df, \tag{2.4}$$

being

$$f = \frac{\omega}{2\pi}. \tag{2.5}$$

The integral transformation cannot be reversed in a unique way, so an AVAR can determine more than one PSD.

2.1.2 Fundamental noises

The modeling of the dynamics of the noise requires to build a noise model including some fundamental noise processes (for example noises with PSD described by a power law, such as $S(f) = \beta f^{-\alpha}$, with f frequency) with known PSDs and AVARs and to tune it in order to obtain an ADEV that is similar to the one found from experimental data.

The objective of this analysis is to construct a state-space model of the noise dynamics, as in (2.6):

$$\begin{cases} \dot{x}(t) = Ax(t) + Bu(t) \\ z(t) = Cx(t) + Dv(t), \end{cases} \tag{2.6}$$

Here x is a state vector containing the values of the fundamental noises, u is an input vector containing independent, white and Gaussian noises used as "driving" noises, z is the total noise and v is another white and Gaussian noise entering the total noise.

A, B and C have dimensions depending on how many fundamental noises are in use, whereas $D = 1$.

Fundamental noises used in this analysis are now listed.

- *White frequency noise* or *Angular Random Walk (ARW)*

  It is a noise characterized by constant PSD $S_{ARW} = N^2$.

  The ADEV is

$$\sigma_{ARW} = \frac{N}{\sqrt{\tau}}, \tag{2.7}$$

that has as logarithmic plot a straight line with slope -0.5. The state representation of ARW, being z_{ARW} its contribution to total noise z, is the one of a white Gaussian noise ω:

$$z(t) = z_{ARW}(t) = \omega(t). \tag{2.8}$$

- *Random walk frequency noise* or *Rate Random Walk (RRW).*

  It is a noise whose PSD $S_{RRW}(f)$ is a power law with exponent 2.

$$S_{RRW}(f) = \left(\frac{K}{2\pi f}\right)^2. \tag{2.9}$$

  The ADEV results to be

$$\sigma_{RRW} = K\sqrt{\frac{\tau}{3}}, \tag{2.10}$$

  that has as logarithmic plot a straight line with slope 0.5. Being z_{RRW} the contribution of RRW to total noise z and ω a white Gaussian noise, the state-space representation is

$$\begin{cases} \dot{z_{RRW}}(t) = \omega(t) \\ z(t) = z_{RRW}(t). \end{cases} \tag{2.11}$$

- *Bias instability.*

  It is a noise due to flickering of electronic components. Given a cut-off frequency f_0, its PSD is defined as follows:

$$S_B(f) = \begin{cases} \frac{B^2}{2\pi f} \text{ for } f < f_0 \\ 0 \text{ for } f > f_0. \end{cases} \tag{2.12}$$

  The ADEV of bias instability has the following expression:

$$\sigma_B(\tau) = \frac{2B^2}{\pi}[ln2 - \frac{\sin^3 x}{2x^2}(\sin x + 4x\cos x) + C_i(2x) - C_i(4x)], \tag{2.13}$$

  where $x = \pi f_0 \tau$ and C_i is the cosine integral function:

$$C_i(x) = -\int_x^{+\infty} \frac{cos(t)}{t} dt. \tag{2.14}$$

Bias instability has a problem: since its PSD is an odd function of frequency, it cannot be factored into a rational transfer function in order to provide a state-space representation. This can be avoided approximating bias instability with Gauss-Markov noise.

- *Gauss-Markov noise (GM)*

  Being z_B the approximation of the bias instability noise's contribution to the total noise z and ω_b a white Gaussian noise with PSD $S(\omega_b) = Q_B$, a Gauss-Markov process is state-space represented as in (2.15):

$$\begin{cases} \dot{z_B}(t) = -\frac{1}{T_B} z_B + \omega_B \\ z(t) = z_B(t). \end{cases} \tag{2.15}$$

  The PSD of the GM process is

$$S_{GM}(f) = \frac{Q_B}{\left(\frac{1}{T_B}\right)^2 + (2\pi f)^2}, \tag{2.16}$$

  and, consequently, the ADEV is:

$$\sigma(\tau) = T_B \left[\frac{Q_B}{\tau} \left(1 - \frac{T_B}{2\tau} (3 - 4e^{-\frac{\tau}{T_B}} + e^{\frac{-2\tau}{T_B}}) \right) \right]^{0.5}. \tag{2.17}$$

- *Drift Rate Ramp noise (R)*

  It is a noise presenting the same PSD and the same ADEV of another noise, the frequency modulated (FM) flicker walk, that has, however, different nature: the FM is an ideal noise, whereas the Rate Ramp noise results from deterministic errors. The PSD of these two noises is a power law with esponent 3:

$$S_R(f) = \frac{R^2}{(2\pi f)^3}. \tag{2.18}$$

In the end, these fundamental noise components are characterized by some coefficients that will be useful for the next steps of this analysis: N, K, T_B, Q_B and R.

The PSD of the total noise is shown in Equation (2.19):

$$S_{tot}(f) = N^2 + \left(\frac{K}{2\pi f}\right)^2 + \frac{Q_B}{\left(\frac{1}{T_B}\right)^2 + (2\pi f)^2} + \frac{R^2}{(2\pi f)^3}. \tag{2.19}$$

2.2 Analysis of Variance (ANOVA)

Analysis of Variance, acronym ANOVA, is a method from inference statistics used to understand variability inside groups of data depending on some factors. It has been developed by Ronald Fisher [9].

ANOVA is extremely useful to determine whether and which factors, through their main effects and their interactions, do or do not play a significant role in determining experimental outcomes.

To understand what ANOVA is, let's follow the approach of [3]. Imagine to have a single factor having a possible levels, to do n experimental observations and to consider the observed value of the quantity of interest as a random variable. This defines the so-called *single-factor* ANOVA.

It is necessary to define a model for the observed data, as in Equation (2.20):

$$y_{ij} = \mu + \tau_i + \epsilon_{ij} \begin{cases} i = 1, 2...a \\ j = 1, 2...n \end{cases} . \tag{2.20}$$

Here μ is a parameter called *overall mean effect*, τ_i identifies the main effect of the i-th level of the factor and ϵ_{ij} is a random error component. Let's indicate the variance of the errors of this model with σ^2.

ANOVA can apply to two different situations. When levels under examination are specifically chosen by the experimenter, conclusions can't be extended to not directly considered levels: this situation is called *fixed effects* model. When the considered levels are a random sample taken within a large number of levels, it is not so important knowing the particular ones investigated, so τ_i is random: this is the so-called *random effect* model.

Let's call

$$\bar{y_i} = \frac{\sum_{j=1}^{n} y_{ij}}{n} = \frac{y_i}{n} \tag{2.21}$$

the average of the observations under the i-th level and

$$\bar{y} = \frac{\sum_{i=1}^{a} \sum_{j=1}^{n} y_{ij}}{an} \tag{2.22}$$

the overall average of the observations.

It is necessary to test the equality of all treatments, that translates in the following hypotheses about main effects:

H_0: $\tau_1 = \tau_2 = ... = \tau_a = 0$
H_1: there is at least one $\tau_i \neq 0$

H_0 is the so-called *null hypothesis* and the ANOVA is the procedure to test it.

A measure of the variability of the data can be the *total sum of squares* (SS_T):

$$SS_T = \sum_{i=1}^{a}\sum_{j=1}^{n}(y_{ij} - \bar{y})^2. \tag{2.23}$$

Note that

$$\sum_{i=1}^{a}\sum_{j=1}^{n}(y_{ij} - \bar{y})^2 = n\sum_{i=1}^{a}(\bar{y_i} - \bar{y})^2 + \sum_{i=1}^{a}\sum_{j=1}^{n}(y_{ij} - \bar{y_i})^2 + 2\sum_{i=1}^{a}\sum_{j=1}^{n}(\bar{y_i} - \bar{y})(y_{ij} - \bar{y}), \tag{2.24}$$

where, however, the last term is zero, because

$$\sum_{j=1}^{n}(y_{ij} - \bar{y_i}) = y_i - n\bar{y_i} = 0, \tag{2.25}$$

so (2.24) turns into (2.26):

$$\sum_{i=1}^{a}\sum_{j=1}^{n}(y_{ij} - \bar{y})^2 = n\sum_{i=1}^{a}(\bar{y_i} - \bar{y})^2 + \sum_{i=1}^{a}\sum_{j=1}^{n}(y_{ij} - \bar{y_i})^2, \tag{2.26}$$

that is the so-called *ANOVA identity*. It tells that the total variability in the data (measured by SS_T) can be partitioned into a sum of squares of the differences *between* the treatment averages and the total average, from now on SS_{Tr}, plus a sum of squares of the differences of data *within* treatments from the treatment average, from now on SS_E, that can be due only to the random error.

Equation (2.26) can be symbolically written as in (2.27):

$$SS_T = SS_{Tr} + SS_E. \tag{2.27}$$

Having a levels of the factor and $an = N$ total observations, SS_T has $N - 1$ degrees of freedom, SS_{Tr} has $a - 1$ degrees of freedom; since each level provides $n - 1$ degrees of freedom, it results that the error has $a(n - 1) = N - a$ degrees of freedom.

Let's now introduce *mean squares* between and within treatments:

$$MS_{Tr} = \frac{SS_{Tr}}{a - 1}; \tag{2.28}$$

$$MS_E = \frac{SS_E}{N - a}. \tag{2.29}$$

If all the null hypotheses are satisfied, both MS_{Tr} and MS_E have to be good estimators of the variance of the model errors σ^2. Consequently, it is necessary to inspect a parameter called F, defined as in (2.30):

$$F = \frac{MS_{Tr}}{MS_E}. \tag{2.30}$$

When F assumes a large value, it means that the null hypotheses are not valid and the dependence of the under-study quantity on that factor is relevant and cannot be neglected. High values of F correspond to low values of the so-called p-value, that represents the probability of experimental outcomes verifying H_0.

In this analysis, it has been necessary to use a different version of the ANOVA, that is useful for experiments with more than one factor and keeps into account also interactions between factors. In a case considering two factors and their interaction, the model of the observed data becomes

$$y_{ij} = \mu + \tau_i + \beta_j + (\tau\beta)_{ij} + \epsilon_{ij}, \tag{2.31}$$

with μ overall mean effect, τ_i effect of the i-th level of the first factor, β_j effect of the j-th level of the second factor and $(\tau\beta)_{ij}$ interaction of the two factors.

The hypotheses regarding main effects become

H_0: $\tau_1 = \tau_2 = ... = \tau_a = 0$
H_1: there is at least one $\tau_i \neq 0$

and

H_0: $\beta_1 = \beta_2 = ... = \beta_b = 0$
H_1: there is at least one $\beta_i \neq 0$

and it is necessary to add hypotheses about the interaction:

H_0: $(\tau\beta)_{ij} = 0$ for all i, j
H_1: there is at least one $(\tau\beta)_{ij} \neq 0$

Data models can be further extended adding other main effects, as many as the factors to keep into account, and other interactions, containing even more than two factors.

What has been previously explained can be generalized to these other versions of the ANOVA and the conclusions are exactly equal, with the parameter F that has the same role even with the interactions.

The *1-way ANOVA* does not keep into account the interactions, the *x-way ANOVA* keeps into account interactions of up to x factors.

All this analysis, however, is valid if and only if data follow the assumed data model and the errors are normally and independently distributed with zero mean and constant variance σ^2. These assumptions have to be checked looking at the Normal Probability Plot of the residuals of the ANOVA, where data lie on an approximately straight line if they are normally distributed.

When the ANOVA has been used in this work, all the necessary computations have been done using the automatic *anovan* tool in MATLAB ®[10], that allows the user to choose between 1-way or 2-ways data model, produces the so-called

ANOVA table containing all values of the sum squares, the mean squares, the F parameters and the p-values and computes the residuals to obtain the Normal Probability Plots.

2.3 ANOVA on AVAR coefficients

In Section (2.1), coefficients N, K, T_B, Q_B and R have been introduced in order to describe the AVARs and the ADEVs of some important noises. Two models of the total noise have been built, one without the Drift Rate Ramp noise, bringing to not consider the R coefficient, and one with it. It is evident that the dependence of these coefficients on experimental conditions can and has to be studied. For each coefficient the study has been conducted on all the three axes of the reference frame and using both ANOVAs with one and two ways.

It has been decided, for the sake of simplicity, to consider only the model without the Rate Ramp noise, that does not include the R coefficient, and to report both the 1-way and the 2-ways ANOVAs. In the analysis done for each coefficient, the most relevant factors and interactions are listed from the most relevant one to the less relevant one.

Coefficient: K
Cartesian axis: x

Analysis of Variance

Source	Sum Sq.	d.f.	Mean Sq.	F	Prob>F
Height	0.0004	1	0.0004	6.41	0.0279
TAV	0.00189	1	0.00189	30.48	0.0002
YF	0.00009	1	0.00009	1.52	0.2432
Light	0	1	0	0.05	0.8274
Error	0.00068	11	0.00006		
Total	0.00307	15			

Constrained (Type III) sums of squares.

Figure 2.1: Table of the 1-way ANOVA of K along x axis

Analysis of Variance

Source	Sum Sq.	d.f.	Mean Sq.	F	Prob>F
Height	0.0004	1	0.0004	13.91	0.0136
TAV	0.00189	1	0.00189	66.1	0.0005
YF	0.00009	1	0.00009	3.3	0.129
Light	0	1	0	0.11	0.7557
Height*TAV	0.00017	1	0.00017	6.06	0.0571
Height*YF	0.0001	1	0.0001	3.44	0.123
Height*Light	0.00002	1	0.00002	0.82	0.4068
TAV*YF	0.00007	1	0.00007	2.5	0.1744
TAV*Light	0.00001	1	0.00001	0.52	0.5016
YF*Light	0.00016	1	0.00016	5.51	0.0657
Error	0.00014	5	0.00003		
Total	0.00307	15			

Constrained (Type III) sums of squares.

Figure 2.2: Table of the 2-ways ANOVA of K along x axis

The most relevant variables here are the TAV, the height, the interaction between height and TAV and the interaction between YF and light.

Coefficient: K
Cartesian axis: y

Analysis of Variance

Source	Sum Sq.	d.f.	Mean Sq.	F	Prob>F
Height	0.00057	1	0.00057	11.8	0.0056
TAV	0.0018	1	0.0018	37.47	0.0001
YF	0.00001	1	0.00001	0.25	0.6249
Light	0.00004	1	0.00004	0.8	0.3905
Error	0.00053	11	0.00005		
Total	0.00295	15			

Constrained (Type III) sums of squares.

Figure 2.3: Table of the 1-way ANOVA of K along x axis

Analysis of Variance

Source	Sum Sq.	d.f.	Mean Sq.	F	Prob>F
Height	0.00057	1	0.00057	32.08	0.0024
TAV	0.0018	1	0.0018	101.85	0.0002
YF	0.00001	1	0.00001	0.69	0.4448
Light	0.00004	1	0.00004	2.17	0.2005
Height*TAV	0.00012	1	0.00012	7.04	0.0452
Height*YF	0.00006	1	0.00006	3.41	0.1243
Height*Light	0.00003	1	0.00003	1.71	0.2477
TAV*YF	0.00008	1	0.00008	4.48	0.088
TAV*Light	0.00002	1	0.00002	1.26	0.3129
YF*Light	0.00012	1	0.00012	7.01	0.0456
Error	0.00009	5	0.00002		
Total	0.00295	15			

Constrained (Type III) sums of squares.

Figure 2.4: Table of the 2-ways ANOVA of K along x axis

Here the most important elements in the dependence are the TAV, the height and the following interactions: height $\times$ TAV, YF $\times$ light, TAV $\times$ YF.

Coefficient: K
Cartesian axis: z

Analysis of Variance

Source	Sum Sq.	d.f.	Mean Sq.	F	Prob>F
Height	0.0003	1	0.0003	5.64	0.0369
TAV	0.00026	1	0.00026	4.91	0.0486
YF	0.00001	1	0.00001	0.23	0.6418
Light	0.0001	1	0.0001	1.95	0.1898
Error	0.00059	11	0.00005		
Total	0.00126	15			

Constrained (Type III) sums of squares.

Figure 2.5: Table of the 1-way ANOVA of K along z axis

Analysis of Variance

Source	Sum Sq.	d.f.	Mean Sq.	F	Prob>F
Height	0.0003	1	0.0003	7.3	0.0427
TAV	0.00026	1	0.00026	6.37	0.053
YF	0.00001	1	0.00001	0.3	0.6096
Light	0.0001	1	0.0001	2.53	0.1726
Height*TAV	0.00015	1	0.00015	3.56	0.118
Height*YF	0.0002	1	0.0002	4.77	0.0807
Height*Light	0.00001	1	0.00001	0.25	0.6367
TAV*YF	0.00002	1	0.00002	0.37	0.5721
TAV*Light	0	1	0	0	0.9555
YF*Light	0.00001	1	0.00001	0.3	0.6078
Error	0.00021	5	0.00004		
Total	0.00126	15			

Constrained (Type III) sums of squares.

Figure 2.6: Table of the 2-ways ANOVA of K along z axis

The K coefficient on the z axis is mostly influenced by the height, the TAV, the interaction between height and YF, the interaction between height and TAV and, in the end, the light.

Coefficient: N
Cartesian axis: x

Analysis of Variance

Source	Sum Sq.	d.f.	Mean Sq.	F	Prob>F
Height	3.67473e-07	1	3.67473e-07	5.52	0.0385
TAV	7.45201e-08	1	7.45201e-08	1.12	0.3126
YF	4.13807e-09	1	4.13807e-09	0.06	0.8076
Light	1.1793e-08	1	1.1793e-08	0.18	0.6818
Error	7.31729e-07	11	6.65208e-08		
Total	1.18965e-06	15			

Constrained (Type III) sums of squares.

Figure 2.7: Table of the 1-way ANOVA of N along x axis

Analysis of Variance

Source	Sum Sq.	d.f.	Mean Sq.	F	Prob>F
Height	3.67473e-07	1	3.67473e-07	4.29	0.0932
TAV	7.45201e-08	1	7.45201e-08	0.87	0.394
YF	4.13807e-09	1	4.13807e-09	0.05	0.8348
Light	1.1793e-08	1	1.1793e-08	0.14	0.7259
Height*TAV	1.03816e-07	1	1.03816e-07	1.21	0.3213
Height*YF	9.08847e-09	1	9.08847e-09	0.11	0.7579
Height*Light	1.70155e-08	1	1.70155e-08	0.2	0.6746
TAV*YF	1.28856e-09	1	1.28856e-09	0.02	0.9072
TAV*Light	5.30887e-10	1	5.30887e-10	0.01	0.9403
YF*Light	1.71322e-07	1	1.71322e-07	2	0.2166
Error	4.28667e-07	5	8.57334e-08		
Total	1.18965e-06	15			

Constrained (Type III) sums of squares.

Figure 2.8: Table of the 2-ways ANOVA of N along x axis

The N coefficient on x axis mostly depends on the height, the interaction between the YF and the light, the interaction between the height and the TAV and the TAV alone.

Coefficient: N
Cartesian axis: y

Analysis of Variance

Source	Sum Sq.	d.f.	Mean Sq.	F	Prob>F
Height	5.92012e-07	1	5.92012e-07	7.33	0.0204
TAV	9.43506e-08	1	9.43506e-08	1.17	0.3028
YF	1.1727e-09	1	1.1727e-09	0.01	0.9062
Light	4.41981e-08	1	4.41981e-08	0.55	0.4748
Error	8.8804e-07	11	8.07309e-08		
Total	1.61977e-06	15			

Constrained (Type III) sums of squares.

Figure 2.9: Table of the 1-way ANOVA of N along y axis

Analysis of Variance

Source	Sum Sq.	d.f.	Mean Sq.	F	Prob>F
Height	5.92012e-07	1	5.92012e-07	7.67	0.0394
TAV	9.43506e-08	1	9.43506e-08	1.22	0.3192
YF	1.1727e-09	1	1.1727e-09	0.02	0.9067
Light	4.41981e-08	1	4.41981e-08	0.57	0.4833
Height*TAV	1.66349e-07	1	1.66349e-07	2.16	0.202
Height*YF	1.35724e-08	1	1.35724e-08	0.18	0.6923
Height*Light	8.62019e-08	1	8.62019e-08	1.12	0.3389
TAV*YF	1.8142e-09	1	1.8142e-09	0.02	0.8841
TAV*Light	2.60619e-08	1	2.60619e-08	0.34	0.5863
YF*Light	2.0825e-07	1	2.0825e-07	2.7	0.1613
Error	3.85791e-07	5	7.71583e-08		
Total	1.61977e-06	15			

Constrained (Type III) sums of squares.

Figure 2.10: Table of the 2-ways ANOVA of N along y axis

In this case the most relevant factors are the height, the YF $\times$ light interaction, the height $\times$ TAV interaction and the TAV alone.

Coefficient: N
Cartesian axis: z

Analysis of Variance

Source	Sum Sq.	d.f.	Mean Sq.	F	Prob>F
Height	7.30391e-11	1	7.30391e-11	0.19	0.674
TAV	3.8653e-10	1	3.8653e-10	0.99	0.3415
YF	2.9574e-10	1	2.9574e-10	0.76	0.4031
Light	1.52625e-09	1	1.52625e-09	3.9	0.0738
Error	4.30229e-09	11	3.91117e-10		
Total	6.58385e-09	15			

Constrained (Type III) sums of squares.

Figure 2.11: Table of the 1-way ANOVA of N along z axis

Analysis of Variance

Source	Sum Sq.	d.f.	Mean Sq.	F	Prob>F
Height	7.30391e-11	1	7.30391e-11	0.15	0.7106
TAV	3.8653e-10	1	3.8653e-10	0.82	0.4075
YF	2.9574e-10	1	2.9574e-10	0.63	0.465
Light	1.52625e-09	1	1.52625e-09	3.23	0.1324
Height*TAV	1.09278e-09	1	1.09278e-09	2.31	0.189
Height*YF	2.52223e-13	1	2.52223e-13	0	0.9825
Height*Light	4.95636e-10	1	4.95636e-10	1.05	0.353
TAV*YF	2.82852e-13	1	2.82852e-13	0	0.9814
TAV*Light	2.39444e-10	1	2.39444e-10	0.51	0.5086
YF*Light	1.08336e-10	1	1.08336e-10	0.23	0.6525
Error	2.36555e-09	5	4.73111e-10		
Total	6.58385e-09	15			

Constrained (Type III) sums of squares.

Figure 2.12: Table of the 2-ways ANOVA of N along z axis

The N coefficient on the z axis mostly depends on the light, the interaction between height and TAV, the interaction between height and light and the TAV.

Coefficient: T_B
Cartesian axis: x

Analysis of Variance

Source	Sum Sq.	d.f.	Mean Sq.	F	Prob>F
Height	2722.9	1	2722.89	1.48	0.2493
TAV	5835.5	1	5835.54	3.17	0.1025
YF	168.9	1	168.88	0.09	0.7676
Light	5240.2	1	5240.23	2.85	0.1196
Error	20241	11	1840.09		
Total	34208.5	15			

Constrained (Type III) sums of squares.

Figure 2.13: Table of the 1-way ANOVA of T_B along x axis

Analysis of Variance

Source	Sum Sq.	d.f.	Mean Sq.	F	Prob>F
Height	2722.9	1	2722.89	1.55	0.2684
TAV	5835.5	1	5835.54	3.32	0.128
YF	168.9	1	168.88	0.1	0.7691
Light	5240.2	1	5240.23	2.98	0.1448
Height*TAV	3148.6	1	3148.61	1.79	0.2383
Height*YF	4410.7	1	4410.67	2.51	0.174
Height*Light	350.6	1	350.65	0.2	0.6738
TAV*YF	16.3	1	16.35	0.01	0.9269
TAV*Light	3527	1	3526.99	2.01	0.2157
YF*Light	1.5	1	1.45	0	0.9782
Error	8786.2	5	1757.25		
Total	34208.5	15			

Constrained (Type III) sums of squares.

Figure 2.14: Table of the 2-ways ANOVA of T_B along x axis

Here the most important dependences are on the TAV, the light, the height $\times$ YF interaction, the TAV $\times$ light interaction and the height.

Coefficient: T_B
Cartesian axis: y

Analysis of Variance

Source	Sum Sq.	d.f.	Mean Sq.	F	Prob>F
Height	3226.3	1	3226.3	0.35	0.5652
TAV	12552.6	1	12552.6	1.37	0.2669
YF	2253.4	1	2253.4	0.25	0.63
Light	8786.1	1	8786.1	0.96	0.3489
Error	100941.3	11	9176.5		
Total	127759.7	15			

Constrained (Type III) sums of squares.

Figure 2.15: Table of the 1-way ANOVA of T_B along y axis

Analysis of Variance

Source	Sum Sq.	d.f.	Mean Sq.	F	Prob>F
Height	3226.3	1	3226.3	0.29	0.6105
TAV	12552.6	1	12552.6	1.15	0.3332
YF	2253.4	1	2253.4	0.21	0.6691
Light	8786.1	1	8786.1	0.8	0.4114
Height*TAV	6052.7	1	6052.7	0.55	0.4906
Height*YF	16612.9	1	16612.9	1.52	0.2728
Height*Light	6156.2	1	6156.2	0.56	0.4871
TAV*YF	804.4	1	804.4	0.07	0.7972
TAV*Light	4219.7	1	4219.7	0.39	0.5619
YF*Light	12357.9	1	12357.9	1.13	0.3366
Error	54737.6	5	10947.5		
Total	127759.7	15			

Constrained (Type III) sums of squares.

Figure 2.16: Table of the 2-ways ANOVA of T_B along y axis

The T_B time on the y axis mainly depends on the interaction between the height and the YF, on the TAV, on the interaction between the YF and the light and on the light alone.

Coefficient: T_B
Cartesian axis: z

Analysis of Variance

Source	Sum Sq.	d.f.	Mean Sq.	F	Prob>F
Height	17542.9	1	17542.9	0.9	0.3622
TAV	17432.7	1	17432.7	0.9	0.3637
YF	22613.5	1	22613.5	1.16	0.3036
Light	13140.8	1	13140.8	0.68	0.4281
Error	213539	11	19412.6		
Total	284268.8	15			

Constrained (Type III) sums of squares.

Figure 2.17: Table of the 1-way ANOVA of T_B along z axis

Analysis of Variance

Source	Sum Sq.	d.f.	Mean Sq.	F	Prob>F
Height	17542.9	1	17542.9	1.01	0.3607
TAV	17432.7	1	17432.7	1.01	0.3621
YF	22613.5	1	22613.5	1.3	0.3052
Light	13140.8	1	13140.8	0.76	0.4239
Height*TAV	21888.3	1	21888.3	1.26	0.3123
Height*YF	23456.6	1	23456.6	1.35	0.2973
Height*Light	23857.9	1	23857.9	1.38	0.2937
TAV*YF	15263.2	1	15263.2	0.88	0.3913
TAV*Light	22864.1	1	22864.1	1.32	0.3029
YF*Light	19487.8	1	19487.8	1.12	0.3376
Error	86721.2	5	17344.2		
Total	284268.8	15			

Constrained (Type III) sums of squares.

Figure 2.18: Table of the 2-ways ANOVA of T_B along z axis

In this case the most important factors and interactions are the height $\times$ light interaction, the height $\times$ YF interaction, the TAV $\times$ light interaction and, in the end, the YF.

Coefficient: Q_B
Cartesian axis: x

Analysis of Variance

Source	Sum Sq.	d.f.	Mean Sq.	F	Prob>F
Height	2.7037e-11	1	2.7037e-11	0.06	0.807
TAV	7.98651e-10	1	7.98651e-10	1.85	0.201
YF	1.61527e-10	1	1.61527e-10	0.37	0.5532
Light	2.06053e-10	1	2.06053e-10	0.48	0.504
Error	4.7486e-09	11	4.3169e-10		
Total	5.94186e-09	15			

Constrained (Type III) sums of squares.

Figure 2.19: Table of the 1-way ANOVA of Q_B along x axis

Analysis of Variance

Source	Sum Sq.	d.f.	Mean Sq.	F	Prob>F
Height	2.7037e-11	1	2.7037e-11	0.05	0.8261
TAV	7.98651e-10	1	7.98651e-10	1.58	0.264
YF	1.61527e-10	1	1.61527e-10	0.32	0.596
Light	2.06053e-10	1	2.06053e-10	0.41	0.551
Height*TAV	4.55098e-10	1	4.55098e-10	0.9	0.3859
Height*YF	2.60699e-10	1	2.60699e-10	0.52	0.5045
Height*Light	2.52713e-10	1	2.52713e-10	0.5	0.5108
TAV*YF	5.97971e-11	1	5.97971e-11	0.12	0.7447
TAV*Light	1.1944e-09	1	1.1944e-09	2.37	0.1846
YF*Light	2.3302e-12	1	2.3302e-12	0	0.9485
Error	2.52356e-09	5	5.04711e-10		
Total	5.94186e-09	15			

Constrained (Type III) sums of squares.

Figure 2.20: Table of the 2-ways ANOVA of Q_B along x axis

The Q_B coefficient on the x axis mainly depends on the interaction between TAV and light, on the TAV itself, on the interaction between height and YF and on the interaction between height and light.

Coefficient: Q_B
Cartesian axis: y

Analysis of Variance

Source	Sum Sq.	d.f.	Mean Sq.	F	Prob>F
Height	8.36111e-12	1	8.36111e-12	0.07	0.7968
TAV	2.43101e-11	1	2.43101e-11	0.2	0.6615
YF	8.39965e-11	1	8.39965e-11	0.7	0.4207
Light	7.82613e-11	1	7.82613e-11	0.65	0.4366
Error	1.32089e-09	11	1.20081e-10		
Total	1.51582e-09	15			

Constrained (Type III) sums of squares.

Figure 2.21: Table of the 1-way ANOVA of Q_B along y axis

Analysis of Variance

Source	Sum Sq.	d.f.	Mean Sq.	F	Prob>F
Height	8.36111e-12	1	8.36111e-12	0.09	0.7754
TAV	2.43101e-11	1	2.43101e-11	0.26	0.6294
YF	8.39965e-11	1	8.39965e-11	0.91	0.3836
Light	7.82613e-11	1	7.82613e-11	0.85	0.3991
Height*TAV	3.65706e-10	1	3.65706e-10	3.97	0.103
Height*YF	2.78279e-11	1	2.78279e-11	0.3	0.6063
Height*Light	1.84655e-10	1	1.84655e-10	2	0.2161
TAV*YF	1.30097e-10	1	1.30097e-10	1.41	0.2881
TAV*Light	1.26118e-10	1	1.26118e-10	1.37	0.2948
YF*Light	2.57137e-11	1	2.57137e-11	0.28	0.6199
Error	4.60774e-10	5	9.21548e-11		
Total	1.51582e-09	15			

Constrained (Type III) sums of squares.

Figure 2.22: Table of the 2-ways ANOVA of Q_B along y axis

Here the most relevant dependences are on the interaction between height and TAV, on the interaction between height and light, on the interaction between TAV and YF and on the interaction between TAV and light.

Coefficient: Q_B
Cartesian axis: z

Analysis of Variance

Source	Sum Sq.	d.f.	Mean Sq.	F	Prob>F
Height	4.64286e-09	1	4.64286e-09	0.29	0.6013
TAV	3.11538e-09	1	3.11538e-09	0.19	0.6679
YF	8.97816e-09	1	8.97816e-09	0.56	0.47
Light	1.09442e-08	1	1.09442e-08	0.68	0.4263
Error	1.76427e-07	11	1.60388e-08		
Total	2.04108e-07	15			

Constrained (Type III) sums of squares.

Figure 2.23: Table of the 1-way ANOVA of Q_B along z axis

Analysis of Variance

Source	Sum Sq.	d.f.	Mean Sq.	F	Prob>F
Height	4.64286e-09	1	4.64286e-09	0.4	0.5536
TAV	3.11538e-09	1	3.11538e-09	0.27	0.6254
YF	8.97816e-09	1	8.97816e-09	0.78	0.4179
Light	1.09442e-08	1	1.09442e-08	0.95	0.3747
Height*TAV	2.77695e-08	1	2.77695e-08	2.41	0.1814
Height*YF	1.92565e-08	1	1.92565e-08	1.67	0.2527
Height*Light	1.43628e-08	1	1.43628e-08	1.25	0.3151
TAV*YF	1.79672e-08	1	1.79672e-08	1.56	0.2672
TAV*Light	1.63675e-08	1	1.63675e-08	1.42	0.2869
YF*Light	2.30571e-08	1	2.30571e-08	2	0.2164
Error	5.76464e-08	5	1.15293e-08		
Total	2.04108e-07	15			

Constrained (Type III) sums of squares.

Figure 2.24: Table of the 2-ways ANOVA of Q_B along z axis

The Q_B coefficient on the z axis mainly depends on: height $\times$ TAV interaction, YF $\times$ light interaction, height $\times$ YF interaction, TAV $\times$ YF interaction, TAV $\times$ light interaction.

2.3.1 Overview of the results

Looking to the above listed ANOVAs, it is evident that:

- K mainly depends on the height, on the TAV and on their interaction;
- N mainly depends on the height, on the interaction between the YF and the light and on the interaction between the height and the TAV;
- No recurrent factors or interactions have been identified when studying T_B;
- The interaction between the height and the TAV and two interactions involving the light seem to have a recurrent influence on Q_B.

From a more general point of view, the most important factors defining the experimental dependences of the AVAR coefficients result to be, in decreasing order, the TAV, the height and the interaction between these two.

Chapter 3

Model identification and Kalman prediction

In this chapter the MOESP-PO algorithm, used to identify models, and the Kalman predictors, used to evaluate the performances of the models, are described.

3.1 MOESP-PO black-box model identification

A *model identification* (or *system identification*) problem is a situation where there is a system whose mathematical model has one or more parameters being uncertain or unknown and it is possible to carry out experiments on the system to collect data that are useful to reduce or remove these uncertainties; in synthesis, doing model identification is trying to incorporate information from data in a mathematical model [11] [12].

Black-box model identification is a particular case of model identification where also the model structure is unknown. It is a very old procedure: something similar to black-box model identification has been done by Isaac Newton to discover gravity.

Black-box model identification is usually performed by transformation into *grey-box model identification*; it means that the first step is the choice of a model structure, then it is possible to estimate parameters. A fundamental goal, here, is to build a model that explains data sufficiently well and at the same time is not too complex.

In our case, the identification process has been conducted through an algorithm called MOESP-PO, that is part of the so-called *subspace* class of model identification algorithms.

Let's consider, at first, a purely deterministic case, for sake of simplicity.

Consider the state-space representation of a finite-dimensional, linear and time-invariant (LTI) system in discrete time, as in Equation (3.1):

$$\begin{cases} x(t+1) = Ax(t) + Bu(t) \\ y(t) = Cx(t) + Du(t) \end{cases} \tag{3.1}$$

For $i > n$ it holds that

$$\begin{bmatrix} y(t) \\ y(t+1) \\ y(t+2) \\ \vdots \\ y(t+i-1) \end{bmatrix} = \begin{bmatrix} C \\ CA \\ CA^2 \\ \vdots \\ CA^{i-1} \end{bmatrix} x(t) + \begin{bmatrix} D & 0 & 0 & \dots & 0 \\ CB & D & 0 & \dots & 0 \\ CAB & CB & D & \dots & 0 \\ \vdots & \vdots & \vdots & \vdots & \vdots \\ CA^{i-1}B & \dots & \dots & CB & D \end{bmatrix} \begin{bmatrix} u(t) \\ u(t+1) \\ u(t+2) \\ \vdots \\ u(t+i-1) \end{bmatrix}. \tag{3.2}$$

This describes the system's behaviour over a finite time interval and, repeating it for various initial time instants, Equation (3.3) is obtained. It is the so-called *data equation*:

$$Y_{tij} = \Gamma_i X_{t,j} + H_i U_{t,i,j}. \tag{3.3}$$

$Y_{t,i,j}$ and $U_{t,i,j}$ are Hankel matrices.

From now on, the general structure of an Hankel matrix, for example $A_{t,i,j}$, will be assumed as

$$A_{t,i,j} = \begin{bmatrix} a(t) & \dots & a(t+j-1) \\ a(t+1) & \dots & a(t+j) \\ \vdots & \ddots & \vdots \\ a(t+i-1) & \dots & a(t+i+j-2) \end{bmatrix}. \tag{3.4}$$

$X_{t,j}$ has the following expression:

$$X_{t,j} = \begin{bmatrix} x(t) & x(t+1) & \dots & x(t+j-1) \end{bmatrix}. \tag{3.5}$$

In 1991, Patrick Dewilde and Michel Verhaegen proposed the MOESP algorithm, that basically has the following steps:

- Construct a projection Π such that $U_{t,i,j}\Pi = 0$
- Use Π to project data equation and recover the column space of Γ_i:

$$Y_{t,i,j}\Pi = \Gamma X_{t,j}\Pi \tag{3.6}$$

- Construct a basis for this column space and estimate the A and C matrices
- Estimate the B and D matrices through the least-squares (LS) estimation method

The projection is given by

$$\Pi = I - U_{t,i,j}^T (U_{t,i,j} U_{t,i,j}^T)^{-1} U_{t,i,j}, \tag{3.7}$$

being careful that this requires $U_{t,i,j} U_{t,i,j}^T$ to be non-singular.
Π can be computed through an RQ factorisation:

$$\begin{bmatrix} U_{t,i,j} \\ Y_{t,i,j} \end{bmatrix} = \begin{bmatrix} R_{11} & 0 \\ R_{21} & R_{22} \end{bmatrix} \begin{bmatrix} Q_1 \\ Q_2 \end{bmatrix} = RQ \tag{3.8}$$

$$QQ^T = \begin{bmatrix} Q_1 Q_1^T & Q_1 Q_2^T \\ Q_2 Q_1^T & Q_2 Q_2^T \end{bmatrix}, \tag{3.9}$$

from which, through some algebraic manipulation, it results that

$$R_{22} = \Gamma_i X_{t,j} Q_2^T, \tag{3.10}$$

so R_{22} has dimensions $il \times il$ and contains information on Γ_i.
If $u(t)$ is such that

$$rank(\begin{bmatrix} X_{t,j} \\ U_{t,i,j} \end{bmatrix}) = n + im, \tag{3.11}$$

it holds that

$$range(R_{22}) = range(\Gamma_i). \tag{3.12}$$

This is not an identifiability condition, since it depends on the state, but is valid if the input u is persistently exciting of order $n+i$, a characteristic implying also that

$$\lim_{N \to \infty} \frac{1}{N} \begin{bmatrix} X_{t,j} \\ U_{t,i,j} \end{bmatrix} \begin{bmatrix} X_{t,j}^T & U_{t,i,j}^T \end{bmatrix} > 0. \tag{3.13}$$

The rank of the estimated column space of Γ_i is reduced through singular value decomposition (SVD) of R_{22} (that is possible being $rank(R_{22}) = n$), because the number of non-zero singular values of R_{22} reveals the order of the system:

$$R_{22} = \begin{bmatrix} U_n & U_n^T \end{bmatrix} \Sigma V^T = \begin{bmatrix} U_n & U_n^T \end{bmatrix} \begin{bmatrix} \Sigma_n & 0 \\ 0 & 0 \end{bmatrix} V^T. \tag{3.14}$$

Matrix C is now estimated as made by the first l rows of Γ_i, while A is computed through *shift invariance*, *i.e.* by solving this linear system:

$$\Gamma_{\uparrow} A = \begin{bmatrix} C \\ CA \\ CA^2 \\ \vdots \\ CA^{i-2} \end{bmatrix} A = \begin{bmatrix} CA \\ CA^2 \\ CA^3 \\ \vdots \\ CA^{i-1} \end{bmatrix} = \Gamma_{\downarrow}. \tag{3.15}$$

It is now time to estimate the B and D matrices.

Through convolution, it is possible to determine the output of the identified model:

$$\hat{y}(t) = Du(t) + \sum_{r=0}^{t-1} CA^{t-r-1}Bu(r). \tag{3.16}$$

It is useful to write Equation (3.16) as a linear regression in the elements of B and D:

$$\hat{y}(t) = \phi_D^T(t)vec(D) + \phi_B^T(t)vec(B), \tag{3.17}$$

with

$$vec(X) = \begin{bmatrix} x_{11} & \dots & x_{m1} & x_{12} & \dots & x_{m2} & x_{1n} & \dots & x_{mn} \end{bmatrix}^T. \tag{3.18}$$

Now, being $A \in R^{m \times n}$ and $B \in R^{r \times s}$, the *Kronecker product* of A and B is a matrix with size $mr \times ns$ defined as

$$A \otimes B = \begin{bmatrix} a_{11}B & a_{12}B & \dots & a_{1n}B \\ a_{21}B & a_{22}B & \dots & a_{2n}B \\ \vdots & \vdots & \vdots & \vdots \\ a_{m1}B & a_{m2}B & \dots & a_{mn}B \end{bmatrix}. \tag{3.19}$$

There is a relationship between the Kronecker product and the *vec* operation. Having $A \in R^{mxn}$, $A \in R^{nxo}$ and $A \in R^{oxp}$, it holds that

$$vec(ABC) = (C^T \otimes A)vec(B). \tag{3.20}$$

Using all this, Equation (3.16) can be written as

$$\hat{y}(t) = [u(t)^T \otimes I_l]vec(D) + (\sum_{r=0}^{t-1} u(r)^T \otimes CA^{t-r-1})vec(B), \tag{3.21}$$

and this allows to find the B and D matrices as the solutions of the least-squares problem of Equation (3.22):

$$B, D = \arg\min_{B,D} \sum_{k=0}^{s} [y(t) - [u(t)^T \otimes I_l]vec(D) - (\sum_{r=0}^{t-1} u(r)^T \otimes CA^{t-r-1})vec(B)]^2. \tag{3.22}$$

In general, however, the considered situation is not at all deterministic, so the state-space representation to be considered is not the one of (3.1), but the one of (3.23):

$$\begin{cases} x(t+1) = Ax(t) + Bu(t) + w(t) \\ y(t) = Cx(t) + Du(t) + v(t), \end{cases} \tag{3.23}$$

where $v(t)$ is the measurement noise and $w(t)$ is the process noise; both noises are considered as zero-mean, white and uncorrelated with $u(t)$.

In this more general case, (3.3) turns into (3.24):

$$Y_{t,i,j} = \Gamma_i X_{t,j} + H_i U_{t_{ij}} + E_i W_{t,i,j} + V_{t,i,j}, \tag{3.24}$$

where $V_{t,i,j}$ and $W_{t,i,j}$ are Hankel matrices.

It follows that the residual is no longer white, so the orthogonal projection procedure does not work anymore, *i.e.* it does not lead to unbiased estimators of the model.

This problem can be solved through the so-called *Instrumental Variables* (IV), assuming to be able to found a Z matrix such that

$$rank(\lim_{N\to\infty} \frac{1}{N}(X_{t,j}\Pi)Z^T) = n \tag{3.25}$$

$$\lim_{N\to\infty} \frac{1}{N}(E_i W_{t,i,j} + V_{t,i,j})Z^T = 0 \tag{3.26}$$

and to estimate the column space of Γ_i from

$$Y_{t,i,j}\Pi Z^T = \Gamma X_{t,j}\Pi Z^T + (E_i W_{t,i,j} + V_{t,i,j})\Pi Z^T \tag{3.27}$$

The term $Y_{t,i,j}\Pi Z^T$ can be computed from the RQ factorisation, holding that

$$\begin{bmatrix} U_{t,i,j} \\ Z \\ Y_{t,i,j} \end{bmatrix} = \begin{bmatrix} R_{11} & 0 & 0 \\ R_{21} & R_{22} & 0 \\ R_{31} & R_{32} & R_{33} \end{bmatrix} \begin{bmatrix} Q_1 \\ Q_2 \\ Q_3 \end{bmatrix}, \tag{3.28}$$

$$Y_{t,i,j}\Pi Z^T = R_{32}R_{22}^T \tag{3.29}$$

and

$$range(\Gamma_i) = range(\lim_{N\to\infty} \frac{1}{N} R_{32}R_{22}^T). \tag{3.30}$$

IVs can be chosen through splitting the available data into two sets of samples to be treated with two separate data equations, the second one shifted ahead with respect to the first, and using previous data as IVs when treating future data; this is the MOESP-PO algorithm, proposed by Michel Verhaegen in 1994.

3.2 Kalman predictors

In this thesis, the MOESP-PO algorithm has been applied to the collected data to identify models having as input $u(t)$ the position data estimated by the odometry system on the UAV and as output $y(t)$ the errors in the estimation of position with respect to the position $p_{MC}(t)$ detected by the motion capture system.

In synthesis:

$$y(t) = u(t) - p_{MC}(t). \tag{3.31}$$

Since the position in a Cartesian reference frame has three components (x, y and z), the produced models are MIMO systems where input, state and output are all vectors with three elements and the state-space matrices are 3×3 matrices.

Furthermore, it has been decided, for the sake of simplicity, to assume that the matrix D is null in all the models.

In these models, the A matrices have turned out to be very close to identity matrices in all cases, whereas the B and C matrices have not shown a systematic trend of the values of their terms; in order to study how the models are influenced by the factors, it has been necessary to consider more general characteristics, as in Section (3.3).

In order to evaluate the performance of the identified models and see how they are able to follow the evolution of the errors, it has been necessary to build and use one-step ahead *Kalman predictors* [13].

3.2.1 Definition

For the sake of simplicity, let's consider a discrete-time system with input $u(t) = 0$ structured as in (3.32):

$$\begin{cases} x(t+1) = Fx(t) + w(t) \\ y(t) = Hx(t) + v(t) \\ x(1) = x_1, \end{cases} \tag{3.32}$$

with v white Gaussian measurement noise with $v \approx G(0, V)$, w white Gaussian process noise with $w \approx G(0, W)$ and $x_1 \approx G(0, P_1)$.

Assuming that the observed interval of time t goes from $t = 0$ to $t = T$, the *prediction* problem is the problem to find estimators for the state given measurements of the output at time instants $t > T$; the *one-step ahead* prediction problem is the prediction problem at time $T + 1$.

It is known that the free response, obtained considering the system with

$$\begin{cases} x(t+1) = Fx(t) \\ x(1) = x_1, \end{cases} \tag{3.33}$$

has as expression

$$x(t) = F^{t-1}x_1, \tag{3.34}$$

whereas the forced response, obtained considering the system with

$$\begin{cases} x(t+1) = Fx(t) + w(t) \\ x(1) = 0, \end{cases} \tag{3.35}$$

is expressed by (3.36):

$$x(t) = \sum_{k=1}^{t-1} F^{t-k} w(k). \tag{3.36}$$

Since (3.34) is Gaussian because it is linear in the Gaussian initial state, and also (3.36) is Gaussian, because it is linear in $w(t)$, the total response, that is the summation of the two, is also Gaussian.

A result from theory called *Bayes rule* allows to state that the optimal one-step ahead state and output predictors have these expressions:

$$\hat{x}(N+1\backslash N) = E[x(N+1)\backslash y^N] \tag{3.37}$$

$$\hat{y}(N+1\backslash N) = E[y(N+1)\backslash y^N]. \tag{3.38}$$

Let's define two quantities that will be often recalled in the following derivation:

$$e(N+1) = y(N+1) - E[y(N+1)\backslash y^N] \tag{3.39}$$

is called the *innovation*, while

$$\nu(N+1) = x(N+1) - E[x(N+1)\backslash y^N] \tag{3.40}$$

is the *state prediction error*.

Now, the output prediction is

$$\begin{aligned} &\hat{y}(N+1\backslash N) = \\ &= E[y(N+1)\backslash y^N] = \\ &= HE[x(N+1)\backslash y^N] + E[v(N+1)\backslash y^N], \end{aligned} \tag{3.41}$$

and, since $E[v(N+1)\backslash y^N] = 0$ because $v(N+1)$ is independent of previous noise samples and of the initial state, that means $v(n+1)$ is *unpredictable* from previous data,

$$\hat{y}(N+1\backslash N) = H\hat{x}(N+1\backslash N). \tag{3.42}$$

Consider now the state prediction:

$$\begin{aligned}
&\hat{x}(N+1\backslash N) = \\
&= E[x(N+1)\backslash y^N] = \\
&= E[x(N+1)\backslash y^{N-1}] + E[x(N+1)\backslash y(N)] = \\
&= E[x(N+1)\backslash y^{N-1}] + E[x(N+1)\backslash e(N)] = \\
&= E[Fx(N) + w(N)\backslash y^{N-1}] + E[x(N+1)\backslash e(N)] = \\
&= FE[x(N)\backslash y^{N-1}] + E[w(N)\backslash y^{N-1}] + E[x(N+1)\backslash e(N)] = \\
&= F\hat{x}(N\backslash N-1) + E[x(N+1)\backslash e(N)].
\end{aligned} \tag{3.43}$$

The second term is zero because $y(N-1)$ is a function of v up to time $N-1$, of w up to time $N-2$ and of x_1 and $w(N)$ is independent of previous samples of the noises and of the initial state, again.

The Bayes rule, again, allows to state that

$$E[x(N+1)\backslash e(N)] = \Lambda_{x(N+1)e(N)}\Lambda^{-1}_{e(N)e(N)}e(N), \tag{3.44}$$

so it is needed to compute the two variance matrices $\Lambda_{x(N+1)e(N)}$ and $\Lambda_{e(N)e(N)}$. After some algebraic passages, it is found that

$$\Lambda_{x(N+1)e(N)} = FE[\nu(N)\nu(N)^T]H^T, \tag{3.45}$$

and, defining

$$P(N) = E[\nu(N)\nu(N)^T], \tag{3.46}$$

Equation (3.45) turns into

$$\Lambda_{x(N+1)e(N)} = FP(N)H^T. \tag{3.47}$$

It is also possible to prove that

$$\Lambda_{e(N)e(N)} = HP(N)H^T + V. \tag{3.48}$$

The complete expression of the predictor is then

$$\hat{x}(N+1\backslash N) = F\hat{x}(N\backslash N-1) + K(N)e(N), \tag{3.49}$$

having defined the predictor's *gain* $K(N)$ (note that $K(N)$ is not constant) as

$$K(N) = FP(N)H^T(HP(N)H^T + V)^{-1}. \tag{3.50}$$

Finally, a strategy to update $P(N)$ is needed. Starting from the definition of the prediction error

$$\nu(N+1) = x(N+1) - \hat{x}(N+1\backslash N) \tag{3.51}$$

and doing some manipulation, it is possible to obtain the *Difference Riccati Equation* (DRE):

$$P(N+1) = FP(N)F^T + W - FP(N)H^T[HP(N)H^T + V]HP(N)F^T, \tag{3.52}$$

with

$$W = E[w(N)w^T(N)]. \tag{3.53}$$

The first two terms together are called *prediction*, the last is called *correction*. To initialize the predictor, let's consider the initial values of the prediction

$$\hat{x}(1\backslash 0) = E[x(1)\backslash y^0] = 0 \tag{3.54}$$

and of the variance of the prediction error

$$P(1) = E[(x(1) - \hat{x}(1\backslash 0))^2] = P_1. \tag{3.55}$$

All these results have been derived under some simplifying assumptions, some of which can actually be removed. An element that is important to add to use Kalman predictors on the identified models is an input $u(t)$, turning the system of Equation (3.32) into this one:

$$\begin{cases} x(t+1) = Fx(t) + Gu(t) + w(t) \\ x(1) = x_1 \\ y(t) = Hx(t) + v(t). \end{cases} \tag{3.56}$$

The input can be included in the above derivation, so the one-step ahead prediction turns into

$$\begin{cases} \hat{x}(N+1\backslash N) = F\hat{x}(N\backslash N-1) + Gu(N) + K(N)(y(N) - \hat{y}(N\backslash N-1)) \\ \hat{x}(1\backslash 0) = x_1 \\ \hat{y}(N\backslash N-1) = H\hat{x}(N\backslash N-1), \end{cases} \tag{3.57}$$

where $K(N)$ and the DRE to update $P(N)$ remain unchanged.

3.2.2 Application

In this thesis, two types of predictors have been considered:

- The first uses all the three components of the position estimation error y and, even if very useful to evaluate the performance of the models, it could not be used in a working contest on an UAV without an onboard motion capture system;
- The second is a partial predictor, since it uses only the vertical component z_y of y, that could be computed onboard if the UAV is equipped with an accurate altitude measurement system, for example a LASER sensor, whose measurement could be used in the error computation.

Each predictor has been built for each one of the 16 identified models, bringing to a total of 32 predictors.

Let's consider the state-space representation of one of the models as in (3.58):

$$\begin{cases} x_m(t+1) = A_m x_m(t) + B_m u_m(t) \\ y_m(t) = C_m x_m(t) \end{cases} \tag{3.58}$$

The corresponding complete predictor has the following structure:

$$\begin{cases} x_{p1}(t+1) = A_{p1}(t) x_{p1}(t) + B_{p1}(t) u_{p1}(t) \\ y_{p1}(t) = C_{p1}(t) x_{p1}(t), \end{cases} \tag{3.59}$$

with

$$A_{p1} = A_m - K C_m, \tag{3.60}$$

$$B_{p1} = \begin{bmatrix} B_m & K \end{bmatrix}, \tag{3.61}$$

$$C_{p1} = C_m \tag{3.62}$$

and

$$u_{p1} = \begin{bmatrix} u_m & y_m \end{bmatrix}, \tag{3.63}$$

being K the gain matrix.

The partial predictor uses only the third column of the C and K matrices, corresponding to the components on the z axis, and has the following structure:

$$\begin{cases} x_{p2}(t+1) = A_{p2} x_{p2}(t) + B_{p2} u_{p2}(t) \\ y_{p2}(t) = C_{p2} x_{p2}(t), \end{cases} \tag{3.64}$$

with

$$A_{p2} = A_m - \begin{bmatrix} K(1,3) \\ K(2,3) \\ K(3,3) \end{bmatrix} \begin{bmatrix} C_m(1,3) \\ C_m(2,3) \\ C_m(3,3) \end{bmatrix}, \tag{3.65}$$

$$B_{p2} = \begin{bmatrix} B_m & \begin{bmatrix} K(1,3) \\ K(2,3) \\ K(3,3) \end{bmatrix} \end{bmatrix}, \tag{3.66}$$

$$C_{p2} = C_m \tag{3.67}$$

and

$$u_{p2} = \begin{bmatrix} u_m & \begin{bmatrix} y_m(1,3) \\ y_m(2,3) \\ y_m(3,3) \end{bmatrix} \end{bmatrix}, \tag{3.68}$$

being, again, K the gain matrix.

To evaluate the validity of these predictors, it is necessary to inspect how much they are able to capture the evolution of the estimation error, that comes from the collected data and is the output of the models.

A first trial to do this has been done using as indicator the percentage relative error on the three axes as a function of the time. Being y the output of the model and yy the output of the considered predictor at the same time instant, the percentage relative error is computed as

$$E_{r\%} = \left(\frac{|y - yy|}{y} \right) * 100. \tag{3.69}$$

This choice, however, has turned out to be not very wise, since when the value of y, that comes from the trajectory described by the drone, becomes very small, $E_{r\%}$ grows towards infinity.

It has been decided, then, to consider the difference E_{abs} between y and yy in absolute value.

Being y_x, y_y and y_z the components of y along the three Cartesian axis and yy_x, yy_y and yy_z the components on the same axes of yy, E_{abs} is computed, at each time instant, as in Equation (3.70):

$$E_{abs} = \sqrt{(y_x - yy_x)^2 + (y_y - yy_y)^2 + (y_z - yy_z)^2}. \tag{3.70}$$

A simple statistical analysis has then been done on E_{abs}, inspecting its mean values μ and the standard deviation σ and looking to how they behave when the levels of the factor is changed.

The following plots, showing how the statistical indicators of E_{abs} variate between the sixteen experimental runs, with an emphasis on the different levels of the factors, have been produced.

As clearly expectable, the partial predictor generates a bigger error than the complete one, because it is based on much less data.

In the following figures, μ and σ of the prediction error of the partial predictor in the run number 5 do not appear, because they are much bigger than in the other runs, so it is better to discard that predictor.

From Figures (3.1) and (3.2), it is evident that the error produced by the complete predictor is bigger in mean and standard deviation at the height of 2 m than at 1 m, a trend that is not present in the case of the partial predictor.

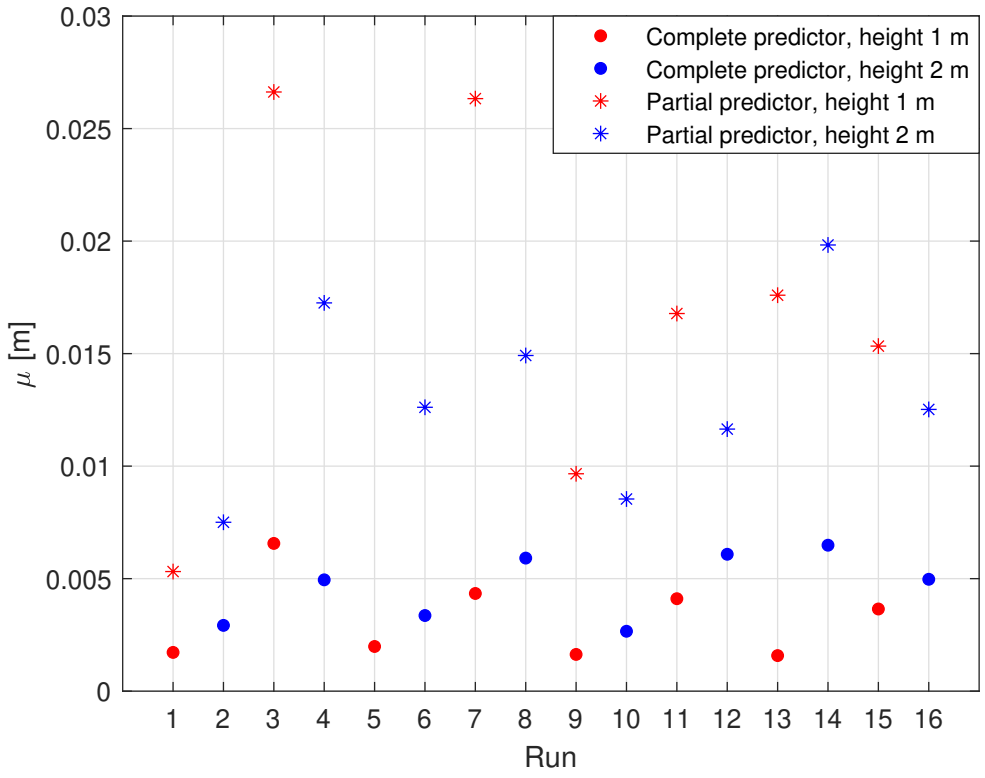

Figure 3.1: Mean values of the prediction error at the two different levels of the height

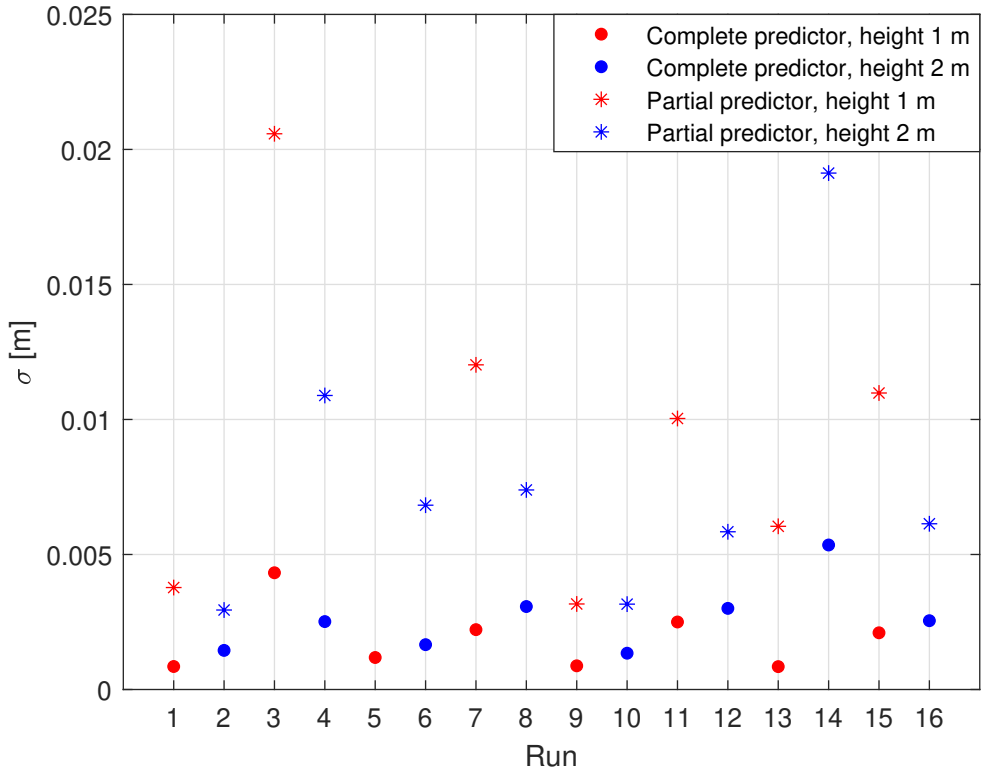

Figure 3.2: Standard deviations of the prediction error at the two different levels of the height

Figures (3.3) and (3.4) show that also the TAV causes a general increase of the statistical indicators of the error when increased (except, again, for the partial predictor in the run number 5, that has not been considered); in this case, such a trend is present in both the types of predictor.

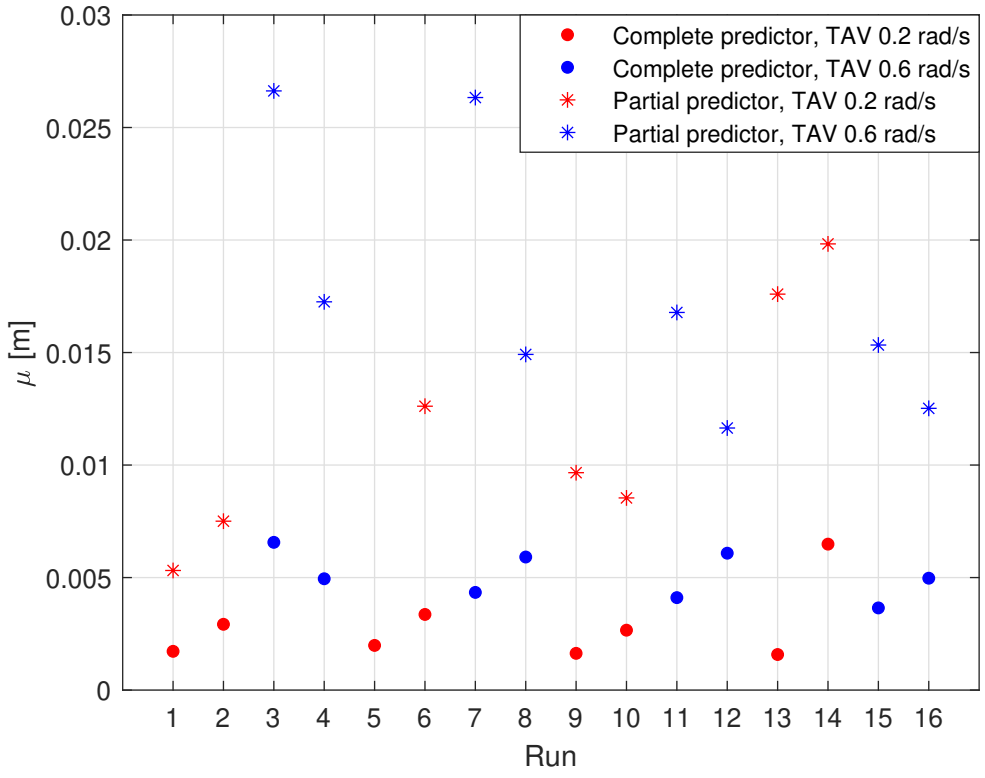

Figure 3.3: Mean values of the prediction error at the two different levels of the TAV

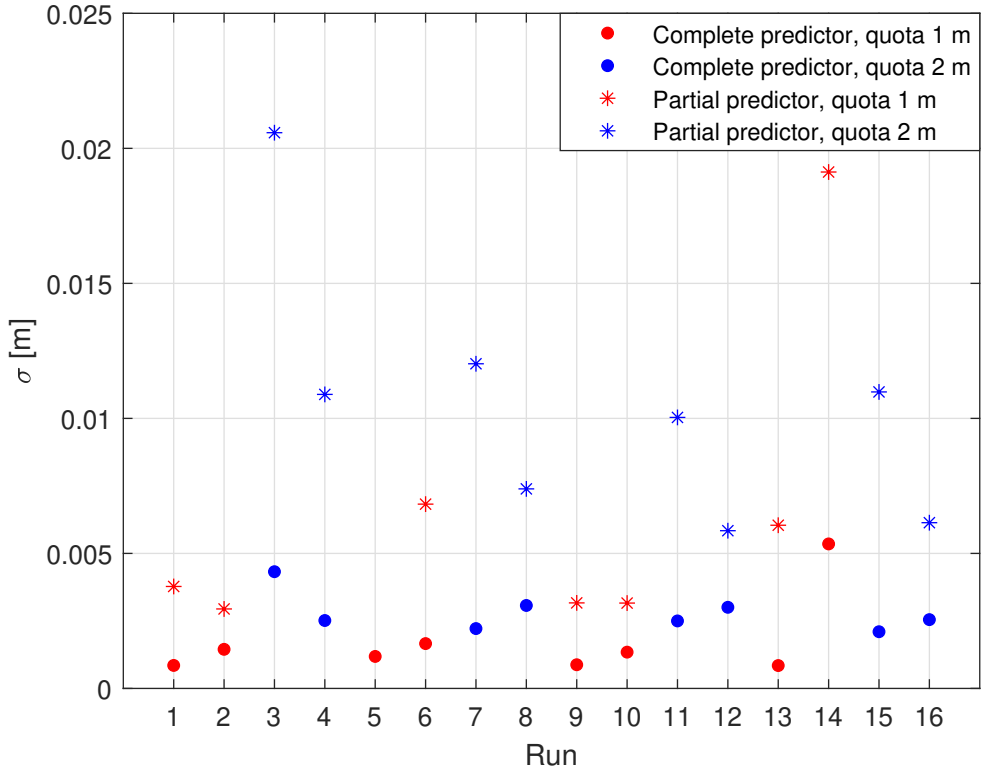

Figure 3.4: Standard deviations of the prediction error at the two different levels of the TAV

Figures (3.5) and (3.6) show how μ and σ of the prediction errors behave when the Yaw Following is enabled or disabled. In this case all the values seem to be similar and a specific influence of the YF is not detected.

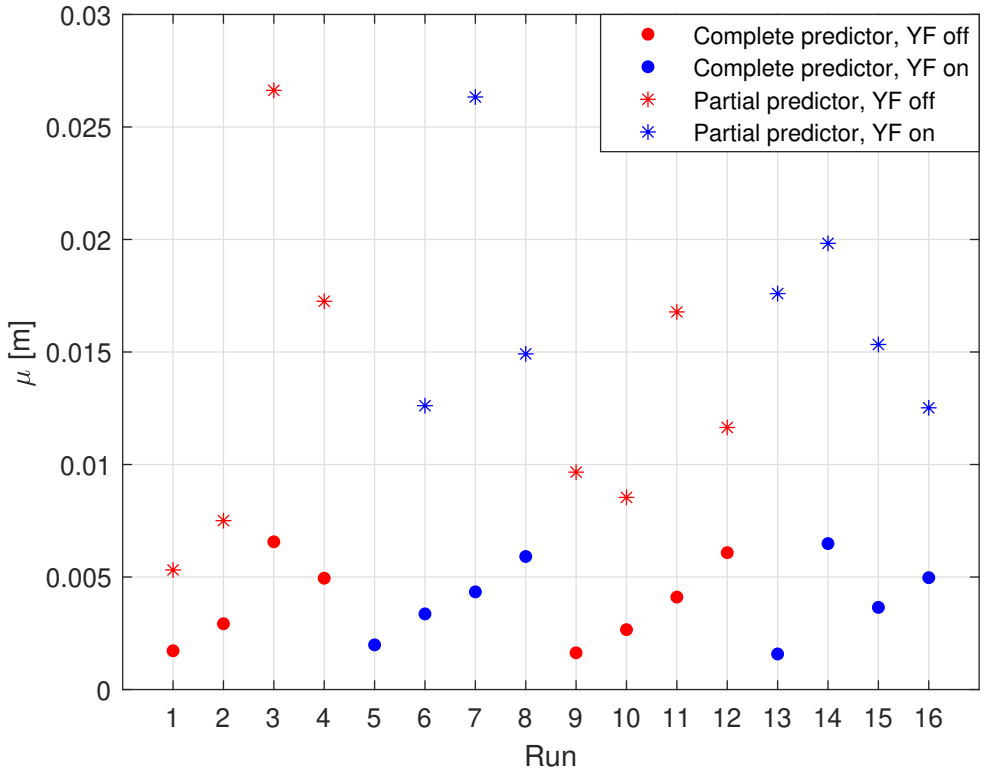

Figure 3.5: Mean values of the prediction error at the two different levels of the YF

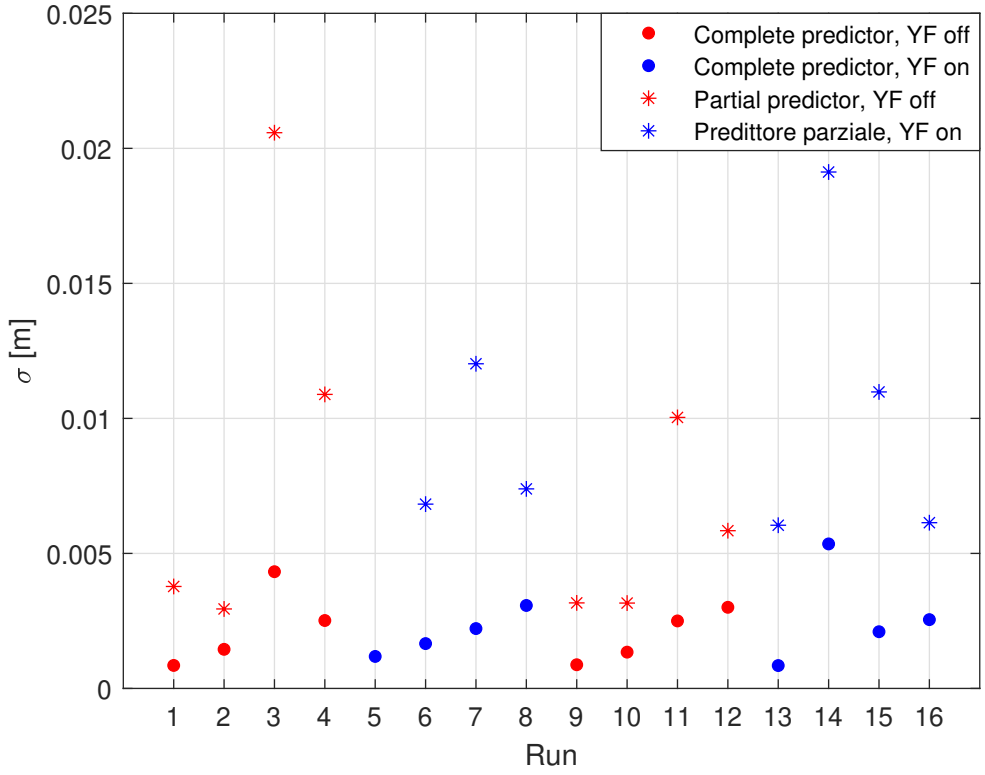

Figure 3.6: Standard deviations of the prediction error at the two different levels of the YF

The last two plots are about the variation of means and standard deviations of errors with the light, that, again, seems not to have a relevant effect, since the values look similar between the two levels.

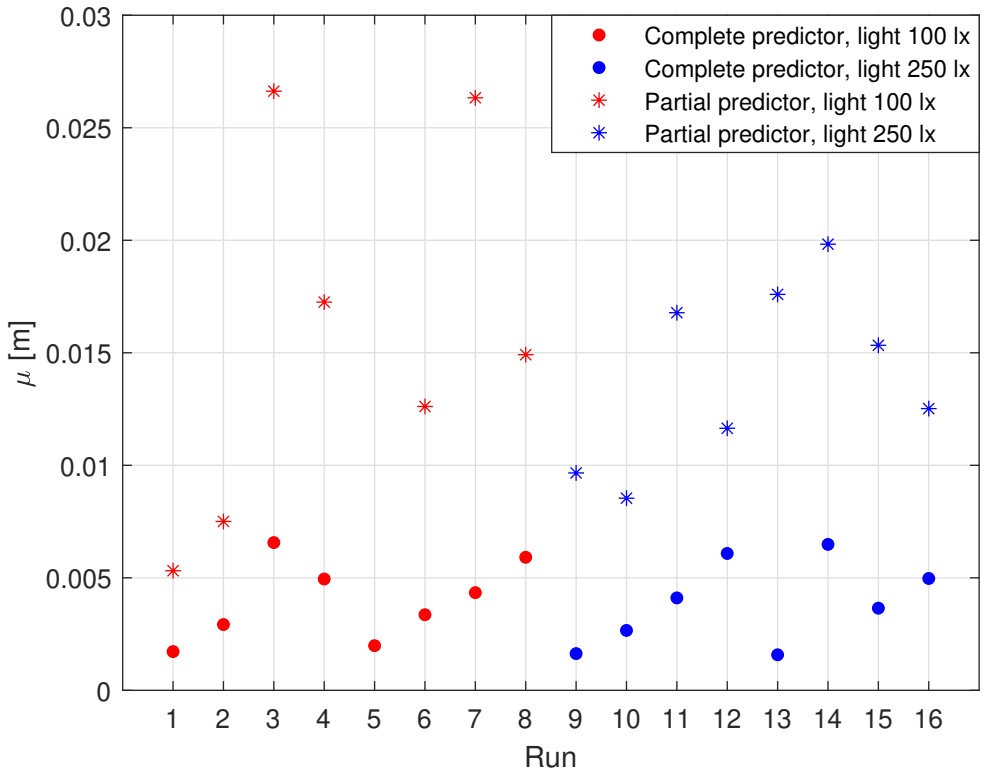

Figure 3.7: Mean values of the prediction error at the two different levels of the light

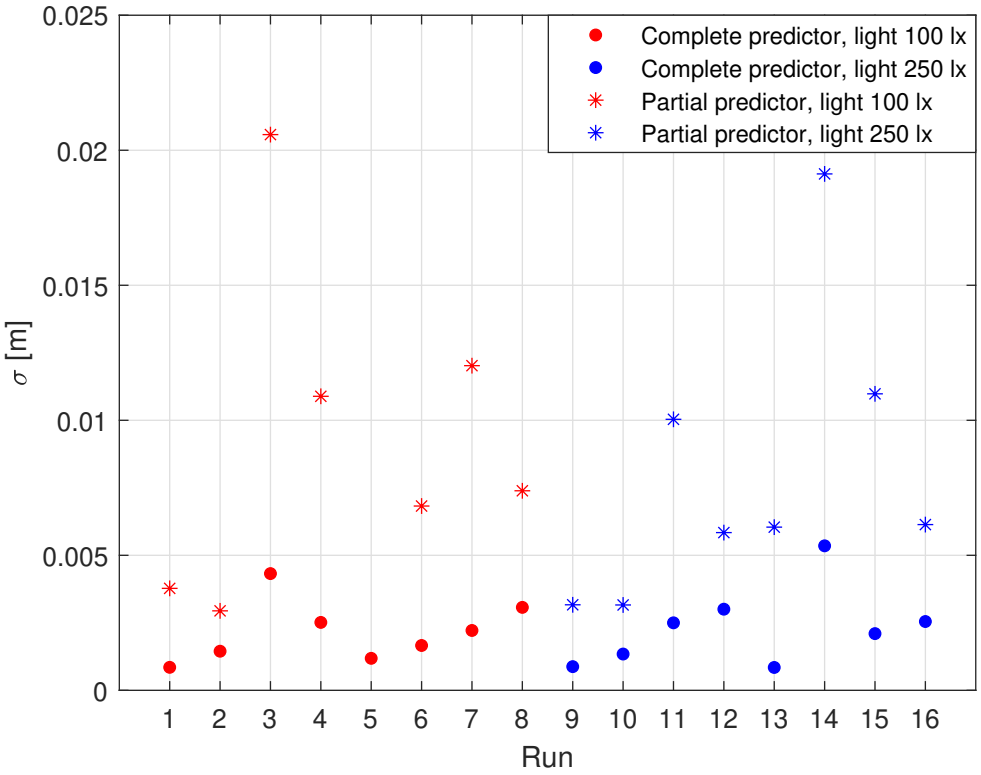

Figure 3.8: Standard deviations of the prediction error at the two different levels of the light

In general, in addition to the run number 5, the other runs that show a big difference between the indicators of the two predictors are the number 3, 4, 6, 7, 8, 11, 14 and 15; the experimental condition that is more present in all them is the TAV of 0.6 rad/s.

3.3 ANOVA on model characteristics

After the inspection of the results from MOESP-PO model identification and Kalman prediction, the dependence from experimental factors of some characteristics of the collected data and of the models has been studied, again, through the ANOVA. These features are:

- Difference between maximum and minimum singular value (σ) of the B matrices (it is a directionality indicator), called from now on $\Delta\sigma_B^{max}$;
- Maximum value (depending on frequency) of the three singular values of the frequency responses matrices $G(j\omega)$, called from now on σ_{G1}^{max}, σ_{G2}^{max}, σ_{G3}^{max} (they are, again, directionality indicators);
- Maximum error on the estimated position with respect to the reference frame origin in absolute value (it is an indicator of the validity of the odometry process): being y_x, y_y, y_z the components of the estimation error on each Cartesian axis, the maximized quantity is defined as $e = \sqrt{y_x^2 + y_y^2 + y_z^2}$.

It has been decided to start doing 2-ways ANOVAs, to check the Normal Probability Plots and then, if the normality of the residuals was not satisfying, to switch to 1-way ANOVA; the 2-way ANOVAs have been discarded only when the residuals were not valid in the central part of the Normal Probability Plot.

Furthermore, in this case, a cross-check on the results from the ANOVAs has been done computing the variation between mean values of the considered quantities at the two levels of the factors.

$\Delta\sigma_B^{max}$: the Normal Probability Plot of the 2-ways ANOVA is shown in Figure (3.9). It is evident that the residuals of the 2-ways ANOVA do not have significant deviations from normality, so the analysis is kept as valid.

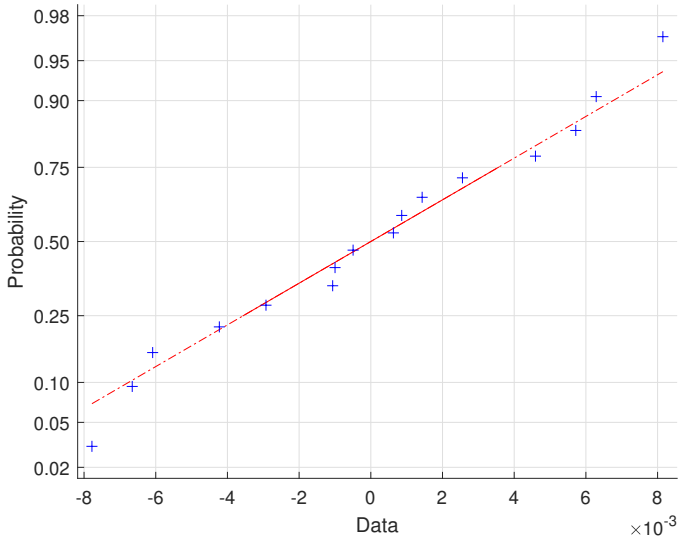

Figure 3.9: Normal Probability Plot of the residuals of the 2-ways ANOVA of $\Delta\sigma_B^{max}$

The ANOVA table is shown into Figure (3.10). The values of F tell that $\Delta\sigma_B^{max}$ mostly depends on the height, on the TAV and on the interaction between the TAV and the YF.

Analysis of Variance

Source	Sum Sq.	d.f.	Mean Sq.	F	Prob>F
Height	0.00013	1	0.00013	1.98	0.2189
TAV	0.00008	1	0.00008	1.2	0.323
YF	0	1	0	0.03	0.8724
Light	0	1	0	0.04	0.8574
Height*TAV	0.00002	1	0.00002	0.3	0.6058
Height*YF	0	1	0	0.02	0.8808
Height*Light	0	1	0	0	0.9786
TAV*YF	0.00008	1	0.00008	1.13	0.3373
TAV*Light	0.00001	1	0.00001	0.12	0.7476
YF*Light	0.00006	1	0.00006	0.86	0.3957
Error	0.00034	5	0.00007		
Total	0.00073	15			

Constrained (Type III) sums of squares.

Figure 3.10: Table of the 2-ways ANOVA of $\Delta\sigma_B^{max}$

This is confirmed by the inspection of the mean variations, shown in Figure (3.11); it is clear that $\Delta\sigma_B^{max}$ increases as all the four factors have their levels increased.

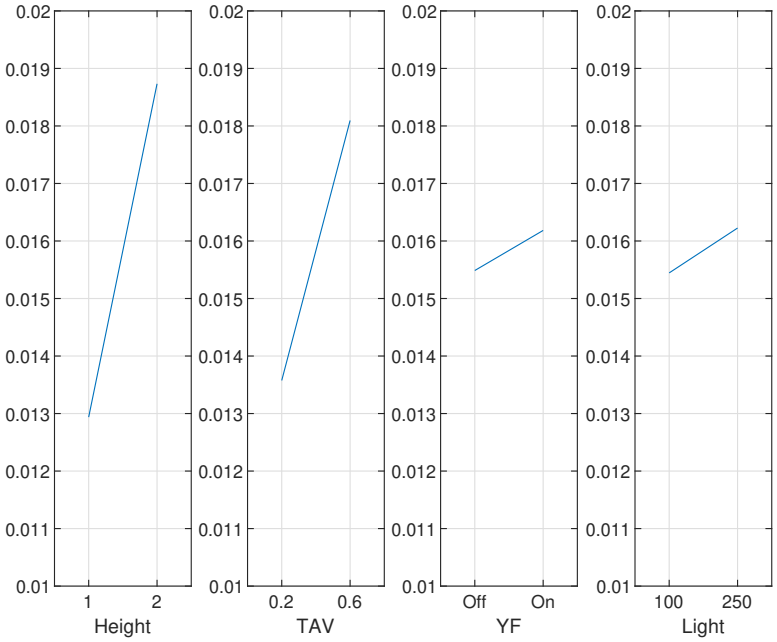

Figure 3.11: Mean variations of $\Delta\sigma_B^{max}$ between the levels of the factors

σ_{G1}^{max}: the Normal Probability Plots of the residuals with the data models, respectively, at 1 and 2 ways, are shown in Figures (3.12) and (3.13). Using 2 ways, residuals seem to not follow normality very well, whereas using only 1 way the situation seems to become better in the central part of the plot, so the 1-way ANOVA has been kept into account.

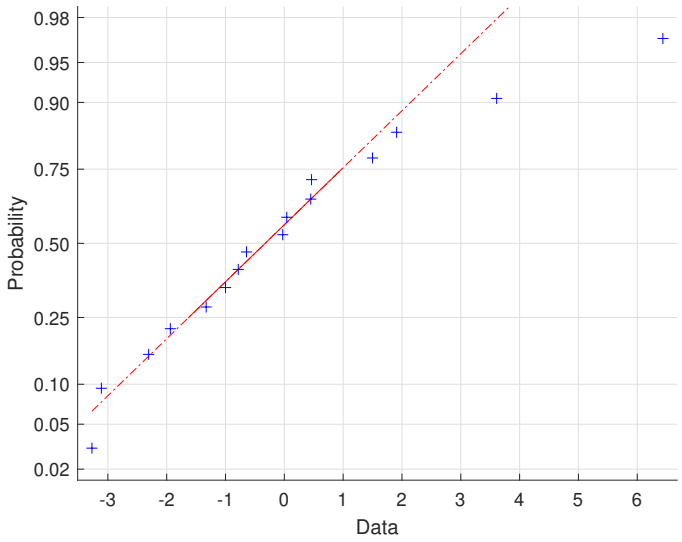

Figure 3.12: Normal Probability of the residuals of the 1-way ANOVA of σ_{G1}^{max}

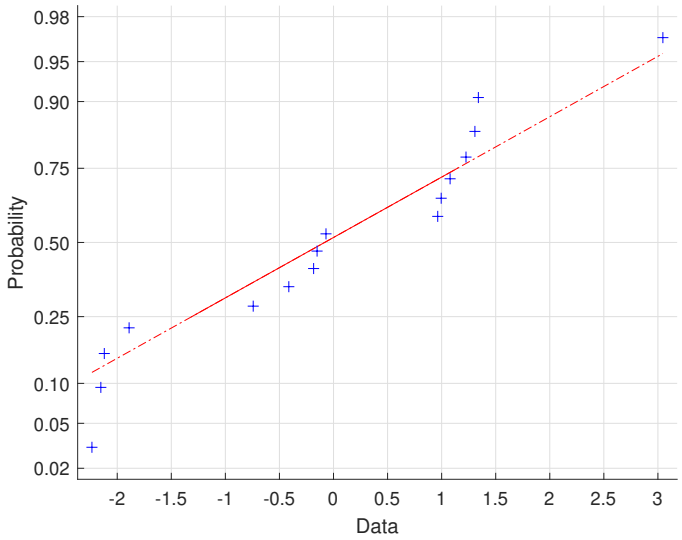

Figure 3.13: Normal Probability Plot of the residuals of the 2-ways ANOVA of σ_{G1}^{max}

The ANOVA reported in Figure (3.14) tells that σ_{G1}^{max} is influenced mainly by the TAV; also the light has a minimum relevance, whereas the other factors are completely irrelevant.

Analysis of Variance

Source	Sum Sq.	d.f.	Mean Sq.	F	Prob>F
Height	0.109	1	0.1094	0.01	0.912
TAV	34.585	1	34.5852	4.05	0.0694
YF	0	1	0.0001	0	0.9977
Light	2.216	1	2.2157	0.26	0.6207
Error	94.007	11	8.5461		
Total	130.917	15			

Constrained (Type III) sums of squares.

Figure 3.14: Table of the 1-way ANOVA of σ_{G1}^{max}

The mean variations, shown in Figure (3.15), confirm the huge relevance of the TAV. The YF has null relevance (as correctly told by the fact that its $F = 0$), while the other factors make σ_{G1}^{max} to grow when their levels are increased.

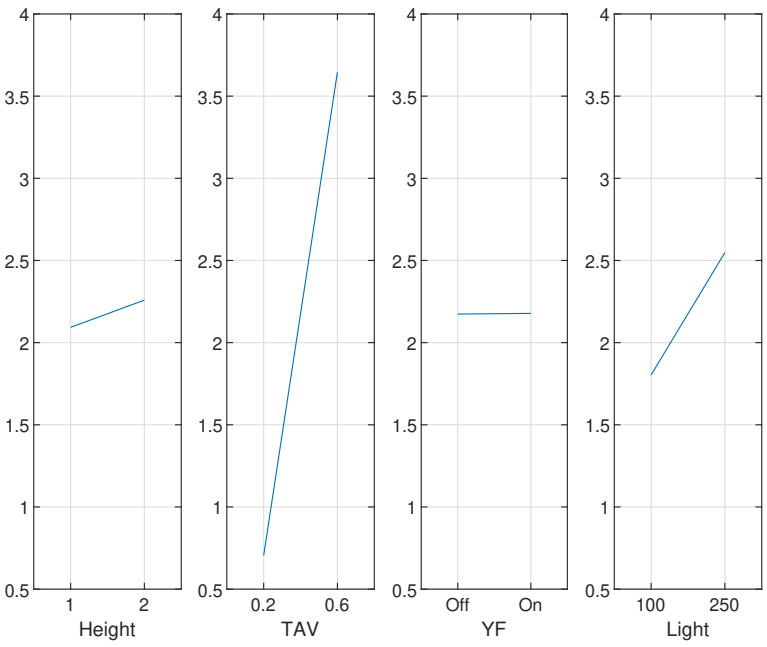

Figure 3.15: Mean variations of σ_{G1}^{max} between the levels of the factors

σ_{G2}^{max}: in this case both the 1-way and the 2-ways ANOVAs have been reported, in order to make a comparison, even if, again, the 1-way one has been considered better, as clearly visible from the Normal Probability Plots in Figures (3.16) and (3.17).

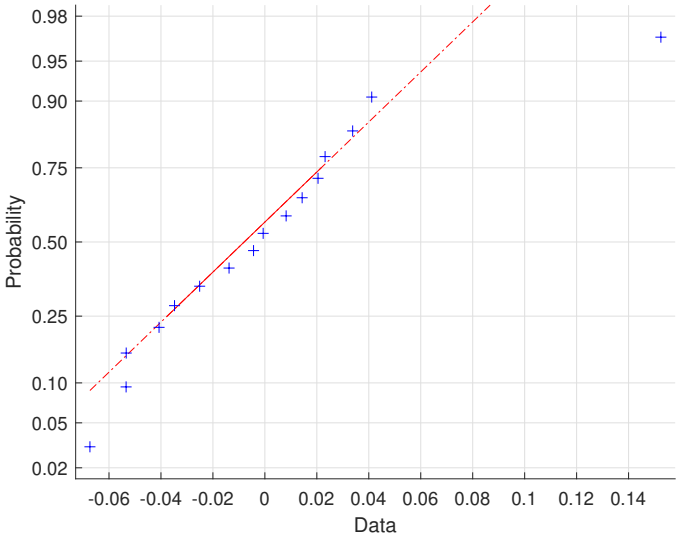

Figure 3.16: Normal Probability Plot of the residuals of the 1-way ANOVA of σ_{G2}^{max}

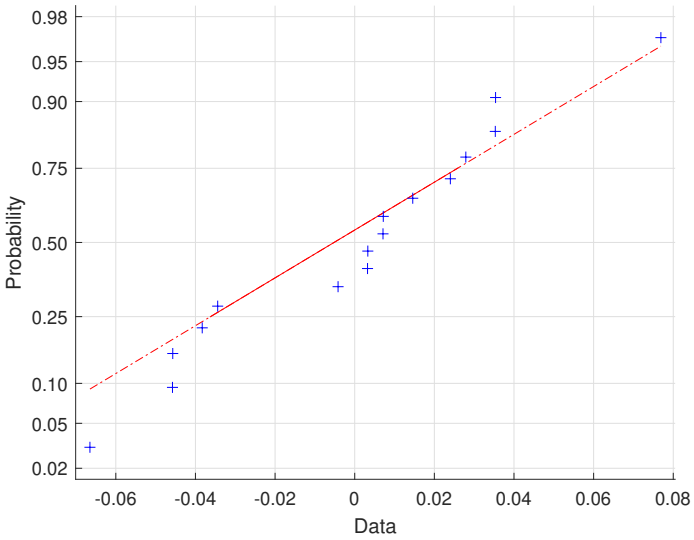

Figure 3.17: Normal Probability Plot of the residuals of the 2-ways ANOVA of σ_{G2}^{max}

The ANOVAs for σ_{G2}^{max} are reported in Figures (3.18) and (3.19). Also in this case the most relevant factor is the TAV and, unlike σ_{G1}^{max}, there is also an influence of the YF. Here the height is not giving any dependence at all ($F = 0$). The most important interactions are the one between the height and the YF and between the TAV and the light, even if with F much lower than single factors.

Analysis of Variance

Source	Sum Sq.	d.f.	Mean Sq.	F	Prob>F
Height	0	1	0	0	0.9772
TAV	0.01999	1	0.01999	5.33	0.0414
YF	0.0111	1	0.0111	2.96	0.1132
Light	0.00103	1	0.00103	0.28	0.6099
Error	0.04124	11	0.00375		
Total	0.07338	15			

Constrained (Type III) sums of squares.

Figure 3.18: Table of the 1-way ANOVA of σ_{G2}^{max}

Analysis of Variance

Source	Sum Sq.	d.f.	Mean Sq.	F	Prob>F
Height	0	1	0	0	0.9792
TAV	0.01999	1	0.01999	4.68	0.0829
YF	0.0111	1	0.0111	2.6	0.168
Light	0.00103	1	0.00103	0.24	0.6437
Height*TAV	0.00004	1	0.00004	0.01	0.9238
Height*YF	0.00708	1	0.00708	1.66	0.2546
Height*Light	0.00255	1	0.00255	0.6	0.4751
TAV*YF	0.00345	1	0.00345	0.81	0.4104
TAV*Light	0.0062	1	0.0062	1.45	0.2823
YF*Light	0.00055	1	0.00055	0.13	0.7334
Error	0.02138	5	0.00428		
Total	0.07338	15			

Constrained (Type III) sums of squares.

Figure 3.19: Table of the 2-ways ANOVA of σ_{G2}^{max}

The mean variations, shown in Figure (3.20), confirm the statistical results again and show that, unlike the other factors, the YF, when its level is increased, produces a decrease in σ_{G2}^{max}.

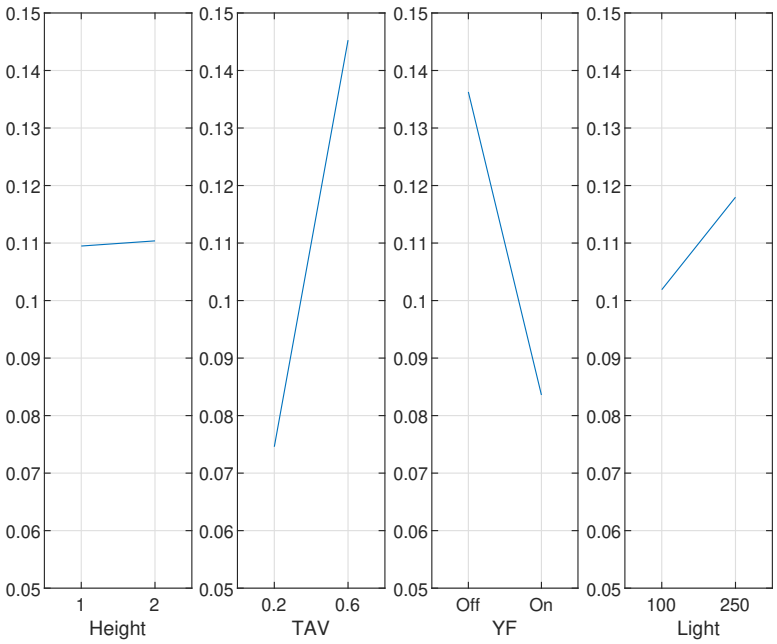

Figure 3.20: Mean variations of σ_{G2}^{max} between the levels of the factors

σ_{G3}^{max}: here the Normal Probability Plot of the residuals of the 2-ways ANOVA, shown in Figure (3.21), does not show big deviations from normality in residuals, so the analysis has been kept in consideration.

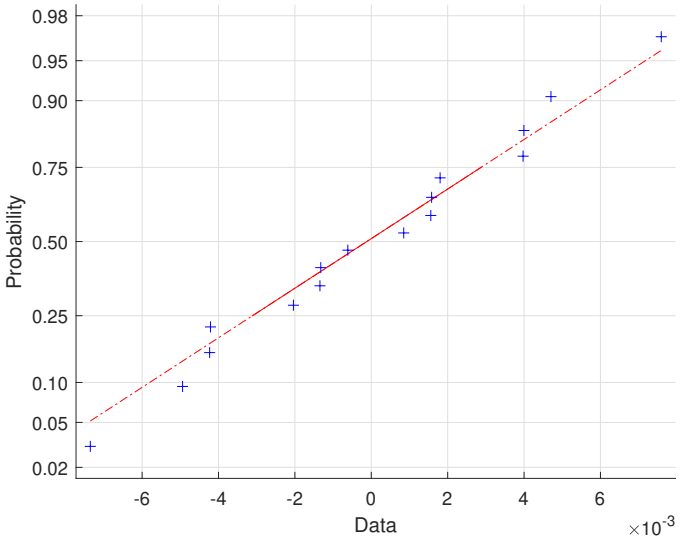

Figure 3.21: Normal Probability Plot of the residuals of the 2-ways ANOVA of σ_{G3}^{max}

The ANOVA is reported in Figure (3.22).

Analysis of Variance

Source	Sum Sq.	d.f.	Mean Sq.	F	Prob>F
Height	0.00003	1	0.00003	0.65	0.4568
TAV	0.00169	1	0.00169	34.83	0.002
YF	0.00175	1	0.00175	35.97	0.0018
Light	0.00001	1	0.00001	0.2	0.677
Height*TAV	0	1	0	0	0.9795
Height*YF	0.00005	1	0.00005	1	0.3629
Height*Light	0.00007	1	0.00007	1.35	0.2984
TAV*YF	0.00041	1	0.00041	8.5	0.0332
TAV*Light	0.00009	1	0.00009	1.9	0.2262
YF*Light	0.00025	1	0.00025	5.23	0.071
Error	0.00024	5	0.00005		
Total	0.00459	15			

Constrained (Type III) sums of squares.

Figure 3.22: Table of the 2-ways ANOVA of σ_{G3}^{max}

There is a big influence of the TAV, of the YF and, even if with less importance, of their interaction; another important interaction is the one between the YF and light.

Also in this case the plots of the mean variations, visible in Figure (3.23), are in line with the ANOVAs' results, portraying the relative influences of the factors, and show that the only factor producing a decrease of σ_{G3}^{max} when its level is increased is the YF.

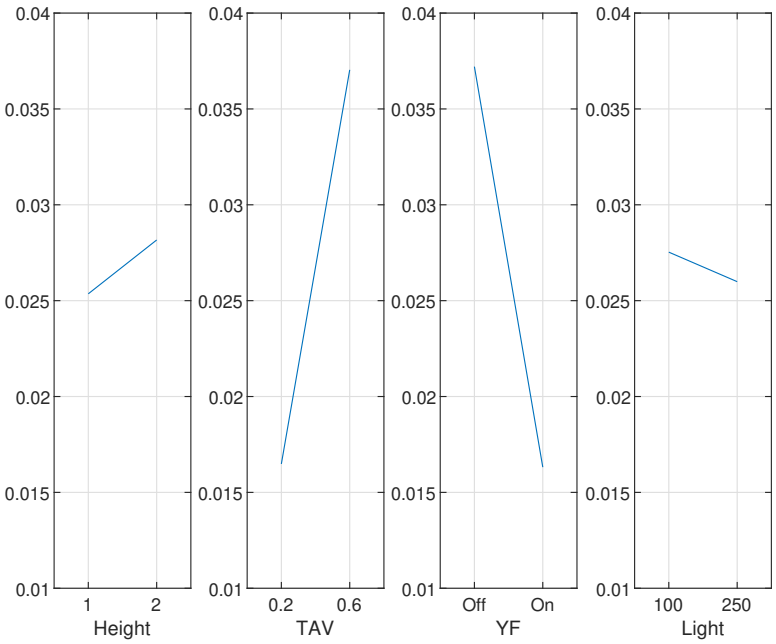

Figure 3.23: Mean variations of σ_{G3}^{max} between the levels of the factors

Estimation error in absolute value e: the 1-way and 2-ways ANOVAs have both been reported, even if in both cases the residuals do not seem very respectful of the normality hypothesis, as visible in the Normal Probability Plots of Figures (3.24) and (3.25).

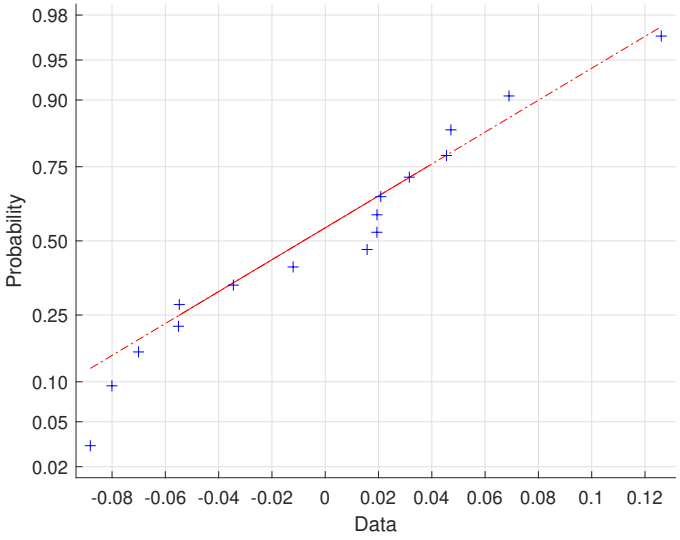

Figure 3.24: Normal Probability Plot of the residuals of the 1-way ANOVA of e

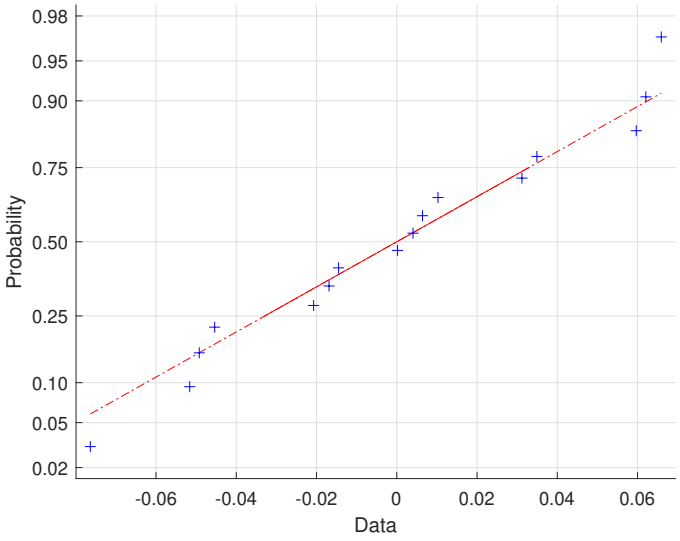

Figure 3.25: Normal Probability Plot of the residuals of the 2-ways ANOVA of e

ANOVAs tell that the factors having the biggest influence on e are the height and the TAV, even if the other two have a not null influence; the 2-ways case shows that the interaction between height and YF is also relevant (the YF alone is not so important).

Analysis of Variance

Source	Sum Sq.	d.f.	Mean Sq.	F	Prob>F
Height	0.01572	1	0.01572	3.21	0.1006
TAV	0.02541	1	0.02541	5.19	0.0437
YF	0.00285	1	0.00285	0.58	0.4618
Light	0.00003	1	0.00003	0.01	0.9407
Error	0.05384	11	0.00489		
Total	0.09785	15			

Constrained (Type III) sums of squares.

Figure 3.26: Table of the 1-way ANOVA of e

Analysis of Variance

Source	Sum Sq.	d.f.	Mean Sq.	F	Prob>F
Height	0.01572	1	0.01572	2.81	0.1547
TAV	0.02541	1	0.02541	4.54	0.0864
YF	0.00285	1	0.00285	0.51	0.5079
Light	0.00003	1	0.00003	0.01	0.9461
Height*TAV	0.00359	1	0.00359	0.64	0.4595
Height*YF	0.01632	1	0.01632	2.91	0.1486
Height*Light	0.00051	1	0.00051	0.09	0.774
TAV*YF	0.00493	1	0.00493	0.88	0.3911
TAV*Light	0.00046	1	0.00046	0.08	0.7857
YF*Light	0	1	0	0	0.9943
Error	0.02801	5	0.0056		
Total	0.09785	15			

Constrained (Type III) sums of squares.

Figure 3.27: Table of the 2-ways ANOVA of e

These results are, again, confirmed, by the mean variations, as visible in Figure (3.28); the YF and the light, when their levels are increased, cause e to decrease.

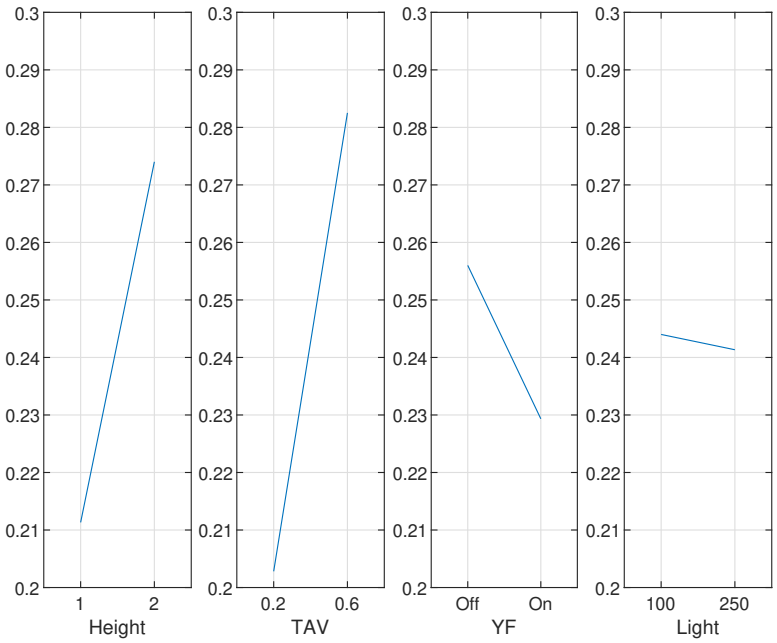

Figure 3.28: Mean variations of e between the levels of the factors

3.3.1 Overview of the results

The above reported ANOVAs tell that the factor causing the biggest changes in the studied characteristics of the models is the TAV, that always cause the under-study feature to highly increase when brought from 0.2 to 0.6 .

The height, when increased, causes a big change (increase) in $\Delta\sigma_B^{max}$ and e, while the activation of the YF produces a big decrease in σ_{G2}^{max} and σ_{G3}^{max}.

The light, in the end, has not a big influence on the studied quantities.

Chapter 4

Parametric modeling

ANOVAs, in the end, explain which variables depend on which factor.

An important step, explained in this chapter, has been trying to construct linear parametrical models of some quantities of interest, doing a linear interpolation through the method of least-squares regression; this has been done on the AVAR coefficients found in the model without the Rate Ramp noise and on the terms of the matrices coming from the identified models.

4.1 Linear regression

The characteristics of the models used for the regressions are reported in Table (4.1).

Number of factors	**Equation**
1	$y = a + bx$
2	$y = a + bx_1 + cx_2$
3	$y = a + bx_1 + cx_2 + dx_3$

Table 4.1: General form of regression models

4.2 Interpolations on AVAR coefficients

Since the ANOVAs done on the AVAR coefficients in Section (2.3) put in evidence that the YF, the only factor with qualitative levels, has an influence on them, so neglecting it would not have been very wise, and since it is not convenient to perform a regression with a variable not having numerical values, it has been decided to split the data in two groups, one containing only the values with the YF and the other only the values without the YF, and to do two ANOVAs and two regressions for each coefficient.

The results of these ANOVAs have been used as driving elements to choose how many and which of the factors was better to use as independent variables in the regression processes, having the AVAR coefficients as dependent variables.

Here it has been considered, again, only the model without the Rate Ramp noise (no R coefficient) and only 1-way ANOVAs have been done, because their residuals were much nearer to normality, so the interactions between the factors have been neglected.

4.2.1 Data without yaw following

Let's list all the ANOVA-based models done on the AVAR coefficients in the eight experimental runs without the YF.

From now on, in the expressions of the models, y will indicate the considered coefficient.

Coefficient: K
Cartesian axis: x
ANOVA: reported in Figure (4.1)

Analysis of Variance

Source	Sum Sq.	d.f.	Mean Sq.	F	Prob>F
Height	0.00005	1	0.00005	0.86	0.4074
TAV	0.00135	1	0.00135	22.93	0.0087
Light	0.0001	1	0.0001	1.74	0.2574
Error	0.00024	4	0.00006		
Total	0.00174	7			

Constrained (Type III) sums of squares.

Figure 4.1: 1-way ANOVA of K on x axis without YF

Model: $y = a + bx$, with x TAV and

$$a = -0.002218623066802 \tag{4.1}$$

$$b = 0.064913963258429 \tag{4.2}$$

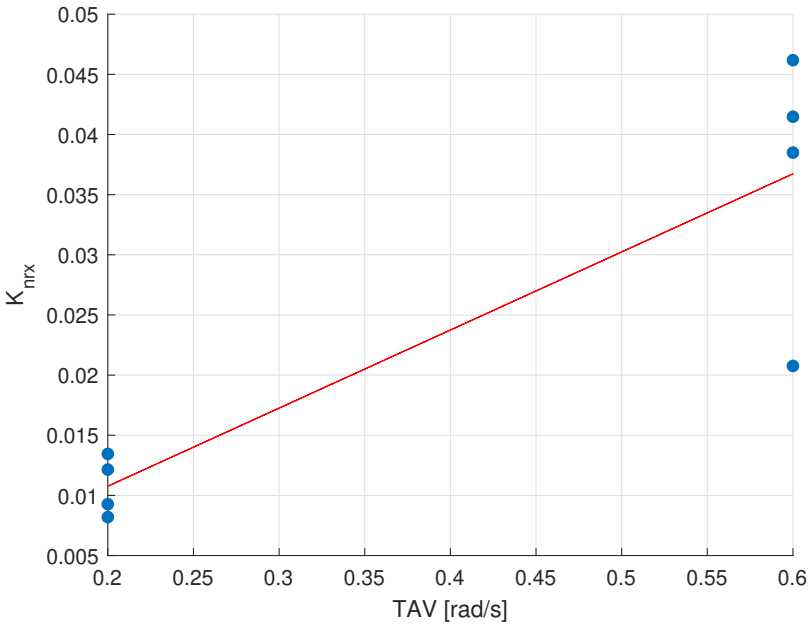

Figure 4.2: Plot of the model for K on x axis without YF

Coefficient: K
Cartesian axis: y
ANOVA: reported in Figure (4.3)

Analysis of Variance

Source	Sum Sq.	d.f.	Mean Sq.	F	Prob>F
Height	0.00013	1	0.00013	2.62	0.1808
TAV	0.00132	1	0.00132	26.79	0.0066
Light	0.00015	1	0.00015	3.05	0.1555
Error	0.0002	4	0.00005		
Total	0.0018	7			

Constrained (Type III) sums of squares.

Figure 4.3: 1-way ANOVA of K on y axis without YF

Model: $y = a + bx_1 + cx_2$, with x_1 TAV, x_2 light and

$$a = -0.007259645073151 \tag{4.3}$$

$$b = 0.064197151770991 \tag{4.4}$$

$$c = -0.000057800048341 \tag{4.5}$$

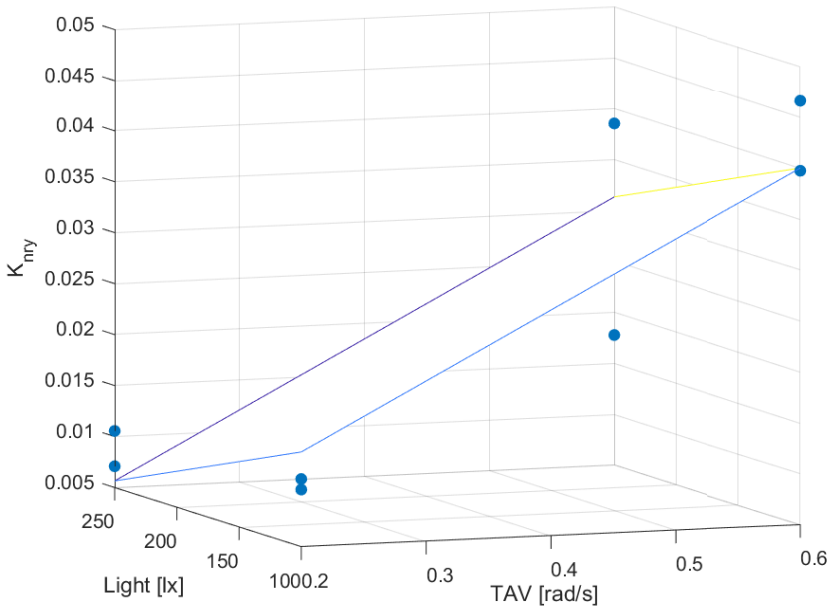

Figure 4.4: Plot of the model for K on y axis without YF

Coefficient: K
Cartesian axis: z
ANOVA: reported in Figure (4.5)

Analysis of Variance

Source	Sum Sq.	d.f.	Mean Sq.	F	Prob>F
Height	0.00001	1	0.00001	0.21	0.6726
TAV	0.0002	1	0.0002	7.55	0.0515
Light	0.00009	1	0.00009	3.53	0.1335
Error	0.00011	4	0.00003		
Total	0.00041	7			

Constrained (Type III) sums of squares.

Figure 4.5: 1-way ANOVA of K on z axis without YF

Model: $y = a + bx_1 + cx_2$, with x_1 TAV, x_2 light and

$$a = -0.001126306931063 \tag{4.6}$$

$$b = 0.025072369784152 \tag{4.7}$$

$$c = 0.000045705586494 \tag{4.8}$$

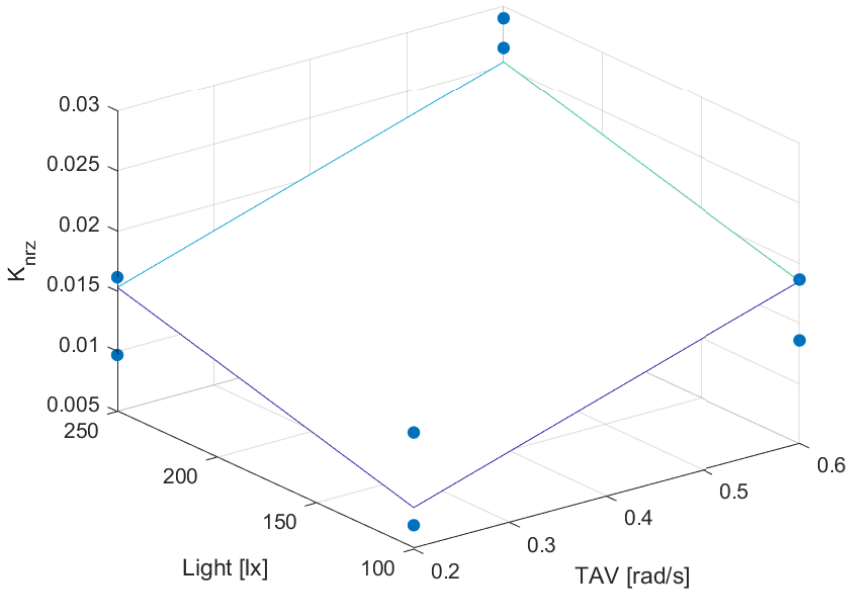

Figure 4.6: Plot of the model for K on z axis without YF

Coefficient: N
Cartesian axis: x
ANOVA: reported in Figure (4.7)

Analysis of Variance

Source	Sum Sq.	d.f.	Mean Sq.	F	Prob>F
Height	1.3049e-07	1	1.3049e-07	1.47	0.2924
TAV	4.77035e-08	1	4.77035e-08	0.54	0.5045
Light	1.36507e-07	1	1.36507e-07	1.54	0.283
Error	3.55587e-07	4	8.88967e-08		
Total	6.70287e-07	7			

Constrained (Type III) sums of squares.

Figure 4.7: 1-way ANOVA of N on x axis without YF

Model: $y = a + bx_1 + cx_2$, with x_1 height, x_2 light and

$$a = 0.233223823824975e - 3 \tag{4.9}$$

$$b = -0.255431130359799e - 3 \tag{4.10}$$

$$c = 0.001741688500999e - 3 \tag{4.11}$$

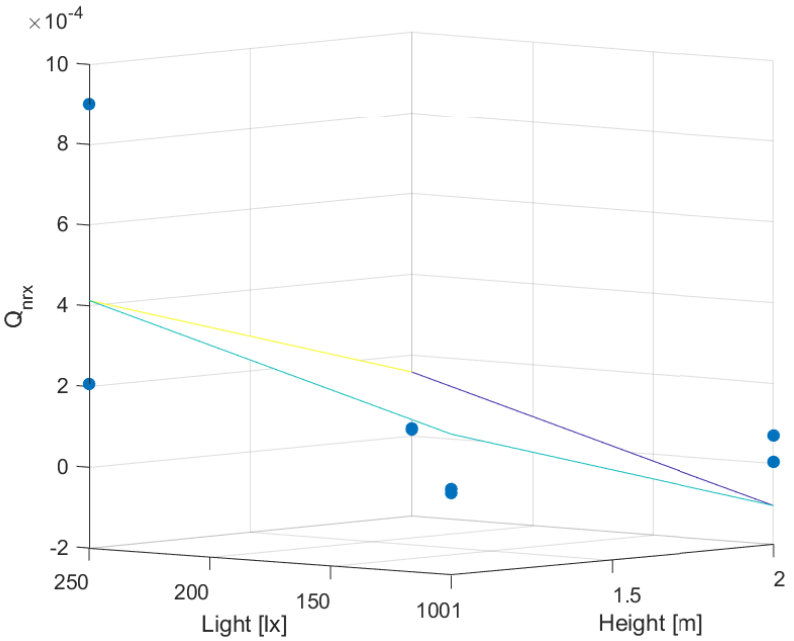

Figure 4.8: Plot of the model for N on x axis without YF

Coefficient: N
Cartesian axis: y
ANOVA: reported in Figure (4.9)

Analysis of Variance

Source	Sum Sq.	d.f.	Mean Sq.	F	Prob>F
Height	2.13154e-07	1	2.13154e-07	1.53	0.2839
TAV	3.49992e-08	1	3.49992e-08	0.25	0.6427
Light	2.22163e-07	1	2.22163e-07	1.59	0.2754
Error	5.57684e-07	4	1.39421e-07		
Total	1.028e-06	7			

Constrained (Type III) sums of squares.

Figure 4.9: 1-way ANOVA of N on y axis without YF

Model: $y = a + bx_1 + cx_2$, with x_1 height, x_2 light and

$$a = 0.313308966020439e - 3 \tag{4.12}$$

$$b = -0.326461368587362e - 3 \tag{4.13}$$

$$c = 0.002221924117212e - 3 \tag{4.14}$$

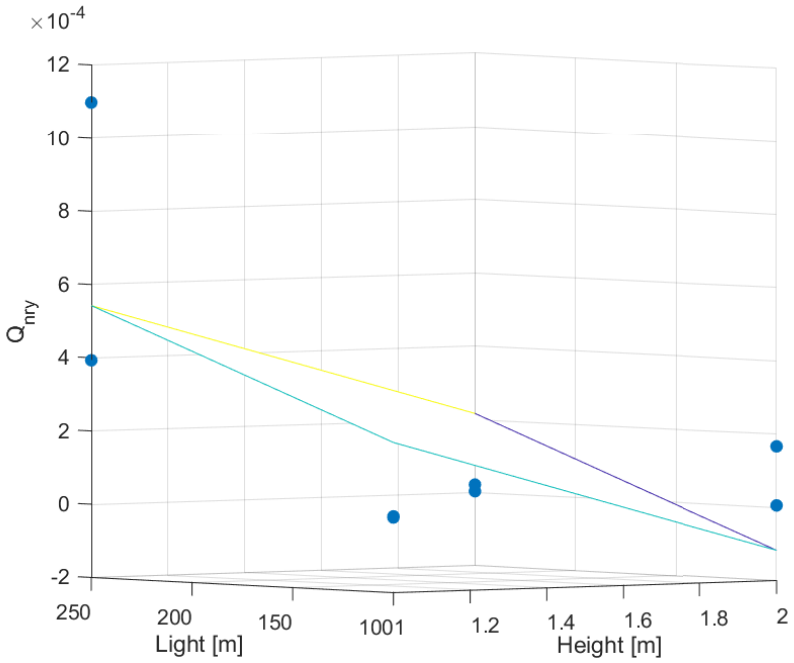

Figure 4.10: Plot of the model for N on y axis without YF

Coefficient: N
Cartesian axis: z
ANOVA: reported in Figure (4.11)

Analysis of Variance

Source	Sum Sq.	d.f.	Mean Sq.	F	Prob>F
Height	3.23536e-11	1	3.23536e-11	0.04	0.8524
TAV	2.03862e-10	1	2.03862e-10	0.25	0.6447
Light	1.22392e-09	1	1.22392e-09	1.49	0.2895
Error	3.28912e-09	4	8.2228e-10		
Total	4.74926e-09	7			

Constrained (Type III) sums of squares.

Figure 4.11: 1-way ANOVA of N on z axis without YF

Model: $y = a + bx$, with x light and

$$a = 0.492929253430033e - 4 \tag{4.15}$$

$$b = -0.001649191622407e - 4 \tag{4.16}$$

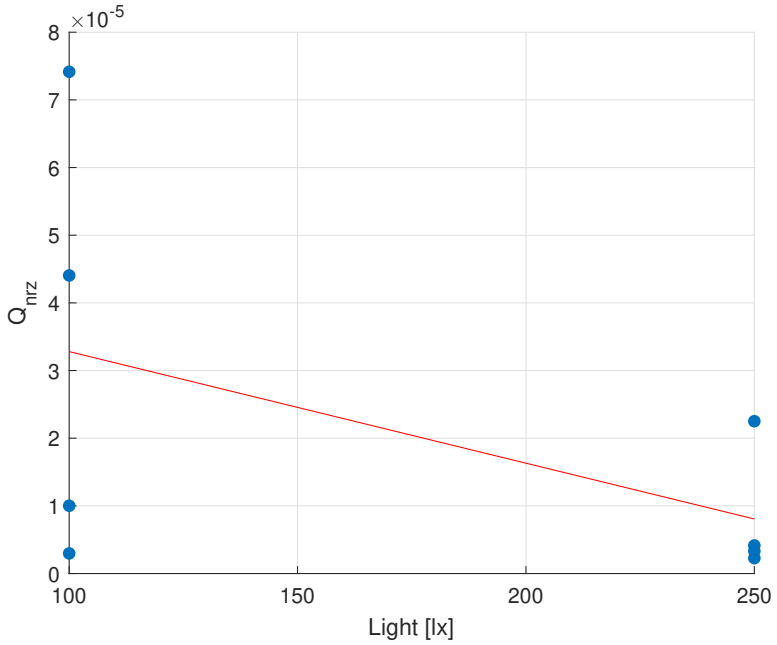

Figure 4.12: Plot of the model for N on z axis without YF

Coefficient: T_B
Cartesian axis: x
ANOVA: reported in Figure (4.13)

Analysis of Variance

Source	Sum Sq.	d.f.	Mean Sq.	F	Prob>F
Height	7032.3	1	7032.3	1.94	0.2364
TAV	3234.8	1	3234.8	0.89	0.3987
Light	2708.1	1	2708.15	0.75	0.4365
Error	14525.5	4	3631.38		
Total	27500.8	7			

Constrained (Type III) sums of squares.

Figure 4.13: 1-way ANOVA of T_B on x axis without YF

Model: $y = a + bx_1 + cx_2 + dx_3$, with x_1 height, x_2 TAV, x_3 light and

$$a = 57.062236898472534 \tag{4.17}$$

$$b = 59.297129266946740 \tag{4.18}$$

$$c = -100.5422890965609 \tag{4.19}$$

$$d = -0.245318340230278 \tag{4.20}$$

Coefficient: T_B
Cartesian axis: y
ANOVA: reported in Figure (4.14)

Analysis of Variance

Source	Sum Sq.	d.f.	Mean Sq.	F	Prob>F
Height	2598.5	1	2598.5	3.12	0.1523
TAV	3500.91	1	3500.91	4.2	0.1098
Light	151.94	1	151.94	0.18	0.6915
Error	3336.32	4	834.08		
Total	9587.67	7			

Constrained (Type III) sums of squares.

Figure 4.14: 1-way ANOVA of T_B on y axis without YF

Model: $y = a + bx_1 + cx_2$, with x_1 TAV, x_2 height and

$$a = 55.958829356058899 \tag{4.21}$$

$$b = -104.5960849546154 \tag{4.22}$$

$$c = 36.045123104501954 \tag{4.23}$$

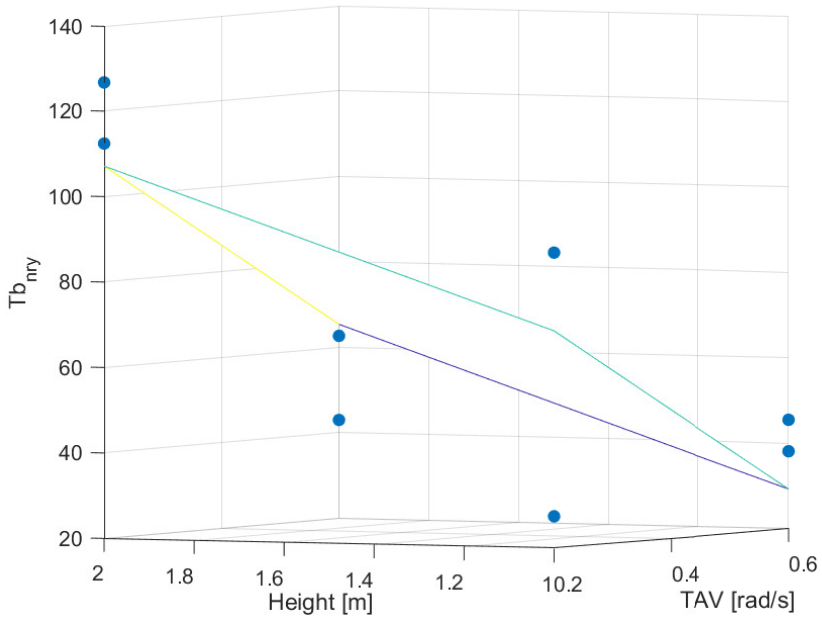

Figure 4.15: Plot of the model for T_B on y axis without YF

Coefficient: T_B
Cartesian axis: z
ANOVA: reported in Figure (4.16)

Analysis of Variance

Source	Sum Sq.	d.f.	Mean Sq.	F	Prob>F
Height	40785.1	1	40785.1	1.06	0.3606
TAV	32659.8	1	32659.8	0.85	0.4082
Light	32317	1	32317	0.84	0.4105
Error	153319.3	4	38329.8		
Total	259081.1	7			

Constrained (Type III) sums of squares.

Figure 4.16: 1-way ANOVA of T_B on z axis without YF

Model: $y = a + bx_1 + cx_2 + dx_3$, with x_1 height, x_2 TAV, x_3 light and

$$a = -85.356064176341945 \tag{4.24}$$

$$b = 142.8024447796917 \tag{4.25}$$

$$c = 319.4712610919590 \tag{4.26}$$

$$d = -0.847440165647982 \tag{4.27}$$

Coefficient: Q_B
Cartesian axis: x
ANOVA: reported in Figure (4.17)

Analysis of Variance

Source	Sum Sq.	d.f.	Mean Sq.	F	Prob>F
Height	2.27823e-10	1	2.27823e-10	0.23	0.6588
TAV	2.1069e-10	1	2.1069e-10	0.21	0.6707
Light	8.22795e-11	1	8.22795e-11	0.08	0.7889
Error	4.01797e-09	4	1.00449e-09		
Total	4.53877e-09	7			

Constrained (Type III) sums of squares.

Figure 4.17: 1-way ANOVA of Q_B on x axis without YF

Model: $y = a + bx_1 + cx_2$, with x_1 height, x_2 TAV and

$$a = 0.101694524685570e - 4 \tag{4.28}$$

$$b = 0.106729373400217e - 4 \tag{4.29}$$

$$c = -0.256594386057576e - 4 \tag{4.30}$$

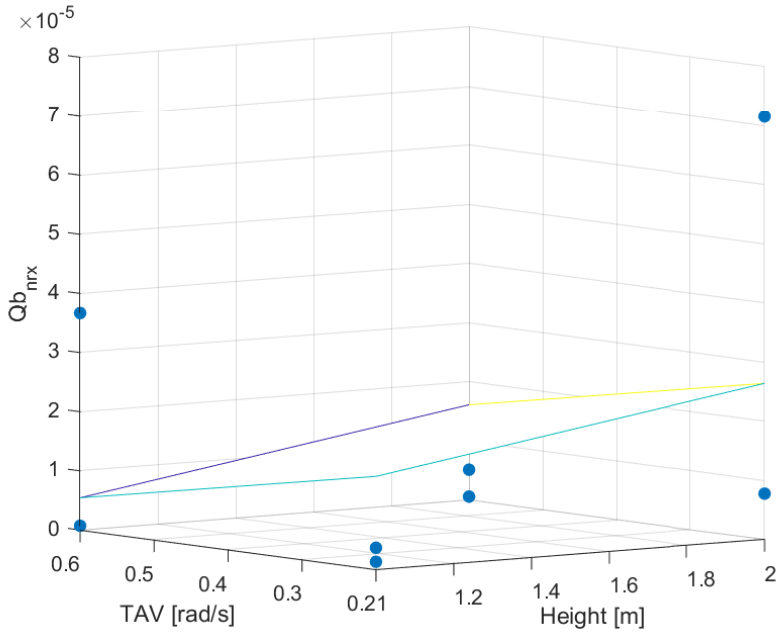

Figure 4.18: Plot of the model for Q_B on x axis without YF

Coefficient: Q_B
Cartesian axis: y
ANOVA: reported in Figure (4.19)

Analysis of Variance

Source	Sum Sq.	d.f.	Mean Sq.	F	Prob>F
Height	2.84092e-12	1	2.84092e-12	0.01	0.9231
TAV	2.0966e-11	1	2.0966e-11	0.08	0.7939
Light	9.68472e-11	1	9.68472e-11	0.36	0.5807
Error	1.07534e-09	4	2.68836e-10		
Total	1.196e-09	7			

Constrained (Type III) sums of squares.

Figure 4.19: 1-way ANOVA of Q_B on y axis without YF

Model: $y = a + bx_1 + cx_2 + dx_3$, with x_1 light, x_2 TAV, x_3 height and

$$a = -0.033977522000897e - 5 \tag{4.31}$$

$$b = 0.004639137082416e - 5 \tag{4.32}$$

$$c = 0.809437223117382e - 5 \tag{4.33}$$

$$d = -0.119183088695481e - 5 \tag{4.34}$$

Coefficient: Q_B
Cartesian axis: z
ANOVA: reported in Figure (4.20)

Analysis of Variance

Source	Sum Sq.	d.f.	Mean Sq.	F	Prob>F
Height	2.14051e-08	1	2.14051e-08	0.79	0.4253
TAV	1.80229e-08	1	1.80229e-08	0.66	0.4615
Light	3.28859e-08	1	3.28859e-08	1.21	0.3335
Error	1.08905e-07	4	2.72264e-08		
Total	1.81219e-07	7			

Constrained (Type III) sums of squares.

Figure 4.20: 1-way ANOVA of Q_B on z axis without YF

Model: $y = a + bx_1 + cx_2 + dx_3$, with x_1 light, x_2 height, x_3 TAV and

$$a = -0.030766130155979e - 3 \tag{4.35}$$

$$b = -0.000854867556257e - 3 \tag{4.36}$$

$$c = 0.103453126015541e - 3 \tag{4.37}$$

$$d = 0.237321972505578e - 3 \tag{4.38}$$

4.2.2 Data with yaw following

Let's list, now, all the ANOVA-based models done on the AVAR coefficients in the eight experimental runs with the YF; y ,again, indicates the considered coefficient.

Coefficient: K
Cartesian axis: x
ANOVA: reported in Figure (4.21)

Analysis of Variance

Source	Sum Sq.	d.f.	Mean Sq.	F	Prob>F
Height	0.00045	1	0.00045	14.91	0.0181
TAV	0.00061	1	0.00061	20.52	0.0106
Light	0.00006	1	0.00006	1.95	0.235
Error	0.00012	4	0.00003		
Total	0.00124	7			

Constrained (Type III) sums of squares.

Figure 4.21: 1-way ANOVA of K on x axis with YF

Model: $y = a + bx_1 + cx_2$, with x_1 TAV, x_2 height and

$$a = -0.020998700796724 \tag{4.39}$$

$$b = 0.043759987614534 \tag{4.40}$$

$$c = 0.014924021403213 \tag{4.41}$$

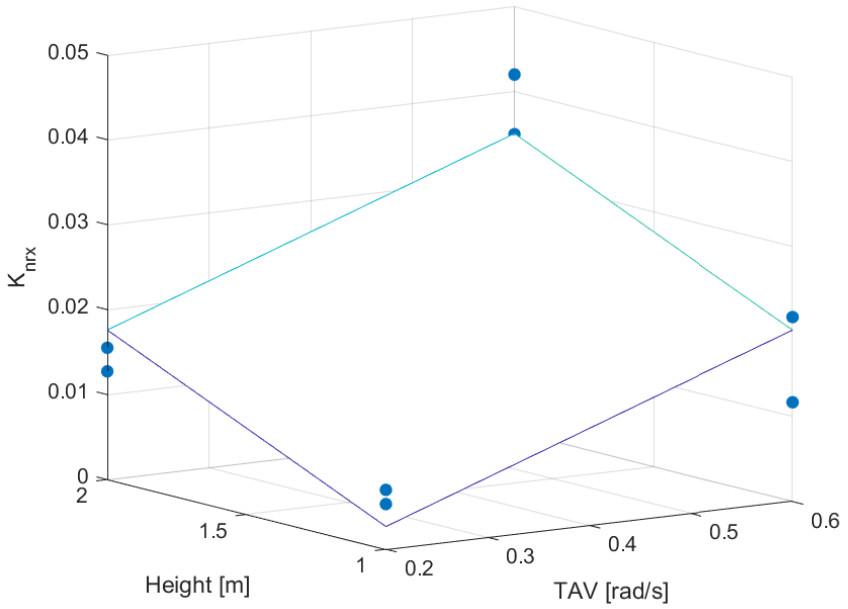

Figure 4.22: Plot of the model for K on x axis with YF

Coefficient: K
Cartesian axis: y
ANOVA: reported in Figure (4.23)

Analysis of Variance

Source	Sum Sq.	d.f.	Mean Sq.	F	Prob>F
Height	0.0005	1	0.0005	29.02	0.0057
TAV	0.00056	1	0.00056	32.74	0.0046
Light	0.00001	1	0.00001	0.71	0.4472
Error	0.00007	4	0.00002		
Total	0.00114	7			

Constrained (Type III) sums of squares.

Figure 4.23: 1-way ANOVA of K on y axis with YF

Model: $y = a + bx_1 + cx_2$, with x_1 TAV, x_2 light and

$$a = -0.019392772537509 \tag{4.42}$$

$$b = 0.041946587940947 \tag{4.43}$$

$$c = 0.015795599832171 \tag{4.44}$$

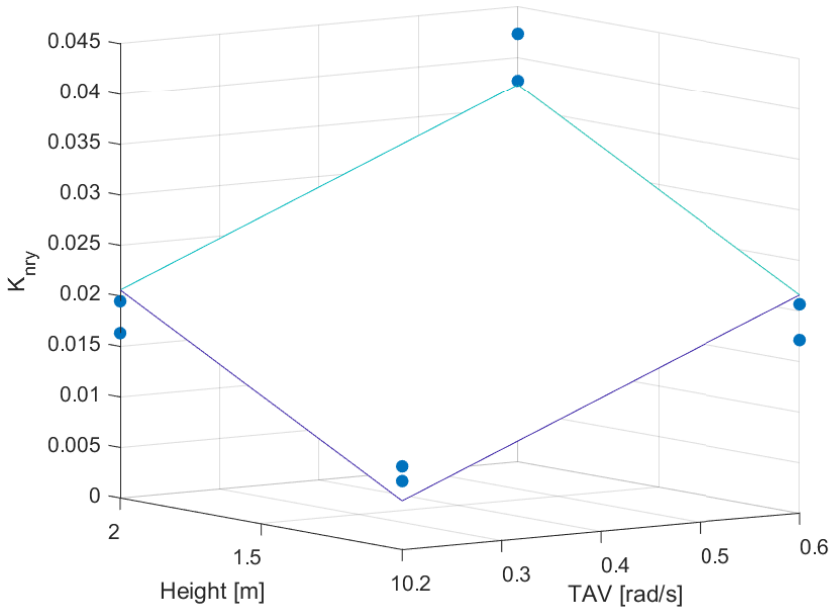

Figure 4.24: Plot of the model for K on y axis with YF

Coefficient: K
Cartesian axis: z
ANOVA: reported in Figure (4.25)

Analysis of Variance

Source	Sum Sq.	d.f.	Mean Sq.	F	Prob>F
Height	0.00049	1	0.00049	7.67	0.0503
TAV	0.00008	1	0.00008	1.18	0.3378
Light	0.00002	1	0.00002	0.35	0.586
Error	0.00026	4	0.00006		
Total	0.00085	7			

Constrained (Type III) sums of squares.

Figure 4.25: 1-way ANOVA of K on z axis with YF

Model: $y = a + bx$, with x height and

$$a = -0.004857761712008 \tag{4.45}$$

$$b = 0.015669830932098 \tag{4.46}$$

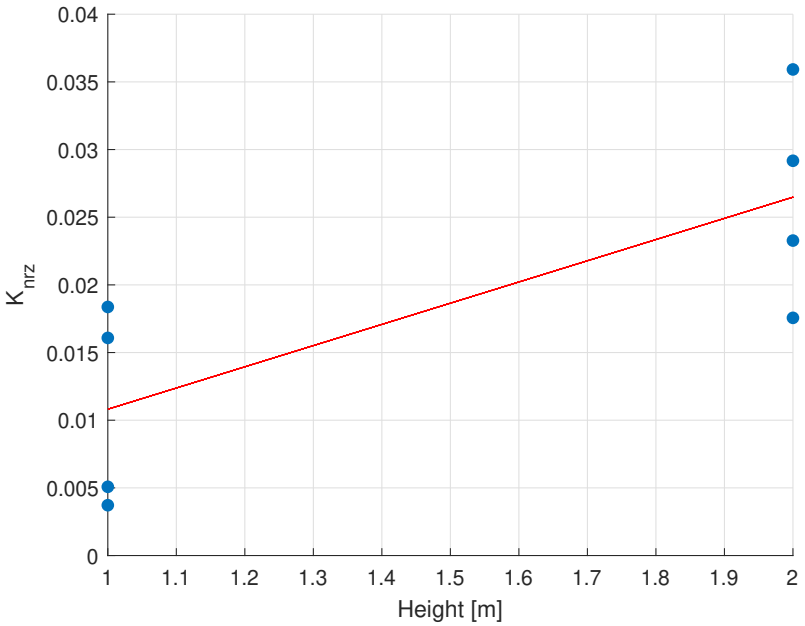

Figure 4.26: Plot of the model for K on z axis with YF

Coefficient: N
Cartesian axis: x
ANOVA: reported in Figure (4.27)

Analysis of Variance

Source	Sum Sq.	d.f.	Mean Sq.	F	Prob>F
Height	2.46072e-07	1	2.46072e-07	5.06	0.0877
TAV	2.81052e-08	1	2.81052e-08	0.58	0.4894
Light	4.66089e-08	1	4.66089e-08	0.96	0.3829
Error	1.94442e-07	4	4.86106e-08		
Total	5.15228e-07	7			

Constrained (Type III) sums of squares.

Figure 4.27: 1-way ANOVA of N on x axis with YF

Model: $y = a + bx$, with x height and

$$a = 0.713183436681427e - 3 \tag{4.47}$$

$$b = -0.350764592305823e - 3 \tag{4.48}$$

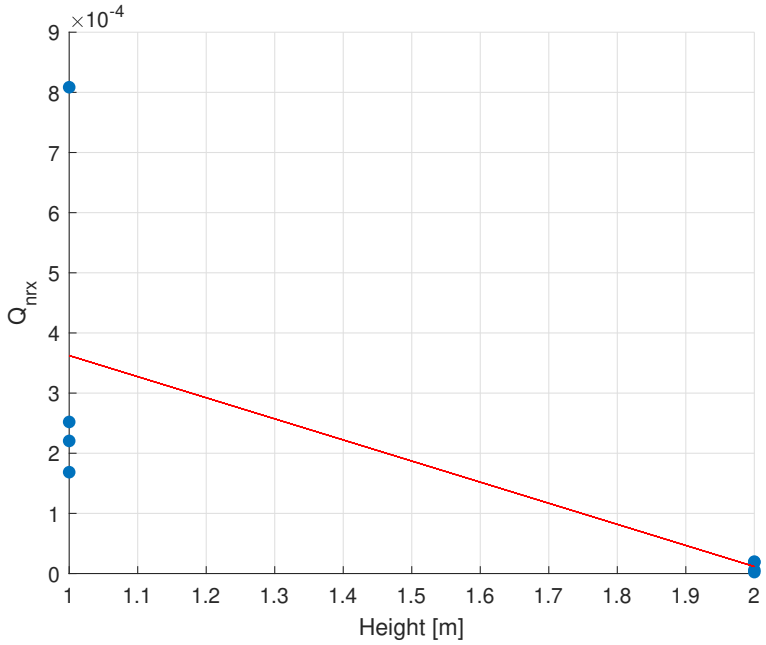

Figure 4.28: Plot of the model for N on x axis with YF

Coefficient: N
Cartesian axis: y
ANOVA: reported in Figure (4.29)

Analysis of Variance

Source	Sum Sq.	d.f.	Mean Sq.	F	Prob>F
Height	3.92431e-07	1	3.92431e-07	14.71	0.0185
TAV	6.11657e-08	1	6.11657e-08	2.29	0.2046
Light	3.02851e-08	1	3.02851e-08	1.14	0.3467
Error	1.0672e-07	4	2.66801e-08		
Total	5.90602e-07	7			

Constrained (Type III) sums of squares.

Figure 4.29: 1-way ANOVA of N on y axis with YF

Model: $y = a + bx$, with x height and

$$a = 0.894019167634692e - 3 \tag{4.49}$$

$$b = -0.442962101016783e - 3 \tag{4.50}$$

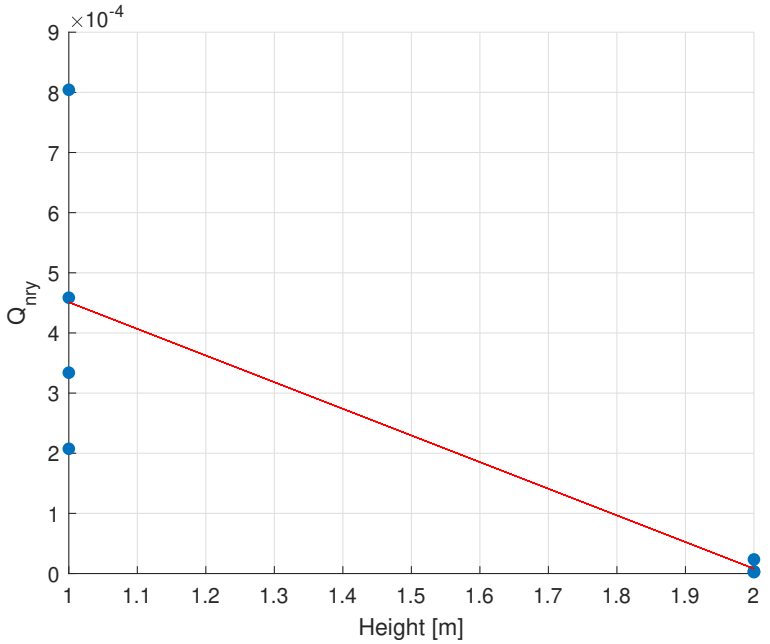

Figure 4.30: Plot of the model for N on y axis with YF

Coefficient: N
Cartesian axis: z
ANOVA: reported in Figure (4.31)

Analysis of Variance

Source	Sum Sq.	d.f.	Mean Sq.	F	Prob>F
Height	4.09378e-11	1	4.09378e-11	0.18	0.6923
TAV	1.8295e-10	1	1.8295e-10	0.81	0.4192
Light	4.10665e-10	1	4.10665e-10	1.82	0.249
Error	9.04296e-10	4	2.26074e-10		
Total	1.53885e-09	7			

Constrained (Type III) sums of squares.

Figure 4.31: 1-way ANOVA of N on z axis with YF

Model: $y = a + bx_1 + cx_2$, with x_1 TAV, x_2 light and

$$a = 0.381154534499600e - 4 \tag{4.51}$$

$$b = -0.239106511750383e - 4 \tag{4.52}$$

$$c = -0.000955295448642e - 4 \tag{4.53}$$

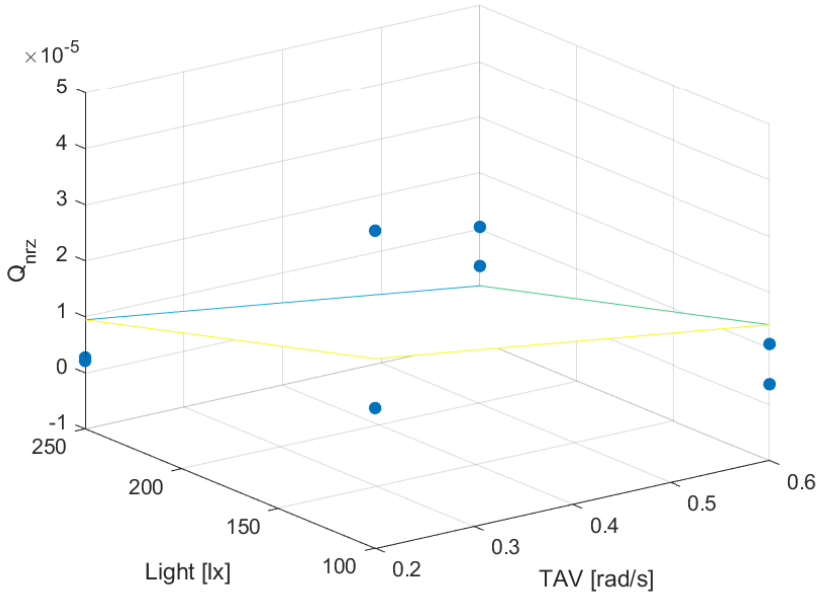

Figure 4.32: Plot of the model for N on z axis with YF

Coefficient: T_B
Cartesian axis: x
ANOVA: reported in Figure (4.33)

Analysis of Variance

Source	Sum Sq.	d.f.	Mean Sq.	F	Prob>F
Height	101.27	1	101.27	0.31	0.6047
TAV	2617.09	1	2617.09	8.13	0.0463
Light	2533.54	1	2533.54	7.87	0.0485
Error	1286.97	4	321.74		
Total	6538.87	7			

Constrained (Type III) sums of squares.

Figure 4.33: 1-way ANOVA of T_B on x axis with YF

Model: $y = a + bx_1 + cx_2$, with x_1 TAV x_2 light and

$$a = 134.0600641529644 \tag{4.54}$$

$$b = -90.4345233867286 \tag{4.55}$$

$$c = -0.2372778726718 \tag{4.56}$$

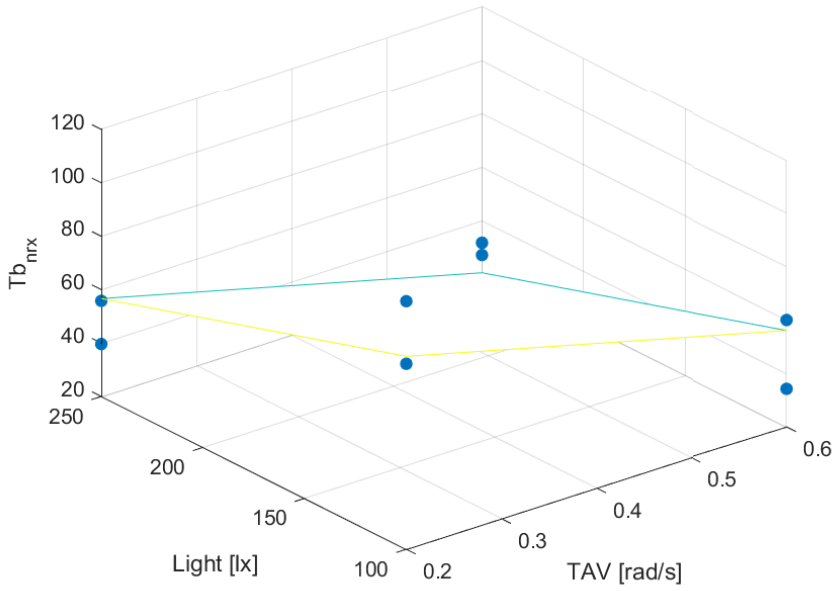

Figure 4.34: Plot of the model for T_B on x axis with YF

Coefficient: T_B
Cartesian axis: y
ANOVA: reported in Figure (4.35)

Analysis of Variance

Source	Sum Sq.	d.f.	Mean Sq.	F	Prob>F
Height	17240.7	1	17240.7	1.02	0.3703
TAV	9856	1	9856	0.58	0.4883
Light	20992	1	20992	1.24	0.3282
Error	67829.9	4	16957.5		
Total	115918.7	7			

Constrained (Type III) sums of squares.

Figure 4.35: 1-way ANOVA of T_B on y axis with YF

Model: $y = a + bx_1 + cx_2 + dx_3$, with x_1 light, x_2 height, x_3 TAV and

$$a = 181.8667337622135 \tag{4.57}$$

$$b = 0.6830003644207 \tag{4.58}$$

$$c = -92.8459520344171 \tag{4.59}$$

$$d = -175.4997015752402 \tag{4.60}$$

Coefficient: T_B
Cartesian axis: z
ANOVA: reported in Figure (4.36)

Analysis of Variance

Source	Sum Sq.	d.f.	Mean Sq.	F	Prob>F
Height	214.36	1	214.364	0.43	0.5495
TAV	36.03	1	36.028	0.07	0.8022
Light	311.63	1	311.633	0.62	0.4753
Error	2012.19	4	503.048		
Total	2574.22	7			

Constrained (Type III) sums of squares.

Figure 4.36: 1-way ANOVA of T_B on z axis with YF

Model: $y = a + bx_1 + cx_2$, with x_1 light, x_2 height and

$$a = 34.111377223048336 \tag{4.61}$$

$$b = 0.083217697322009 \tag{4.62}$$

$$c = -10.352885861998592 \tag{4.63}$$

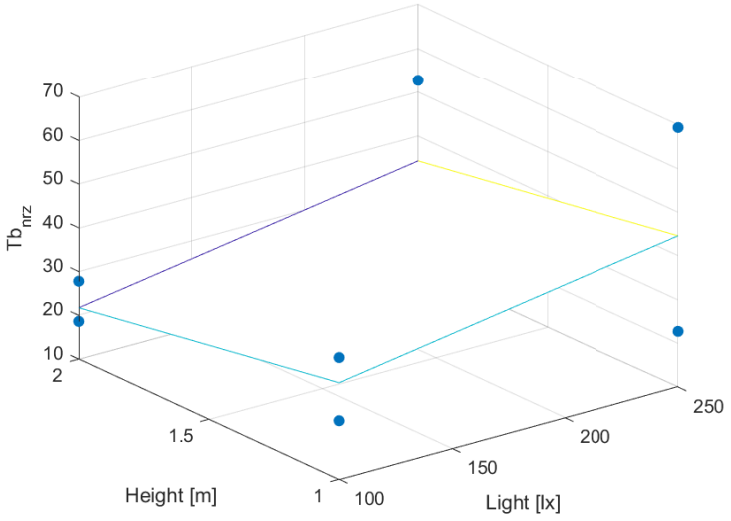

Figure 4.37: Plot of the model for T_B on z axis with YF

Coefficient: Q_B
Cartesian axis: x
ANOVA: reported in Figure 4.38

Analysis of Variance

Source	Sum Sq.	d.f.	Mean Sq.	F	Prob>F
Height	5.99124e-11	1	5.99124e-11	0.59	0.4861
TAV	6.47758e-10	1	6.47758e-10	6.35	0.0653
Light	1.26104e-10	1	1.26104e-10	1.24	0.3284
Error	4.07795e-10	4	1.01949e-10		
Total	1.24157e-09	7			

Constrained (Type III) sums of squares.

Figure 4.38: 1-way ANOVA of Q_B on x axis with YF

Model: $y = a + bx$, with x TAV and

$$a = 0.275570501634261e - 4 \tag{4.64}$$

$$b = -0.449915860176829e - 4 \tag{4.65}$$

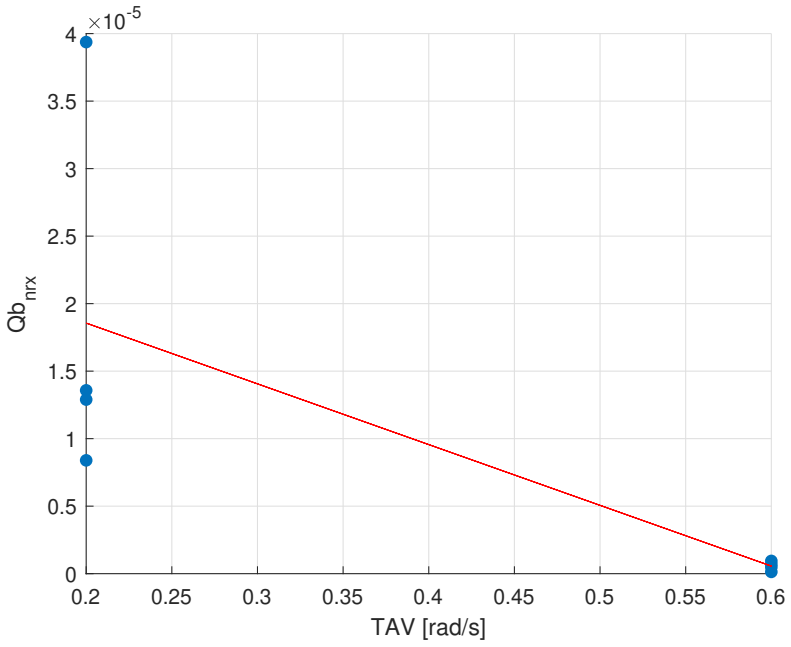

Figure 4.39: Plot of the model for Q_B on x axis with YF

Coefficient: Q_B
Cartesian axis: y
ANOVA: reported in Figure (4.40)

Analysis of Variance

Source	Sum Sq.	d.f.	Mean Sq.	F	Prob>F
Height	3.33481e-11	1	3.33481e-11	2.15	0.2161
TAV	1.33441e-10	1	1.33441e-10	8.62	0.0425
Light	7.12783e-12	1	7.12783e-12	0.46	0.5346
Error	6.19104e-11	4	1.54776e-11		
Total	2.35828e-10	7			

Constrained (Type III) sums of squares.

Figure 4.40: 1-way ANOVA of Q_B on y axis with YF

Model: $y = a + bx$, with x TAV and

$$a = 0.128145104308231e - 4 \tag{4.66}$$

$$b = -0.204206864633445e - 4 \tag{4.67}$$

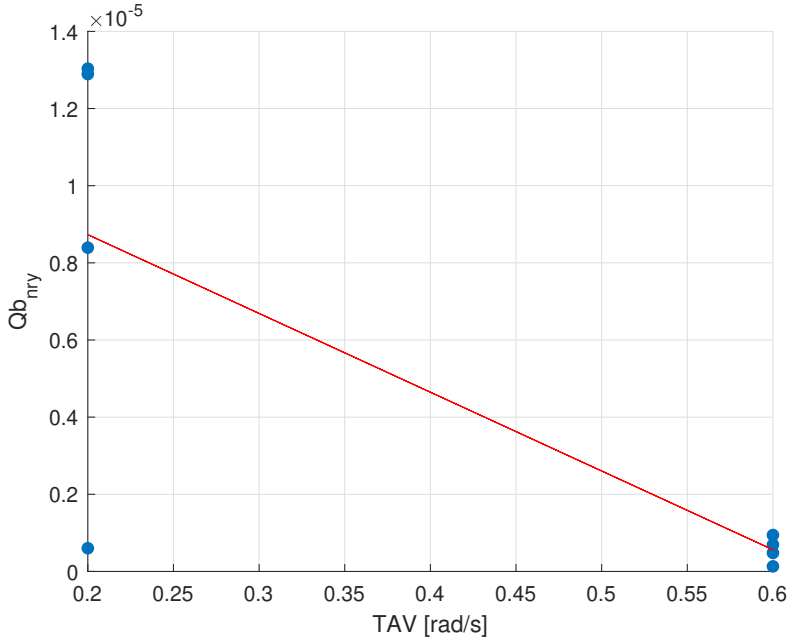

Figure 4.41: Plot of the model for Q_B on y axis with YF

Coefficient: Q_B
Cartesian axis: z
ANOVA: reported in Figure (4.42)

Analysis of Variance

Source	Sum Sq.	d.f.	Mean Sq.	F	Prob>F
Height	2.49424e-09	1	2.49424e-09	1.38	0.3056
TAV	3.05968e-09	1	3.05968e-09	1.69	0.2634
Light	1.11538e-09	1	1.11538e-09	0.62	0.4764
Error	7.24079e-09	4	1.8102e-09		
Total	1.39101e-08	7			

Constrained (Type III) sums of squares.

Figure 4.42: 1-way ANOVA of Q_B on z axis with YF

Model: $y = a + bx_1 + cx_2$, with x_1 TAV, x_2 height and

$$a = 0.114449047778092e - 3 \tag{4.68}$$

$$b = -0.097782942500976e - 3 \tag{4.69}$$

$$c = -0.035314610255495e - 3 \tag{4.70}$$

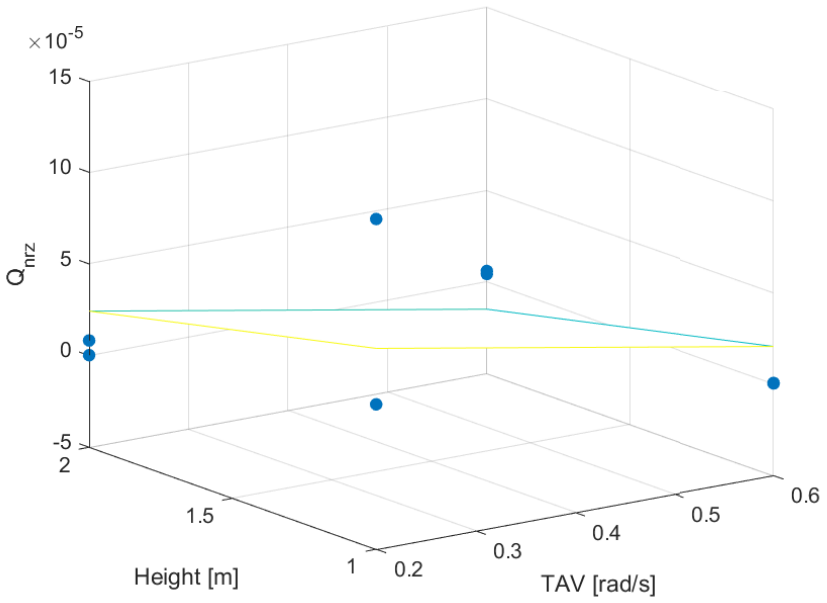

Figure 4.43: Plot of the model for Q_B on z axis with YF

4.2.3 Overview of the results

Tables (4.2) and (4.3) sum up all the previously illustrated analysis, showing for each of the AVAR coefficients how many and what independent variables have been used.

In the case without the YF all the variables have been used in an almost equal manner, even if the TAV has been used once more than the other two, whereas in the case with the YF the light has come into play much less times. The coefficients T_B and Q_B require more variables than K and N to be parametrically modeled. It is noticed that, in general, in the case with the YF the models for T_B and Q_B are simpler than in the case without the YF, whereas the other two coefficients do not exibit such a regularity.

Coefficient	Axis	Height	TAV	Light
K	x		✓	
K	y		✓	✓
K	z		✓	✓
N	x	✓		✓
N	y	✓		✓
N	z			✓
T_B	x	✓	✓	✓
T_B	y	✓	✓	
T_B	z	✓	✓	✓
Q_B	x	✓	✓	
Q_B	y	✓	✓	✓
Q_B	z	✓	✓	✓

Table 4.2: Summary of the used independent variables for AVAR coefficients without YF

Coefficient	Axis	Height	TAV	Light
K	x	✓	✓	
K	y	✓	✓	
K	z	✓		
N	x	✓		
N	y	✓		
N	z		✓	✓
T_B	x		✓	✓
T_B	y	✓	✓	✓
T_B	z	✓		✓
Q_B	x		✓	
Q_B	y		✓	
Q_B	z	✓	✓	

Table 4.3: Summary of the used independent variables for AVAR coefficients with YF

4.3 Interpolations on matrices

It has been decided, then, to try to make linear parametric models also on the terms of the A, B, C and K matrices coming from the identified models and from the Kalman predictors [14].

In this case, for the sake of simplicity, only one factor has been considered, choosing the TAV since the previous steps have revealed that it is very relevant.

The linear regression process has not been done on all terms, but only on the ones that show a non-negligible variation between the two levels of the factor; for the other terms it has been taken a constant value equal to the average of all the values.

The choice of what terms to interpolate has been conducted not through ANOVAs or other statistical tools, but simply looking to two macroscopic indicators:

- The difference between the range of values covered by the terms at the two factors' level
- The difference between the mean values of the terms at the two factors' level

The second indicator has been given more importance than the first one in the choice of the terms, because it has turned out to be more conservative.

Doing all the calculations, the following four matrices, calling x the value of the TAV, have been obtained. It is clear that the TAV produces a much larger variability on the C and K matrices rather than on the A and B matrices.

$$A = \begin{bmatrix} 0.997934 & -0.0118058 & 0.0037696 \\ 5.079863e-4 & 0.980773 & 0.021803 - 0.0169617x \\ -3.651178e-5 & -0.0070356 & 0.9616464 - 0.0196969x \end{bmatrix} \tag{4.71}$$

$$B = \begin{bmatrix} -5.827294e-4 & 3.945836e-4 & -4.058273e-4 \\ 0.0022336 & 1.579183e-4 & -0.0013049 \\ 8.404396e-4 & -0.003858 & 3.5994212e-4 \end{bmatrix} \tag{4.72}$$

$$C = \begin{bmatrix} 0.068151 - 0.1236792x & -0.1303572 + 0.1157025x & 0.006166 \\ -0.1140281 + 0.287701x & -0.08805 + 0.330028x & 0.0343085 + 0.0504399x \\ -0.0410961 & -0.2104276 + 0.4704582x & 0.1479916 - 0.0654206x \end{bmatrix} \tag{4.73}$$

$$K = \begin{bmatrix} 0.4085824 - 0.6858456x & 0.421089 + 0.8898056x & -0.350039 + 0.6850546x \\ -0.2424603 - 0.0212521x & -0.2026322 + 1.0614513x & -0.8039088 + 1.664683x \\ 0.5752862 - 1.50499x & -0.0229125 - 0.1215274x & 0.2118715 \end{bmatrix} \tag{4.74}$$

Conclusions

This thesis had as objectives to model the dynamics of a Visual Odometry system and to find some systematic relationships between the characteristics and the conditions of the environment where the system is operated; the studied features have been taken from the dynamics of the noise and of the error, the first identified through the AVAR technique, the second through the MOESP-PO black-box technique.

The LS regression technique has allowed to build parametric models of part of the data and the ANOVA technique has been extremely useful to understand what factors had been better to use as independent variables and, more generally, what factors have a relevant influence on the selected dynamic features.

It is evident that the height and the Trajectory Angular Velocity (TAV), both individually and through their interaction, are much more important in changing all the studied variables (AVAR coefficients, prediction errors and characteristics of the models) than the setting of the Yaw Following (YF) and the environmental light; about the last two factors, in some cases it has been turned out to be more important their interactions rather than their main effects.

An important step of the work, that has not been done only for logistic reasons, is the *validation* of the results from model identification and parametric modeling [11].

To carry out a validation, basically, it is necessary, at first, to check if the characteristics of the identified models are compatible with the prior knowledge about the system, then it is required to collect some new data, for example repeating all or only some of the experiments that provided the data that have been used, to do again the identification and modeling processes on these new data and to check if the new results are coherent with the ones from the first identification.

When it is not possible to collect new data, it is often possible to do a *cross-validation*, that basically consists in splitting the available data set in two parts, one to be used to do the identification process and the other to be used to validate it; in this case it has been decided that, since the available data were not so much even from the beginning of the work, a further splitting of them would have not been very wise.

Here there are reported some ideas that could allow to repeat this analysis in a better manner:

- Make flights longer or use a more complex trajectory;
- Introduce other factors in the design of the experiments, in addition to the already used ones
- Use more than two levels for each factor;
- In the parts of the work involving the coefficients of the AVAR, use the model that includes also the Rate Ramp noise, with the R coefficient;
- Carry out each experiment more than once, in order to have multiple data sets corresponding to the same conditions and to make the identification and the validation with only one experimental campaign.

It is evident, in synthesis, that the analysis can be improved through a more complex experimental campaign and/or through the collection of a bigger amount of data, as implied by all the above-listed solutions.

Bibliography

[1] D. Scaramuzza. Tutorial on Visual Odometry. *Robotics and Perception Group, University of Zurich*, 2011.

[2] M.O.A. Aqel, Ismail N.B., Marhaban M.H., and Saripan M.I. Review of visual odometry: types, approaches, challenges and applications. *SpringerPlus*, 2016.

[3] D.C. Montgomery. *Design and Analysis of Experiments, Ninth Edition*. Wiley, 2017.

[4] F. Chiarlo. A statistical analysis of position estimation error in visual odometry. *School of Industrial and Information Engineering, Politecnico di Milano*, 2021.

[5] KDE2315XF-965 - UAS BLDC Brushless Motor - KDE Direct.

[6] Zed website.

[7] OptiTrack website.

[8] M. Lovera and G. Roggi. Visual odometry error modeling for multicopter UAVs. *Dipartimento di Scienze e Tecnologie Aerospaziali, Politecnico di Milano*, 2022.

[9] Analysis of variance - Wikipedia, The Free Encyclopedia.

[10] N-way analysis of variance - MATLAB anovan - MathWorks Italia.

[11] M. Lovera. Introduction to model identification. *Dipartimento di Scienze e Tecnologie Aerospaziali, Politecnico di Milano*, 2020.

[12] M. Lovera. Identification of MIMO linear models: introduction to subspace methods. *Dipartimento di Scienze e Tecnologie Aerospaziali, Politecnico di Milano*, 2021.

[13] M. Lovera. Kalman prediction and filtering. *Dipartimento di Scienze e Tecnologie Aerospaziali, Politecnico di Milano*, 2020.

[14] Hecker S. and Pfifer H. Generation of optimal linear parametric models for lft-based robust stability analysis and control design. *IEEE Transactions on Control System Technology*, 2011.